REPORT ON A HELICOPTER-BORNE VERSATILE TIME DOMAIN ELECTROMAGNETIC (VTEM) GEOPHYSICAL SURVEY

Denyes-Swayze, Dore and Heenan Blocks

Foleyet, Ontario

For:

Red Pine Exploration Inc.

By

Geotech Ltd.

245 Industrial Parkway North

Aurora, Ont., CANADA, L4G 4C4

Tel: 1.905.841.5004

Fax: 1.905.841.0611

www.geotech.ca

Email: info@geotech.ca

Survey flown in May, 2009

Project 9067

July, 2009

TABLE OF CONTENTS

APPENDICES

LIST OF FIGURES

LIST OF TABLES

REPORT ON A HELICOPTER-BORNE VERSATILE TIME DOMAIN ELECTROMAGNETIC SURVEY

Denyes-Swayze, Dore and Heenan blocks
Foleyet, Ontario

Executive Summary

During May 13th to May 24th, 2009 Geotech Ltd. carried out a helicopter-borne geophysical survey for Red Pine Exploration Inc. over the Denyes-Swayze, Dore and Heenan blocks situated near Foleyet, Ontario, Canada.

Principal geophysical sensors included a versatile time domain electromagnetic (VTEM) system, a cesium magnetometer and an airborne gamma ray spectrometer. Ancillary equipment included a GPS navigation system and a radar altimeter. A total of 955 line-kilometres were flown.

The survey operations were based in the Timber Camp, Ontario, near the survey area. In-field data quality assurance and preliminary processing were carried out on a daily basis during the acquisition phase. Preliminary and final data processing, including generation of final digital data and map products were undertaken from the office of Geotech Ltd. in Aurora, Ontario.

The processed survey results are presented as electromagnetic stacked profiles, and as a colour grid of the B-field EM late time channels, total magnetic intensity, time constants (Tau) and gamma ray spectrometry products.

Digital data includes all electromagnetic, magnetic and gamma ray spectrometry products, plus ancillary data including the waveform.

The survey report describes the procedures for data acquisition, processing, final image presentation and the specifications for the digital data set. The survey results have been briefly described in a summary interpretation, in support of the EM anomaly picking, and EM time-constant (Tau) analysis that were performed together with magnetic and spectrometric data analysis.

1. INTRODUCTION

1.1 General Considerations

These services are the result of the Agreement made between Geotech Ltd. and Red Pine Exploration Inc. to perform a helicopter-borne geophysical survey over Denyes-Swayze, Dore and Heenan blocks located south-west of Foleyet, Ontario, Canada (Figure 1).

Jacob McKinnon acted on behalf of Red Pine Exploration Inc. during the data acquisition and data processing phases of this project.

The geophysical surveys consisted of helicopter borne EM using the versatile time-domain electromagnetic (VTEM) system, aeromagnetics using a cesium magnetometer and a gamma ray spectrometer system. A total of 955 line-km of geophysical data were acquired during the survey. The survey area is shown in Figure 2.

The crew was based at the Timber Camp, south-west of the town of Foleyet, Ontario, for the acquisition phase of the survey. Survey flying started on May 13th and was completed on May 24th, 2009.

Data quality control and quality assurance, and preliminary data processing were carried out on a daily basis during the acquisition phase of the project. Final data processing followed immediately after the end of the survey. Final reporting, data presentation and archiving were completed from the Aurora office of Geotech Ltd. in July, 2009.

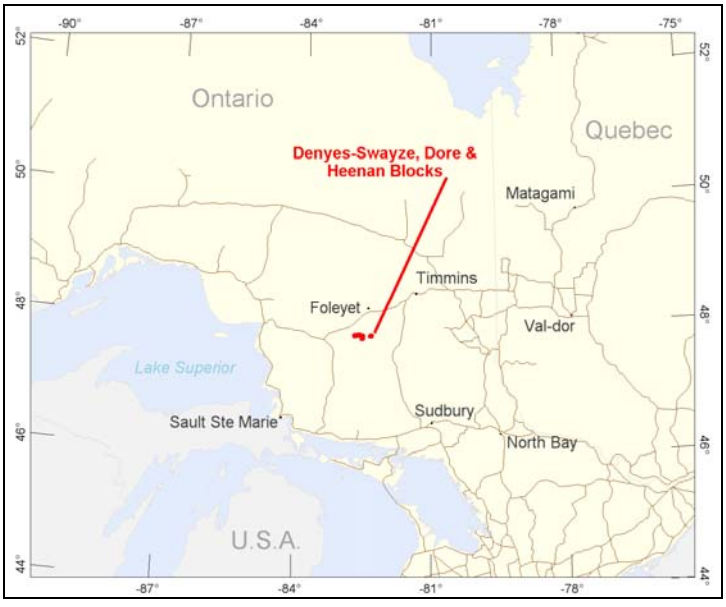

Figure 1 - Property Location

1.2 Survey and System Specifications

The survey blocks are located approximately 45 kilometers south-west of Foleyet, Ontario as shown in Figure 2.

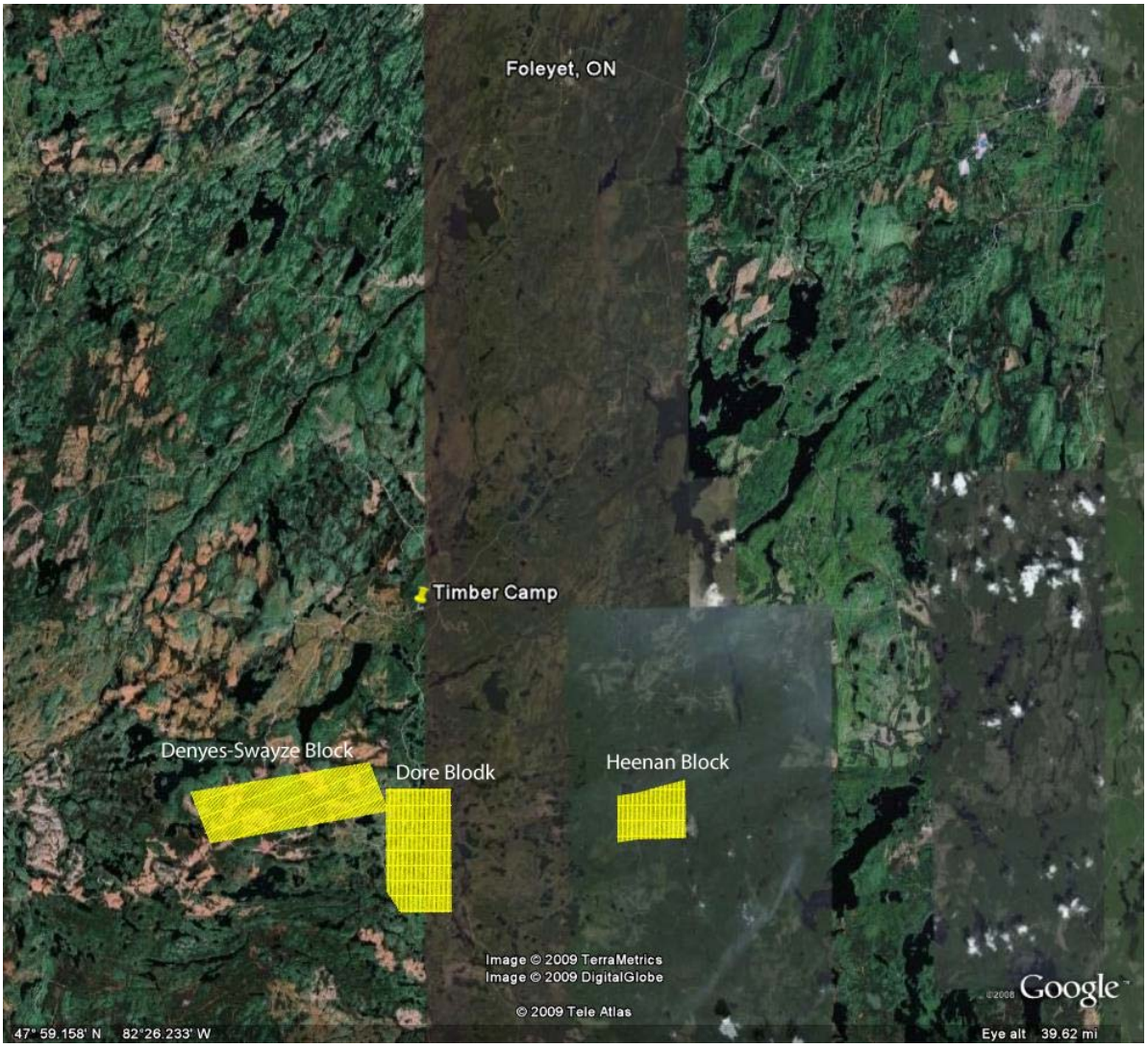

Figure 2 – Google Image with survey site location

All three blocks were flown at 100 metre traverse line spacing wherever possible with flight directions of N 1° E / N 181° E for the Dore and Heenan blocks and at N 160° E / N 340° E for the Denyes-Swayze block while the tie lines were flown perpendicular to the traverse lines at a spacing of 1000 metres with a flight direction of N 91°E / N 271°E for the Dore and Heenan blocks and at N 70° E / N 250° E for the Denyes-Swayze block. For more detailed information on the flight spacing and direction see Table 1.

1.3 Topographic Relief and Cultural Features

Topographically, the blocks exhibit a shallow relief covering a total of 87.5 square kilometers for all three blocks, with an elevation ranging from 377 to 457 metres above sea level (see Figure 3). The survey areas show no visible signs of culture however, there a few small roads and many small rivers running through the surveys connecting various small lakes and wetlands.

The Ontario mining claims, which are shown in Appendix A, are plotted on all maps. The blocks are covered by NTS (National Topographic Survey) of Canada sheets 041O15 and 041O16.

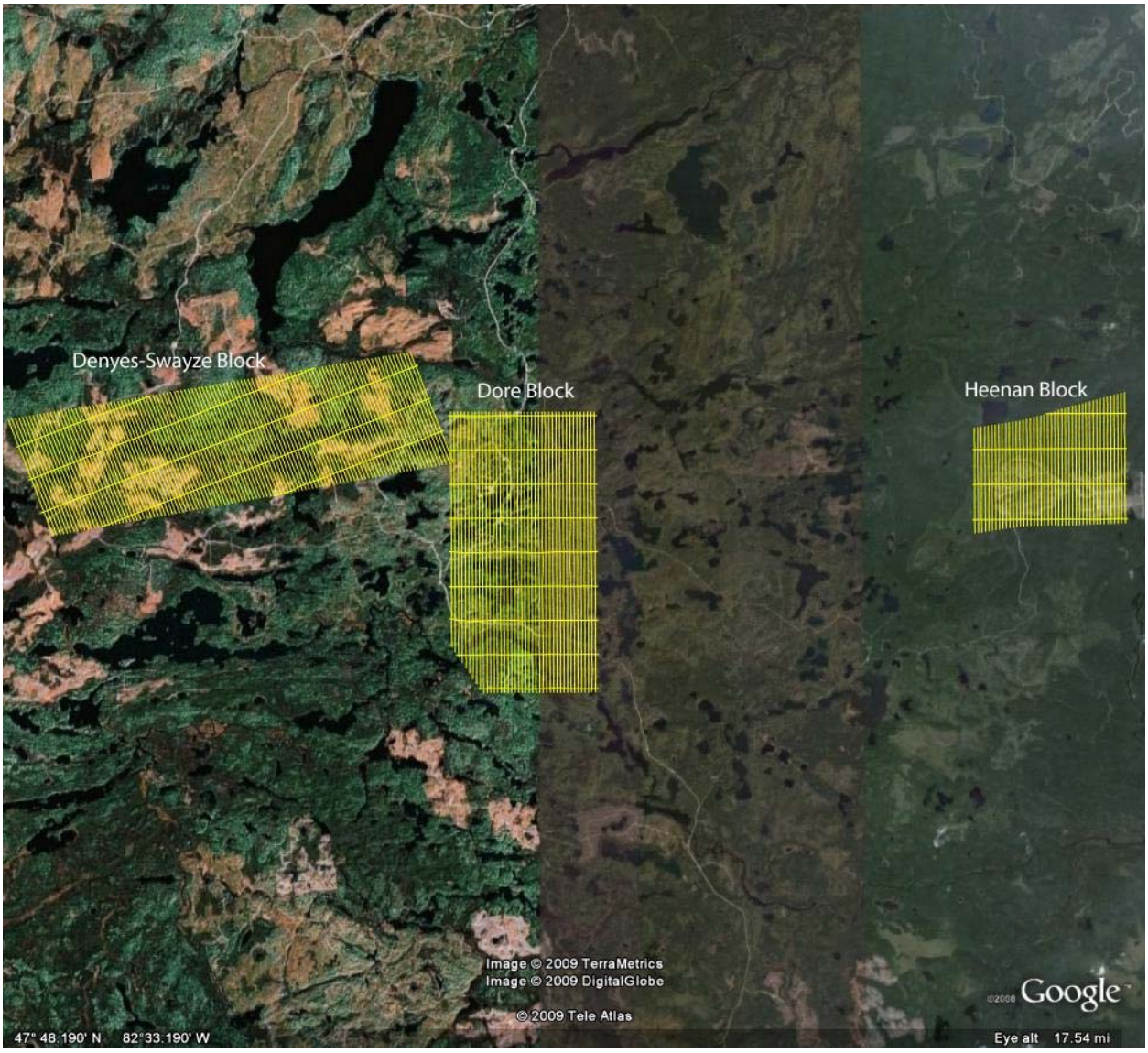

Figure 3 - Google Earth Image with Flight Path

2. DATA ACQUISITION

2.1 Survey Area

The survey blocks (see Location map in Appendix A and Figure 2) and general flight specifications are as follows:

Table 1 - Survey Specifications

Survey blocks	Line spacing (m)	Area (Km^2)	Planned Line-km	Actual line-km[1]	Flight direction	Line number
Denyes	Traverse: 100	40.4	393.8	399.8	N 160° E / N 340° E	L1010 - 2150
	Tie: 1000		38.8	39.3	N 70° E / N 250° E	T2500 - 2540
Dore	Traverse: 100	32.8	327.0	329.2	N 1° E / N 181° E	L3000 - 3410
	Tie: 1000		36.4	37.2	N 91° E / N 271° E	T3500 - 3580
Heenan	Traverse: 100	14.3	142.5	143.5	N 1° E / N 181° E	L4000 - 4430
	Tie: 1000		16.0	16	N 91° E / N 271° E	T4500 - 4530
Total		87.5	954.5	965		

Survey block boundaries co-ordinates are provided in Appendix B.

2.2 Survey Operations

Survey operations were based at the Timber Camp, located near Foleyet, Ontario during the survey period of May 13th to May 24th, 2009. The following table shows the timing of the flying.

Table 2 - Survey schedule

Date	Crew Location	Flight #	Block	Km flown	Comments
05-13-2009	Timber Camp				System Installation
05-14-2009	Timber Camp				System Installation
05-15-2009	Timber Camp				System Installation – test flight
05-16-2009	Timber Camp				No Production due to bad weather
05-17-2009	Timber Camp				No Production due to bad weather
05-18-2009	Timber Camp	1	Dore	143	Production
05-19-2009	Timber Camp				No Production due to technical problem
05-20-2009	Timber Camp	2, 3	Dore	171	Production
05-21-2009	Timber Camp	4	Dore	50	Limited production due to weather
05-22-2009	Timber Camp	5, 6, 7	Denyes	300	Production
05-23-2009	Timber Camp	8, 9	Denyes/Heenan	207	Production
05-24-2009	Timber Camp	10	Heenan	84	Production - Job Complete

1 Note: The Actual line kilometres displayed, which exceed the Planned line-km amount as described in the navigation (NAV) files, represent the total flown kilometres contained in the final databases.

2.3 Flight Specifications

During the survey the helicopter was maintained at a mean height of 77 metres above the ground with a nominal survey speed of 80 km/hour. This allowed for a nominal EM sensor terrain clearance of 42 metres and a magnetic sensor clearance of 64 metres.

The data recording rates of the data acquisition was 0.1 second for electromagnetics, magnetometer and 0.2 second for altimeter and GPS. This translates to a geophysical reading about every 2 metres along flight track. Navigation was assisted by a CDGPS receiver and data acquisition system, which reports GPS co-ordinates as latitude/longitude and directs the pilot over a pre-programmed survey flight path.

The operator was responsible for monitoring of the system integrity. He also maintained a detailed flight log during the survey, tracking the times of the flight as well as any unusual geophysical or topographic feature.

On return of the aircrew to the base camp the survey data was transferred from a compact flash card (PCMCIA) to the data processing computer. The data were then uploaded via ftp to the Geotech office in Aurora for daily quality assurance and quality control by qualified personnel, operating remotely.

2.4 Aircraft and Equipment

2.4.1 Survey Aircraft

The survey was flown using a Euro copter Aerospatiale (Astar) 350 B3 helicopter, registration C-GEOZ. The helicopter was operated by Gateway Helicopters Ltd. and Geotech Ltd. Installation of the geophysical and ancillary equipment was carried out by Geotech Ltd.

2.4.2 Electromagnetic System

The electromagnetic system was a Geotech Time Domain EM (VTEM) system. The configuration is as indicated in Figure 4.

The standard VTEM Receiver and transmitter coils are concentric-coplanar and Z-direction oriented. The receiver system for the project also included a coincident-coplanar X-direction sensor to mean the in-line dB/dt and calculate B-Field responses. All loops were towed at a mean distance of 35 metres below the aircraft as shown in Figures 4 and 6. The receiver decay recording scheme is shown diagrammatically in Figure 5.

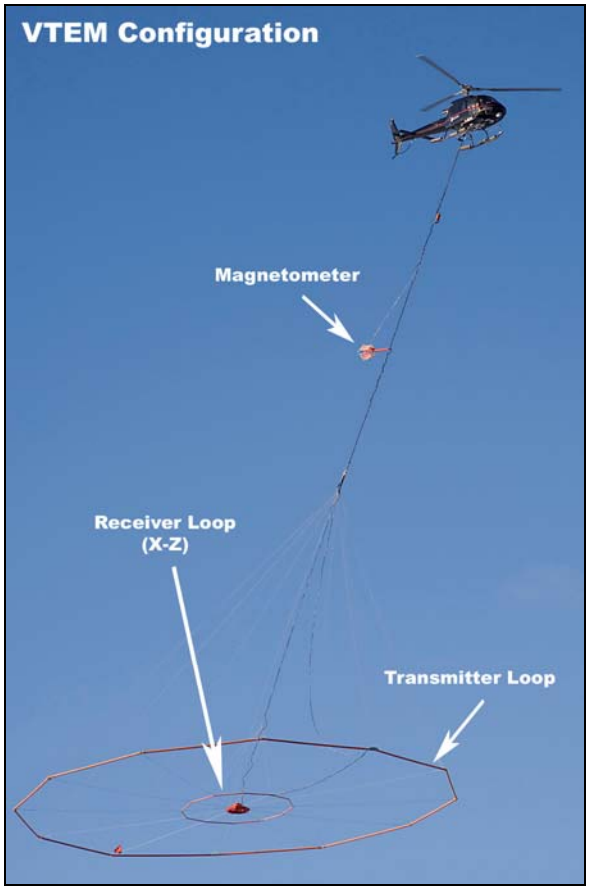

Figure 4 - VTEM Configuration

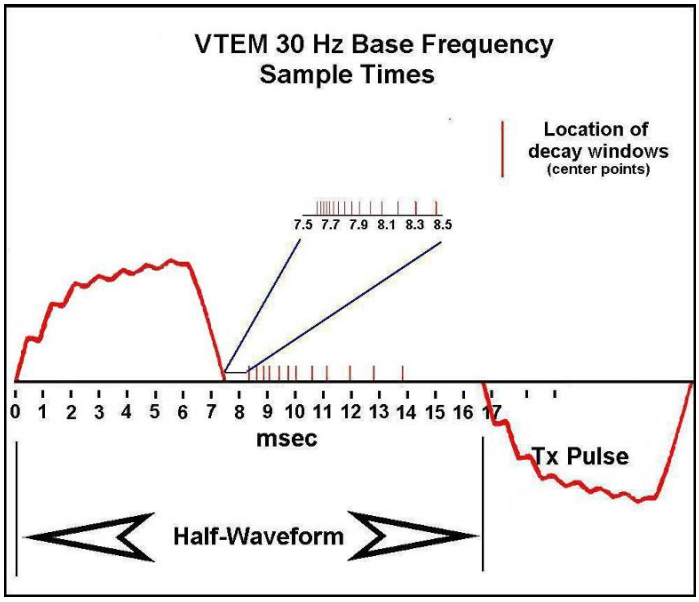

Figure 5 - VTEM waveform & Sample Times

The VTEM decay sampling scheme is shown in Table 3 below. Twenty-four time measurement gates (ch10 to ch33) were used for the final data processing in the range from 120 to 6578 µsec, as shown in Table 5.

Table 3 - Decay Sampling Scheme

VTEM Decay Sampling scheme[2]				
Array Index	(Microseconds)			
	Time Gate	Start	End	Width
0	5	0	10	10
1	16	10	21	11
2	21	16	26	10
3	31	26	37	11
4	42	37	47	10
5	52	47	57	10
6	62	57	68	11
7	73	68	78	11
8	83	78	91	13
9	99	91	110	19
10	120	110	131	21
11	141	131	154	24
12	167	154	183	29
13	198	183	216	34
14	234	216	258	42
15	281	258	310	53
16	339	310	373	63
17	406	373	445	73
18	484	445	529	84
19	573	529	628	99
20	682	628	750	123
21	818	750	896	146
22	974	896	1063	167
23	1151	1063	1261	198
24	1370	1261	1506	245
25	1641	1506	1797	292
26	1953	1797	2130	333
27	2307	2130	2526	396
28	2745	2526	3016	490
29	3286	3016	3599	583
30	3911	3599	4266	667
31	4620	4266	5058	792
32	5495	5058	6037	979
33	6578	6037	7203	1167
34	7828	7203	8537	1334
35	9245	8537	10120	1584

[2] Note: Measurement times-delays are referenced to time-zero marking the end of the transmitter current turn-off, as illustrated in Figure 5 and Appendix C.

VTEM system parameters:

Transmitter Section
- Transmitter coil diameter: 26 metres
- Number of turns: 4
- Transmitter base frequency: 30 Hz
- Peak current: 190 A
- Pulse width: 7.5 ms
- Pulse width: Duty cycle: 45%
- Peak dipole moment: 404, 000 nIA
- Nominal terrain clearance: 46 metres

Receiver Section

X-Coil
- X Coil diameter: 0.32 m
- Number of turns: 245
- Effective coil area: 19.69 m^2

Z-Coil
- Z-Coil coil diameter: 1.2 m
- Number of turns: 100.
- Effective coil area: 113.04 m^2

Magnetometer
- Nominal terrain clearance: 64 metres

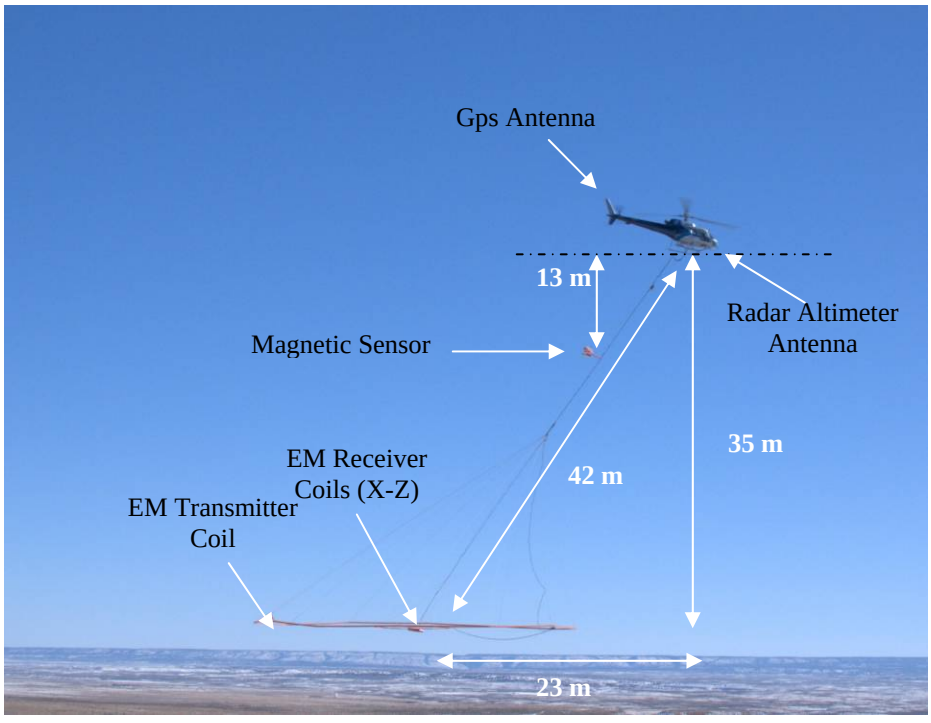

Figure 6 - VTEM system configuration

2.4.3 Airborne magnetometer

The magnetic sensor utilized for the survey was a Geometrics optically pumped caesium vapour magnetic field sensor, mounted in a separate bird, 13 metres below the helicopter, as shown in Figure 6. The sensitivity of the magnetic sensor is 0.02 nanoTesla (nT) at a sampling interval of 0.1 seconds. The magnetometer sends the measured magnetic field strength as nanoTesla to the data acquisition system via the RS-232 port.

2.4.4 Radar Altimeter

A Terra TRA 3000/TRI 40 radar altimeter was used to record terrain clearance. The antenna was mounted beneath the bubble of the helicopter cockpit.

2.4.5 Airborne Gamma Ray Spectrometer

The Airborne gamma ray spectrometer utilized for the survey was an RSI ARGS RSX-5 (Radiation Solutions Inc. Airborne Gamma Ray Spectrometer 500), mounted on the interior floor of the helicopter cabin. A temperature and barometric pressure sensor is located on the outside of the helicopter and connected to the auxiliary port of the detector unit. The RSX-5 is equipped with four, 4.2 litre (1024cu in.) downward looking Nal (Sodium Iodide) crystals and one 4.2 litre (256cu in.) upward looking Nal crystal. The resolution of the crystals is <8.5%, with 1024 channels at a sampling interval of 1 second. Temperature and barometric pressure are also acquired at an interval of 1 second.

The gamma ray spectrometer data are acquired and stored in the internal memory of the RSX-5. Once the survey is completed the acquired data can then download onto a USB drive from the RSX-5 detector pack. The RSX-5 maintains the measured total counts, potassium, equivalent Thorium, and equivalent Uranium as counts per second in its internal memory. During the survey RadAssist Software (Radiation solutions Inc., 2008) is utilized by Geotech data acquisition system and displayed on the LCD screen. This allows the operator to monitor the integrity of the RSX-5 detector pack to ensure it is running properly.

2.4.6 GPS Navigation System

The navigation system used was a Geotech PC104 based navigation system utilizing a NovAtel's CDGPS (Canada-Wide Differential Global Positioning System Correction Service) enabled Propak V3-RT20 GPS receiver. Geotech's Navigation software, using a full screen display with controls in front of the pilot, allows him to direct the flight. A NovAtel GPS antenna is mounted on the helicopter tail (Figure 6). As many as 14 GPS and two CDGPS satellites may be monitored at any one time. The positional accuracy or circular error probability (CEP) is 1.8 m, with CDGPS active, it is 0.6 m. The co-ordinates of the blocks were set-up prior to the survey and the information was fed into the airborne navigation system.

2.4.7 Digital Acquisition System

A Geotech data acquisition system recorded the digital survey data on an internal compact flash card. Data is displayed on an LCD screen as traces to allow the operator to monitor the integrity of the system. The data type and sampling interval as provided in Table 4.

Table 4 - Acquisition Sampling Rates

DATA TYPE	SAMPLING
TDEM	0.1 sec
Magnetometer	0.1 sec
GPS Position	0.2 sec
Spectrometer	1 sec
Pressure and Temperature	1 sec
Radar Altimeter	0.2 sec

2.4.8 Base Station

A combined magnetometer/GPS base station was utilized on this project. A Geometrics Caesium vapour magnetometer was used as a magnetic sensor with a sensitivity of 0.001 nT. The base station was recording the magnetic field together with the GPS time at 1 Hz on a base station computer.

The base station magnetometer sensor was installed where the crew was housed, on the north-west side of the Timber Camp (47° 56’ 2270" N, 82° 34’ 4104" W), away from electric transmission lines and moving ferrous objects such as motor vehicles. The base station data were backed-up to the data processing computer at the end of each survey day.

3. PERSONNEL

The following Geotech Ltd. personnel were involved in the project.

Field:

Project Managers:	Lee Harper (Office)
Data QC/QA:	Neil Fiset (Office)
Crew chief:	Robert Rus
Operator:	Robert Rus

The survey pilot and the mechanical engineer were employed directly by the helicopter operator – Geotech Ltd. / Gateway Helicopters Inc.

Pilots:	Bruno Prieur
Mechanical Engineer:	Igor Tsirkot Alexander Prikhodko

Office:

Data QA/QC:	Neil Fiset
EM & Magnetic data processing:	Marta Orta
Spectrometric data processing:	Alexander Prikhodko
Final data QA/QC:	Neil Fiset
Interpretation notes:	Marta Orta
Mapping / Reporting:	Wendy Acorn

Data acquisition phase was carried out under the supervision of Andrei Bagrianski, P. Geo, Surveys Manager. Processing phase was carried out under the supervision of Jean Legault, P. Geo, Manager of Processing and Interpretation. The overall contract management and customer relations were by Quentin Yarie.

4. DATA PROCESSING AND PRESENTATION

Data compilation and processing were carried out by the application of Geosoft OASIS Montaj and programs proprietary to Geotech Ltd.

4.1 Flight Path

The flight path, recorded by the acquisition program as WGS 84 latitude/longitude, was converted into the NAD83 Datum, UTM Zone 17 North coordinate system in Oasis Montaj.

The flight path was drawn using linear interpolation between X,Y positions from the navigation system. Positions are updated every second and expressed as UTM easting's (x) and UTM northing's (y).

4.2 Electromagnetic Data

A three stage digital filtering process was used to reject major sferic events and to reduce system noise. Local sferic activity can produce sharp, large amplitude events that cannot be removed by conventional filtering procedures. Smoothing or stacking will reduce their amplitude but leave a broader residual response that can be confused with geological phenomena. To avoid this possibility, a computer algorithm searches out and rejects the major sferic events. The filter used was a 16 point non-linear filter.

The signal to noise ratio was further improved by the application of a low pass linear digital filter. This filter has zero phase shift which prevents any lag or peak displacement from occurring, and it suppresses only variations with a wavelength less than about 1 second or 15 metres. This filter is a symmetrical 1 sec linear filter.

The results are presented as stacked profiles of EM voltages for the time gates, in linear - logarithmic scale for both B-field and dB/dt response in the Z component and dB/dt response in the X component. The early dB/dt time channel recorded at 0.339 milliseconds after the termination of the impulse is also presented as contour colour image.

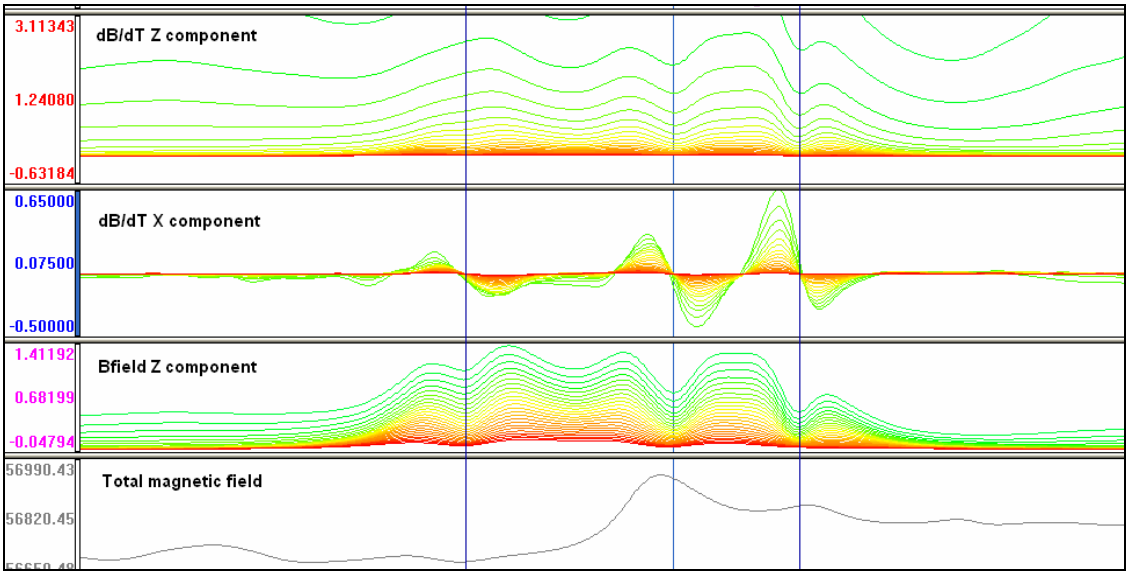

Figure 7 - VTEM X Component data

Graphical representations of the VTEM transmitter current waveform and output voltage of the receiver coil are shown in Appendix C.

Generalized modeling results of VTEM data, written by consultant Roger Barlow and Nasreddine Bournas, P. Geo., are shown in Appendix E.

An explanation of the EM time constant (Tau) calculation is provided in Appendix F.

4.2.1 VTEM X Component Polarity

VTEM X component data do not exhibit maxima or minima above conductors; in fact they produce cross-over type anomalies. The crossover polarity sign convention for VTEM X component polarity is according to the right hand rule for multi-component transient electromagnetic methods.

For the north-south lines at the Dore and Heenan blocks the sign convention for the X in-line component crossover is positive-negative pointing south to north for tabular conductor's perpendicular to the profile (Figure 8). Similarly, for the southeast – northwest lines of the Denyes-Swayze block, the X Component polarity is positive to negative pointing NW to SE. X component data for alternating/opposite flight directions have been reversed (multiplied by negative one) in the final database to account for this polarity convention.

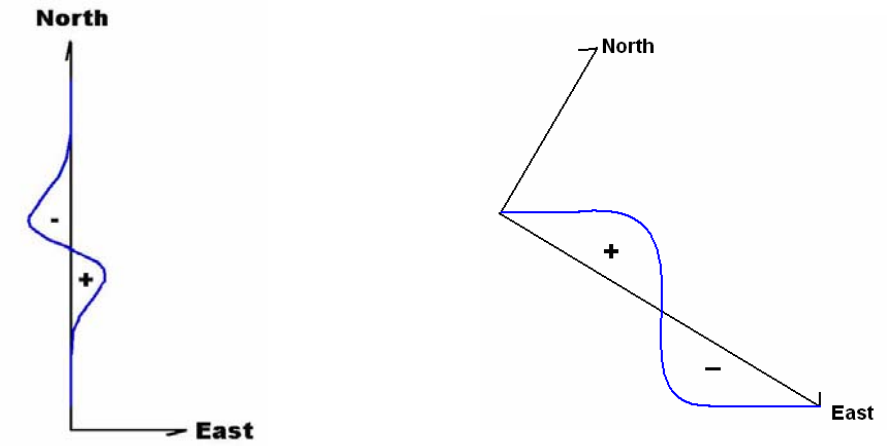

Figure 8 - VTEM X Component Polarity Convention for the Dore and Heenan blocks (left) and Denyes-Swayze block (right).

4.3 Electromagnetic Anomaly selection

The EM data were subjected to an anomaly recognition process using all time domain geophysical channels and using both the B-Field and dB/dt profiles. However, based on the low conductance detected through the survey area, the dB/dt was relied upon for the EM anomaly selection and analysis process. The resulting EM anomaly picks are presented as overlays on all maps.

Each individual conductor pick is represented by an anomaly symbol classified according to calculated conductance[3]. Identified anomalies were classified into one of five categories (Figure 9). The anomaly symbol is accompanied by postings denoting the calculated dB/dt conductance, calculated dB/dt decay constant (Tau)[4], and the dip direction for all dipping thin-plates[5]. Each symbol is also given an identification letter label, unique to each flight line. The anomaly symbol legend is given below.

[3]Note: Conductance values were obtained from the dB/dt EM time constant (Tau) whose relationship was calculated using Maxwell forward modeling algorithm (EMIT Technology Ltd. Pty. Midland, WA, AU). The conductance model utilized was for a vertical tabular plate, with horizontal dimensions of 10 x 100 metres by 1000 metres vertical (N. Bournas, Geotech Ltd., pers. comm.., 09/2008).

[4] Note: An explanation of the EM time constant (Tau) approach to VTEM data is provided in Appendix F.

[5] Note: For vertically dipping thin plates (i.e., producing symmetric double peak anomalies – see Appendix E) and prism-like (single peak anomaly), a dip direction was assigned.

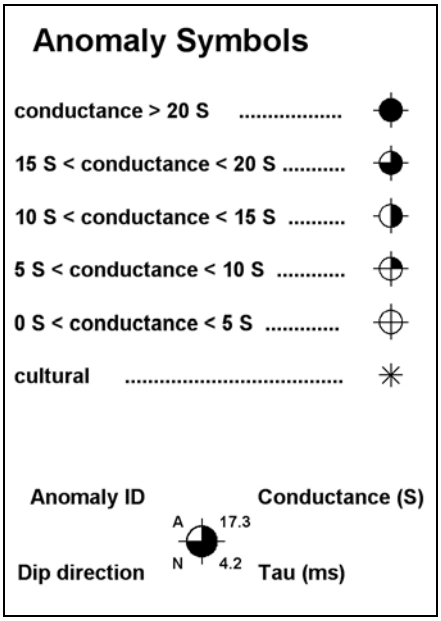

Figure 9 - EM Anomaly Symbols

EM anomaly symbols are presented in all final maps, i.e. VTEM profiles, total magnetic intensity and spectrometric grids. The anomalous responses have been picked on each line, reviewed and edited by the interpreter on a line by line basis to discriminate between bedrock, overburden and culture conductors. The VTEM anomalies and calculated parameters have been created in XYZ format for each block as per table 7. The identified time domain electromagnetic VTEM anomalies are listed in Appendix G.

4.4 Magnetic Data

The processing of the magnetic data involved the correction for diurnal variations by using the digitally recorded ground base station magnetic values. The base station magnetometer data was edited and merged into the Geosoft GDB database on a daily basis. The aeromagnetic data was corrected for diurnal variations by subtracting the observed magnetic base station deviations.

Tie line levelling was carried out by adjusting intersection points along traverse lines. A micro-levelling procedure was applied to remove persistent low-amplitude components of flight-line noise remaining in the data.

The corrected magnetic data was interpolated between survey lines using a random point gridding method to yield x-y grid values for a standard grid cell size of approximately 0.25 cm at the mapping scale. The Minimum Curvature algorithm was used to interpolate values onto a rectangular regular spaced grid.

The magnetic derivative analysis was obtained using algorithms developed inside the Geosoft Magmap ^{TM} platform. This FFT-based analysis is performed directly onto the Geosoft grids or the final corrected total magnetic intensity data.

4.5 Gamma-ray Spectrometer Data

The processing of the spectrometric data involved the transformation of the spectra into energy windows, corrections for aircraft and cosmic background, radon background correction, stripping corrections, height reducing to standard atmosphere using measured barometric pressure and temperature and to nominal height. The applied corrections were based on calibrations made before and during survey. The results of these calibrations and tests can be found on the digital archive.

Micro levelling procedures were applied to the data to remove minor residual noises.

The spectrometric data were processed and saved in a separate Geosoft GDB database because of different sampling rates to the VTEM-magnetic data. Table 6 presents the database channels for the processed gamma-ray spectrometer data.

5. DELIVERABLES

5.1 Survey Report

The survey report describes the data acquisition, processing, and final presentation of the survey results. The survey report is provided in two paper copies and digitally in PDF format.

5.2 Maps

Final maps were produced at scale of 1:10,000. The coordinate/projection system used was NAD 83, UTM Zone 17 North. All maps show the flight path trace and topographic data; latitude and longitude are also noted on maps. Mineral claims, provided by the Ontario Ministry of Northern Development and Mines, are also presented on each map.

The preliminary and final results of the survey are presented as EM profiles, an early-time gate gridded EM channel, color magnetic TMI and various spectrometer contour maps. The following maps are presented on paper;

- VTEM B-field profiles, Time Gates 0.234 – 6.578 ms in linear - logarithmic scale over total magnetic intensity colour image and EM anomalies.
- VTEM dB/dt profiles, Time Gates 0.234 – 6.578 ms in linear – logarithmic scale and EM anomalies.
- VTEM dB/dt Time Gate 0.339 ms colour image and contours, and EM anomalies.
- Total magnetic intensity (TMI) colour image and contours, and EM anomalies.
- Tilt Derivative of TMI
- Calculated Time Constant (Tau) for B-Field and dB/dt with EM anomalies
- Gamma-ray Spectrometer Potassium, equivalent Uranium and equivalent Thorium total counts colour image and contours, and EM anomalies.
- Gamma-ray Spectrometer Potassium levels colour image and contours, and EM anomalies.
- Gamma-ray Spectrometer equivalent Uranium levels colour image and contours, and EM anomalies.
- Gamma-ray Spectrometer equivalent Thorium levels colour image and contours, and EM anomalies.
- Gamma-ray Spectrometer equivalent Thorium / Potassium ratio colour image and contours, and EM anomalies.

5.3 Digital Data

- Two copies of the data and maps on DVD were prepared to accompany the report. Each DVD contains a digital file of the line data in Geosoft Oasis Montaj GDB format as well as the maps in Geosoft Oasis Montaj MAP and PDF format.

- DVD structure.

  There are two (2) main directories;

  Data contains databases, grids and maps, as described below.

  Report contains a copy of the report and appendices in PDF format.

  Databases in Geosoft GDB format, containing the channels listed in Table 5.

Table 5 - Geosoft GDB Data Format.

Channel name	Units	Description
X:	metres	NAD83 / UTM zone 17N
Y:	metres	NAD83 / UTM zone 17N
Z:	metres	GPS antenna elevation (ASL)
Lat:	Decimal Degrees	NAD 83 Latitude data
Lon:	Decimal Degrees	NAD 83 Longitude data
Gtime1:	Seconds of the day	GPS time
Date:	yyyy/mm/dd	Flight data
FltNo:		Flight number
Radar:	metres	helicopter terrain clearance from radar altimeter
Radarb:	metres	EM bird terrain clearance from radar altimeter
DEM:	metres	Digital Elevation Model
BaseMag:	nT	Magnetic diurnal variation data
Mag1:	nT	Raw Total Magnetic field data
Mag2:	nT	Lag and Diurnal corrected Total Magnetic field data
Mag3:	nT	Leveled Total Magnetic field data
SFz[10]:	pV/(A*m^4)	Z dB/dt 120 microsecond time channel
SFz[11]:	pV/(A*m^4)	Z dB/dt 141 microsecond time channel
SFz[12]:	pV/(A*m^4)	Z dB/dt 167 microsecond time channel
SFz[13]:	pV/(A*m^4)	Z dB/dt 198 microsecond time channel
SFz[14]:	pV/(A*m^4)	Z dB/dt 234 microsecond time channel
SFz[15]:	pV/(A*m^4)	Z dB/dt 281 microsecond time channel
SFz[16]:	pV/(A*m^4)	Z dB/dt 339 microsecond time channel
SFz[17]:	pV/(A*m^4)	Z dB/dt 406 microsecond time channel
SFz[18]:	pV/(A*m^4)	Z dB/dt 484 microsecond time channel
SFz[19]:	pV/(A*m^4)	Z dB/dt 573 microsecond time channel
SFz[20]:	pV/(A*m^4)	Z dB/dt 682 microsecond time channel
SFz[21]:	pV/(A*m^4)	Z dB/dt 818 microsecond time channel
SFz[22]:	pV/(A*m^4)	Z dB/dt 974 microsecond time channel
SFz[23]:	pV/(A*m^4)	Z dB/dt 1151 microsecond time channel
SFz[24]:	pV/(A*m^4)	Z dB/dt 1370 microsecond time channel
SFz[25]:	pV/(A*m^4)	Z dB/dt 1641 microsecond time channel
SFz[26]:	pV/(A*m^4)	Z dB/dt 1953 microsecond time channel
SFz[27]:	pV/(A*m^4)	Z dB/dt 2307 microsecond time channel
SFz[28]:	pV/(A*m^4)	Z dB/dt 2745 microsecond time channel
SFz[29]:	pV/(A*m^4)	Z dB/dt 3286 microsecond time channel
SFz[30]:	pV/(A*m^4)	Z dB/dt 3911 microsecond time channel
SFz[31]:	pV/(A*m^4)	Z dB/dt 4620 microsecond time channel
SFz[32]:	pV/(A*m^4)	Z dB/dt 5495 microsecond time channel
SFz[33]:	pV/(A*m^4)	Z dB/dt 6578 microsecond time channel

Channel name	Units	Description
BFz[10]:	(pV*ms)/(A*m^4)	Z B-field 120 microsecond time channel
BFz[11]:	(pV*ms)/(A*m^4)	Z B-field 141 microsecond time channel
BFz[12]:	(pV*ms)/(A*m^4)	Z B-field 167 microsecond time channel
BFz[13]:	(pV*ms)/(A*m^4)	Z B-field 198 microsecond time channel
BFz[14]:	(pV*ms)/(A*m^4)	Z B-field 234 microsecond time channel
BFz[15]:	(pV*ms)/(A*m^4)	Z B-field 281 microsecond time channel
BFz[16]:	(pV*ms)/(A*m^4)	Z B-field 339 microsecond time channel
BFz[17]:	(pV*ms)/(A*m^4)	Z B-field 406 microsecond time channel
BFz[18]:	(pV*ms)/(A*m^4)	Z B-field 484 microsecond time channel
BFz[19]:	(pV*ms)/(A*m^4)	Z B-field 573 microsecond time channel
BFz[20]:	(pV*ms)/(A*m^4)	Z B-field 682 microsecond time channel
BFz[21]:	(pV*ms)/(A*m^4)	Z B-field 818 microsecond time channel
BFz[22]:	(pV*ms)/(A*m^4)	Z B-field 974 microsecond time channel
BFz[23]:	(pV*ms)/(A*m^4)	Z B-field 1151 microsecond time channel
BFz[24]:	(pV*ms)/(A*m^4)	Z B-field 1370 microsecond time channel
BFz[25]:	(pV*ms)/(A*m^4)	Z B-field 1641 microsecond time channel
BFz[26]:	(pV*ms)/(A*m^4)	Z B-field 1953 microsecond time channel
BFz[27]:	(pV*ms)/(A*m^4)	Z B-field 2307 microsecond time channel
BFz[28]:	(pV*ms)/(A*m^4)	Z B-field 2745 microsecond time channel
BFz[29]:	(pV*ms)/(A*m^4)	Z B-field 3286 microsecond time channel
BFz[30]:	(pV*ms)/(A*m^4)	Z B-field 3911 microsecond time channel
BFz[31]:	(pV*ms)/(A*m^4)	Z B-field 4620 microsecond time channel
BFz[32]:	(pV*ms)/(A*m^4)	Z B-field 5495 microsecond time channel
BFz[33]:	(pV*ms)/(A*m^4)	Z B-field 6578 microsecond time channel
SFx[10]:	pV/(A*m^4)	X dB/dt 120 microsecond time channel
SFx[11]:	pV/(A*m^4)	X dB/dt 141 microsecond time channel
SFx[12]:	pV/(A*m^4)	X dB/dt 167 microsecond time channel
SFx[13]:	pV/(A*m^4)	X dB/dt 198 microsecond time channel
SFx[14]:	pV/(A*m^4)	X dB/dt 234 microsecond time channel
SFx[15]:	pV/(A*m^4)	X dB/dt 281 microsecond time channel
SFx[16]:	pV/(A*m^4)	X dB/dt 339 microsecond time channel
SFx[17]:	pV/(A*m^4)	X dB/dt 406 microsecond time channel
SFx[18]:	pV/(A*m^4)	X dB/dt 484 microsecond time channel
SFx[19]:	pV/(A*m^4)	X dB/dt 573 microsecond time channel
SFx[20]:	pV/(A*m^4)	X dB/dt 682 microsecond time channel
SFx[21]:	pV/(A*m^4)	X dB/dt 818 microsecond time channel
SFx[22]:	pV/(A*m^4)	X dB/dt 974 microsecond time channel
SFx[23]:	pV/(A*m^4)	X dB/dt 1151 microsecond time channel
SFx[24]:	pV/(A*m^4)	X dB/dt 1370 microsecond time channel
SFx[25]:	pV/(A*m^4)	X dB/dt 1641 microsecond time channel
SFx[26]:	pV/(A*m^4)	X dB/dt 1953 microsecond time channel
SFx[27]:	pV/(A*m^4)	X dB/dt 2307 microsecond time channel
SFx[28]:	pV/(A*m^4)	X dB/dt 2745 microsecond time channel
SFx[29]:	pV/(A*m^4)	X dB/dt 3286 microsecond time channel
SFx[30]:	pV/(A*m^4)	X dB/dt 3911 microsecond time channel
SFx[31]:	pV/(A*m^4)	X dB/dt 4620 microsecond time channel
SFx[32]:	pV/(A*m^4)	X dB/dt 5495 microsecond time channel
SFx[33]:	pV/(A*m^4)	X dB/dt 6578 microsecond time channel
BFx[10]:	(pV*ms)/(A*m^4)	X B-field 120 microsecond time channel
BFx[11]:	(pV*ms)/(A*m^4)	X B-field 141 microsecond time channel

Channel name	Units	Description
BFx[12]:	(pV*ms)/(A*m^4)	X B-field 167 microsecond time channel
BFx[13]:	(pV*ms)/(A*m^4)	X B-field 198 microsecond time channel
BFx[14]:	(pV*ms)/(A*m^4)	X B-field 234 microsecond time channel
BFx[15]:	(pV*ms)/(A*m^4)	X B-field 281 microsecond time channel
BFx[16]:	(pV*ms)/(A*m^4)	X B-field 339 microsecond time channel
BFx[17]:	(pV*ms)/(A*m^4)	X B-field 406 microsecond time channel
BFx[18]:	(pV*ms)/(A*m^4)	X B-field 484 microsecond time channel
BFx[19]:	(pV*ms)/(A*m^4)	X B-field 573 microsecond time channel
BFx[20]:	(pV*ms)/(A*m^4)	X B-field 682 microsecond time channel
BFx[21]:	(pV*ms)/(A*m^4)	X B-field 818 microsecond time channel
BFx[22]:	(pV*ms)/(A*m^4)	X B-field 974 microsecond time channel
BFx[23]:	(pV*ms)/(A*m^4)	X B-field 1151 microsecond time channel
BFx[24]:	(pV*ms)/(A*m^4)	X B-field 1370 microsecond time channel
BFx[25]:	(pV*ms)/(A*m^4)	X B-field 1641 microsecond time channel
BFx[26]:	(pV*ms)/(A*m^4)	X B-field 1953 microsecond time channel
BFx[27]:	(pV*ms)/(A*m^4)	X B-field 2307 microsecond time channel
BFx[28]:	(pV*ms)/(A*m^4)	X B-field 2745 microsecond time channel
BFx[29]:	(pV*ms)/(A*m^4)	X B-field 3286 microsecond time channel
BFx[30]:	(pV*ms)/(A*m^4)	X B-field 3911 microsecond time channel
BFx[31]:	(pV*ms)/(A*m^4)	X B-field 4620 microsecond time channel
BFx[32]:	(pV*ms)/(A*m^4)	X B-field 5495 microsecond time channel
BFx[33]:	(pV*ms)/(A*m^4)	X B-field 6578 microsecond time channel
SFxc[10]:	pV/(A*m^4)	X dB/dt 120 microsecond time channel direction corrected
SFxc[11]:	pV/(A*m^4)	X dB/dt 141 microsecond time channel direction corrected
SFxc[12]:	pV/(A*m^4)	X dB/dt 167 microsecond time channel direction corrected
SFxc[13]:	pV/(A*m^4)	X dB/dt 198 microsecond time channel direction corrected
SFxc[14]:	pV/(A*m^4)	X dB/dt 234 microsecond time channel direction corrected
SFxc[15]:	pV/(A*m^4)	X dB/dt 281 microsecond time channel direction corrected
SFxc[16]:	pV/(A*m^4)	X dB/dt 339 microsecond time channel direction corrected
SFxc[17]:	pV/(A*m^4)	X dB/dt 406 microsecond time channel direction corrected
SFxc[18]:	pV/(A*m^4)	X dB/dt 484 microsecond time channel direction corrected
SFxc[19]:	pV/(A*m^4)	X dB/dt 573 microsecond time channel direction corrected
SFxc[20]:	pV/(A*m^4)	X dB/dt 682 microsecond time channel direction corrected
SFxc[21]:	pV/(A*m^4)	X dB/dt 818 microsecond time channel direction corrected
SFxc[22]:	pV/(A*m^4)	X dB/dt 974 microsecond time channel direction corrected
SFxc[23]:	pV/(A*m^4)	X dB/dt 1151 microsecond time channel direction corrected
SFxc[24]:	pV/(A*m^4)	X dB/dt 1370 microsecond time channel direction corrected
SFxc[25]:	pV/(A*m^4)	X dB/dt 1641 microsecond time channel direction corrected
SFxc[26]:	pV/(A*m^4)	X dB/dt 1953 microsecond time channel direction corrected
SFxc[27]:	pV/(A*m^4)	X dB/dt 2307 microsecond time channel direction corrected
SFxc[28]:	pV/(A*m^4)	X dB/dt 2745 microsecond time channel direction corrected
SFxc[29]:	pV/(A*m^4)	X dB/dt 3286 microsecond time channel direction corrected
SFxc[30]:	pV/(A*m^4)	X dB/dt 3911 microsecond time channel direction corrected
SFxc[31]:	pV/(A*m^4)	X dB/dt 4620 microsecond time channel direction corrected
SFxc[32]:	pV/(A*m^4)	X dB/dt 5495 microsecond time channel direction corrected
SFxc[33]:	pV/(A*m^4)	X dB/dt 6578 microsecond time channel direction corrected
BFxc[10]:	(pV*ms)/(A*m^4)	X B-field 120 microsecond time channel direction corrected
BFxc[11]:	(pV*ms)/(A*m^4)	X B-field 141 microsecond time channel direction corrected
BFxc[12]:	(pV*ms)/(A*m^4)	X B-field 167 microsecond time channel direction corrected
BFxc[13]:	(pV*ms)/(A*m^4)	X B-field 198 microsecond time channel direction corrected

Channel name	Units	Description
BFxc[14]:	(pV*ms)/(A*m^4)	X B-field 234 microsecond time channel direction corrected
BFxc[15]:	(pV*ms)/(A*m^4)	X B-field 281 microsecond time channel direction corrected
BFxc[16]:	(pV*ms)/(A*m^4)	X B-field 339 microsecond time channel direction corrected
BFxc[17]:	(pV*ms)/(A*m^4)	X B-field 406 microsecond time channel direction corrected
BFxc[18]:	(pV*ms)/(A*m^4)	X B-field 484 microsecond time channel direction corrected
BFxc[19]:	(pV*ms)/(A*m^4)	X B-field 573 microsecond time channel direction corrected
BFxc[20]:	(pV*ms)/(A*m^4)	X B-field 682 microsecond time channel direction corrected
BFxc[21]:	(pV*ms)/(A*m^4)	X B-field 818 microsecond time channel direction corrected
BFxc[22]:	(pV*ms)/(A*m^4)	X B-field 974 microsecond time channel direction corrected
BFxc[23]:	(pV*ms)/(A*m^4)	X B-field 1151 microsecond time channel direction corrected
BFxc[24]:	(pV*ms)/(A*m^4)	X B-field 1370 microsecond time channel direction corrected
BFxc[25]:	(pV*ms)/(A*m^4)	X B-field 1641 microsecond time channel direction corrected
BFxc[26]:	(pV*ms)/(A*m^4)	X B-field 1953 microsecond time channel direction corrected
BFxc[27]:	(pV*ms)/(A*m^4)	X B-field 2307 microsecond time channel direction corrected
BFxc[28]:	(pV*ms)/(A*m^4)	X B-field 2745 microsecond time channel direction corrected
BFxc[29]:	(pV*ms)/(A*m^4)	X B-field 3286 microsecond time channel direction corrected
BFxc[30]:	(pV*ms)/(A*m^4)	X B-field 3911 microsecond time channel direction corrected
BFxc[31]:	(pV*ms)/(A*m^4)	X B-field 4620 microsecond time channel direction corrected
BFxc[32]:	(pV*ms)/(A*m^4)	X B-field 5495 microsecond time channel direction corrected
BFxc[33]:	(pV*ms)/(A*m^4)	X B-field 6578 microsecond time channel direction corrected
TauSF:	ms	Time constant (Tau) calculated from dB/dt data
TauBF:	ms	Time constant (Tau) calculated from B-Field data
PLM:		60 Hz power line monitor

Electromagnetic B-field and dB/dt data is found in array channel format between indexes 10 – 33, as described above.

- Database of the gamma ray spectrometer data in Geosoft GDB format, containing the channels described in Table 6.

Table 6 - Geosoft GDB Spectrometer Data Format.

Channel Name	Description
X:	X positional data (meters – NAD83, UTM zone 17 north)
Y:	Y positional data (meters –NAD83, UTM zone 17 north)
Z:	GPS antenna elevation (meters - ASL)
Longitude	Longitude (decimal degree)
Latiitude	Latitude (decimal degree)
Radar:	Helicopter (SPEC eq) radar Terrain Clearance (meters)
PresF	Barometric Pressure (hPa)
TmprtF	Temperature, Celcius
DEM:	Digital elevation model (meters)
Gtime:	GPS time (seconds of the day)
D_K	uncorrected Potassium Count (counts per sec) Downward looking
D_U	uncorrected Uranium Count (counts per sec) Downward looking
D_Th	uncorrected Thorium Count (counts per sec) Downward looking
D_TC	uncorrected Total Count (counts per sec) Downward looking

Channel Name	Description
D_Cos	uncorrected Cosmic Count (counts per sec) Downward looking
Up_K	uncorrected Potassium Count (counts per sec) Upward looking
Up_U	uncorrected Uranium Count (counts per sec) Upward looking
Up_Th	uncorrected Thorium Count (counts per sec) Upward looking
Up_TC	uncorrected Total Count (counts per sec) Upward looking
Up_Cos	uncorrected Cosmic Count (counts per sec) Upward looking
C_K	Potassium (%)Concentrations (under calibratoin coefficients of the equipment)
C_U	Uranium (ppm) Concentrations (under calibratoin coefficients of the
C_Th	Thorium (ppm) Concentrations (under calibratoin coefficients of the equipment)
Kfin	Corrected Potassium Count (counts per sec)
Ufin	Corrected Uranium count (counts per sec)
Thfin	Corrected Thorium Count (counts per sec)
TCfin	Corrected Total Count (counts per sec)

- Databases of selected anomalies in Geosoft GDB format, contains the channels described in Table 7.

Table 7 - Geosoft database for selected EM anomalies

Channel name	Units	Description
AnomID:		Letter indicating the Anomaly ID
Anom_type:		Anomaly type
X:	metres	NAD83 / UTM zone 17N
Y:	metres	NAD83 / UTM zone 17N
Z:	metres	GPS antenna elevation (ASL)
Radarb:	metres	EM bird terrain clearance from radar altimeter
Conductance:	Siemens	Estimated conductance
TauSF:	milliseconds	Time constant, calculated from dB/dt data
TauBF:	milliseconds	Time constant, calculated from B-Field data
Dipping:		Dip direction
Cultural_effect		“Yes” if the anomaly is affected by cultural components

- Database of the VTEM Waveform “9067_Waveform_final.gdb” in Geosoft GDB format, containing the following channels:

Time: Sampling rate interval, 10.416 microseconds
Rx_Volt: Output voltage of the receiver coil (Volt)
Tx_Curr: Output current of the transmitter (Amp)

- Grids in Geosoft GRD format, as follows:

SFz339_bb:	Z-coil dB/dt Channel 16 (Time Gate 0.339 ms)
TMI_bb:	Total Magnetic Intensity (nT)
Tilt_bbt:	Magnetic Tilt derivative (radians)
TauSF_bb:	dB/dt Calculated Time Constant (Tau)
TauBF_bb:	B-Field Calculated Time Constant (Tau)
Kfin_bb:	Potassium Levels (K)
Ufin_bb:	Equivalent Uranium (eU)
TCfin_bb:	K, eU, and eTh Total Counts
Thfin_bb:	Equivalent Thorium (eTh)
ratioThK_bb :	Thorium / Potassium Ratio

Where bb represents the block name (ie: Kfin_Dore)

A Geosoft .GRD file has a .GI metadata file associated with it, containing grid projection information. A grid cell size of 25 metres was used.

- Maps at 1:10,000 scales in Geosoft MAP format, as follows:

9067_bfield_10K_bb:	B-field Z Component profiles, Time Gates 0.234 – 6.578 ms in linear logarithmic scale, with TMI colour image and EM anomalies.
9067_dbdt_10K_bb:	dB/dt Z Component profiles, Time Gates 0.234 – 6.578 ms in linear logarithmic scale with EM anomalies.
9067_SF339_10K_bb:	VTEM dB/dt Time Gate 0.339 ms colour image and EM anomalies.
9067_TMI_10K_bb:	Total magnetic intensity (TMI) colour image and contours, and EM anomalies.
9067_Tilt_10K_bb:	Tilt Derivative of TMI with EM anomalies.
9067_TauSF_10K _bb:	VTEM dB/dt Z Component Calculated Time Constant with EM anomalies.
9067_X_Coil_10K_bb:	VTEM X Component profiles, Time Gates 0.281 – 1.641 ms in linear logarithmic scale and EM anomalies.
9067_RADTC_10K_bb:	Gamma Ray Spectrometer Potassium, equivalent Uranium and equivalent Thorium total counts colour image and EM anomalies.
9067_RADK_10K_bb:	Gamma Ray Spectrometer Potassium levels colour image and EM anomalies.
9067_RADeU_10K_bb:	Gamma Ray Spectrometer equivalent Uranium levels colour image and EM anomalies.

9067_RADeTh_10K_bb: Gamma Ray Spectrometer equivalent Thorium levels colour image and EM anomalies.
9067_RADeThK_10K_bb:Gamma Ray Spectrometer equivalent Thorium / Potassium ratio colour image and EM anomalies.

Where bb represents the block name (ie: 9067_TMI_10K_Dore.map)

Maps are also presented in PDF format.

1:50,000 topographic vectors were taken from the NRCAN Geogratis database at; http://geogratis.gc.ca/geogratis/en/index.html.

- Google Earth files *9067_RedPine.kml* showing the flight path of the block. Free versions of Google Earth software from: http://earth.google.com/download-earth.html

6. PRELIMINARY INTERPRETATION

6.1 EM Analysis

Several groups of EM anomalies favourable for gold mineralization are identified in the three blocks of study, as shown in Figure 10 below.

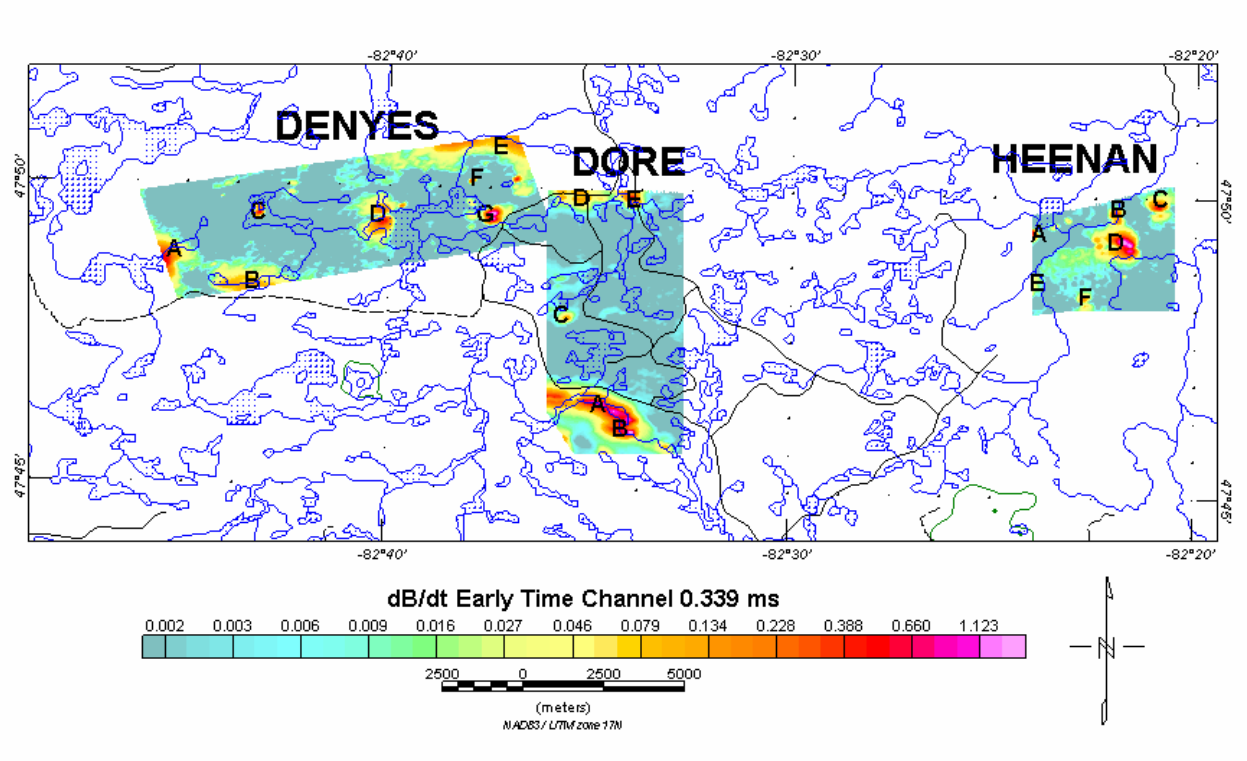

Figure 10 - Groups of EM anomalies in the blocks of study

Low values of conductance are detected in the area of study. Hence, the EM analysis is based on the early time response. Figure 10 shows the dB/dt early time 0.339 ms image for the Denyes-Swayze, Dore and Heenan blocks.

Detailed comments on each block are found in the following sections.

6.1.1 EM Anomalies of Interest – Denyes-Swayze Block

Seven groups of anomalies from A to G are identified in the Denyes-Swayze block as shown in Figure 10 above.

Figure 11 presents the EM time-constant (Tau) image generated from the early time dB/dt response (0.234 to 0.484 millisecond after the end of the impulse). EM anomaly symbols are also shown for better definition of the relatively small values of conductance detected in the survey area.

The EM time-constant (Tau) results were generated using Geotech's proprietary software on the dB/dt and B-field data from the Z-coil response. The "sliding Tau" method (see Appendix F for calculation details), stopped at the early time gate of 0.484 ms after the end of the impulse (index 18 in the EM array), suggesting that no highly conductive targets are present in the survey area.

Denyes-Swayze block shows the lowest values of conductance (Sec. 4.2) in the survey area, varying from 0.5 to 8 Siemens.

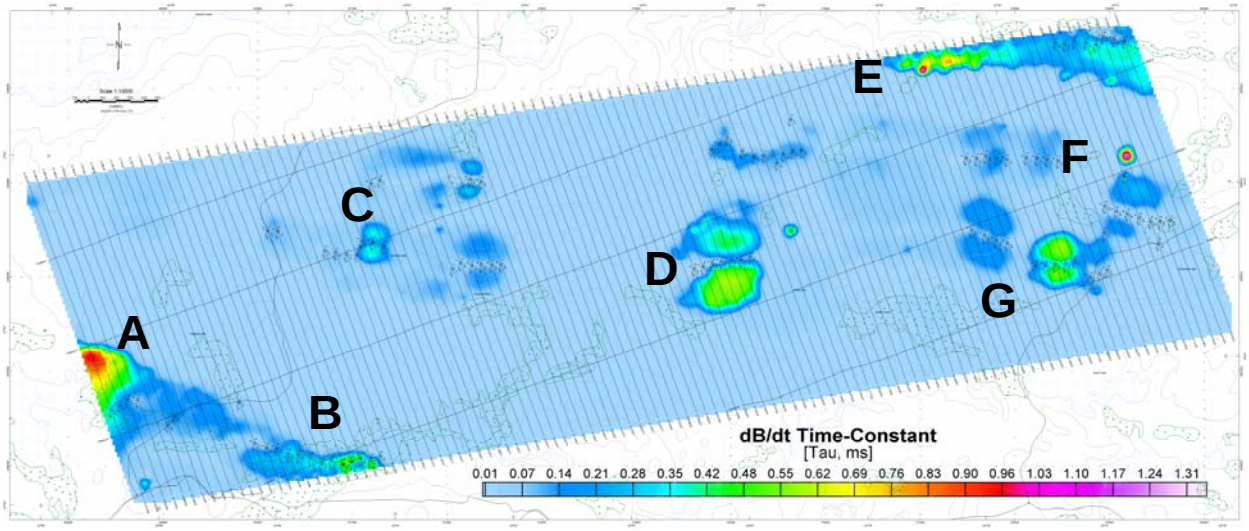

Figure 11 – Tau (dB/dt, Z-coil) image and EM anomaly symbols of Denyes-Swayze block.

Anomaly F, at the east end of Denyes-Swayze Block, is selected for further analysis. It is detected from Line 1950 to L2040, with visible signal in B-Field and dB/dt data until the beginning of the late times.

Its response indicates a plate-shape model, with dip direction varying from north to south in both the east and the west part of the anomaly. Weaker signal is detected on L2000.

Figure 12 shows the Anomaly F on the dB/dt Z-coil early time channel 0.339ms image. The east-west trend of this target, hosted by mafic to intermediate metavolcanic rocks, could be favorable for a gold-quartz vein, typical of gold deposit around the Timmins area (Dubé and Gosselin, 2007)[6].

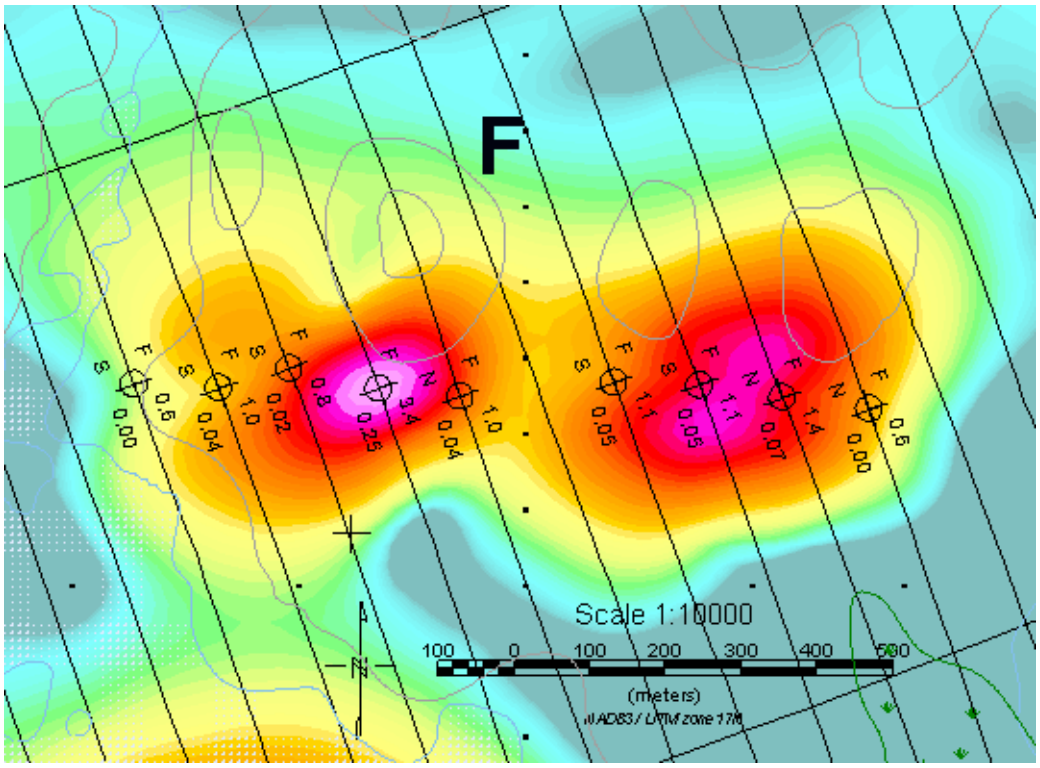

Figure 12 - dB/dt Z-coil 0.339ms image of Anomaly F, Denyes-Swayze block

[6] Dubé, B., and Gosselin, P., 2007, Greenstone-hosted quartz-carbonate vein deposits, in Goodfellow, W.D., ed., Mineral Deposits of Canada: A Synthesis of Major Deposit-Types, District Metallogeny, the Evolution of Geological Provinces, and Exploration Methods: Geological Association of Canada, Mineral Deposits Division, Special Publication No. 5, p. 49-73.

6.1.2 EM Anomalies of Interest – Dore Block

Five groups of anomalies are identified in Dore block, named from A to E, as shown previously in Figure 10. Their estimated conductance (see section 4.3) varies from 0.5 to 21 Siemens.

Figure 13 presents the EM time-constant (Tau) image generated from the early time dB/dt Z-coil response with EM anomaly symbols.

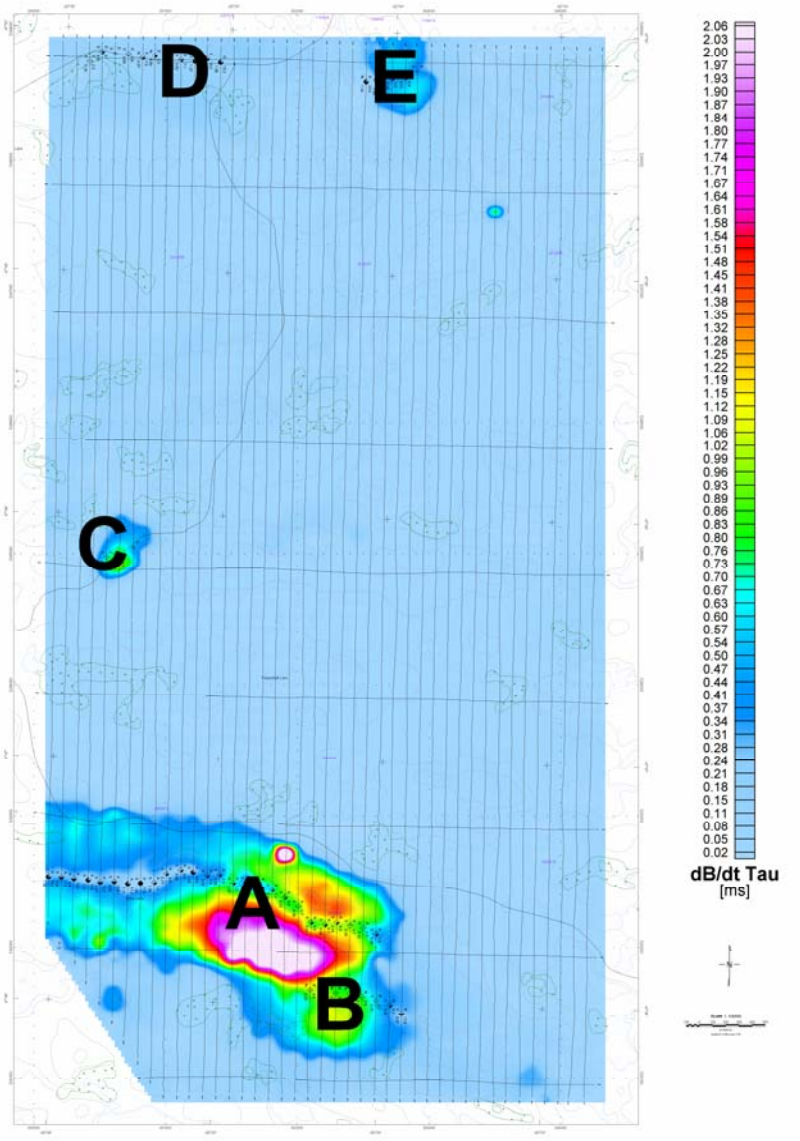

Figure 13 - Tau (dB/dt, Z-coil) image and EM anomalies over Dore block

Anomaly A and B, located in the southern part of the block on Bayly Lake and Wakami River, are selected for further discussion.

Anomaly A is detected from Line 3000 to L3270, including tie line T3570. Its signal is visible in B-Field and dB/dt data until the late time 1.953ms recorded after the end of the impulse. A consistent response from dB/dt data indicates a thin plate model with dip direction to the south, confirmed by its corresponding cross-over in the X-coil response (see section 4.2.1). Highest values of conductance are observed in the west part of anomaly A, as shown in Figure 13.

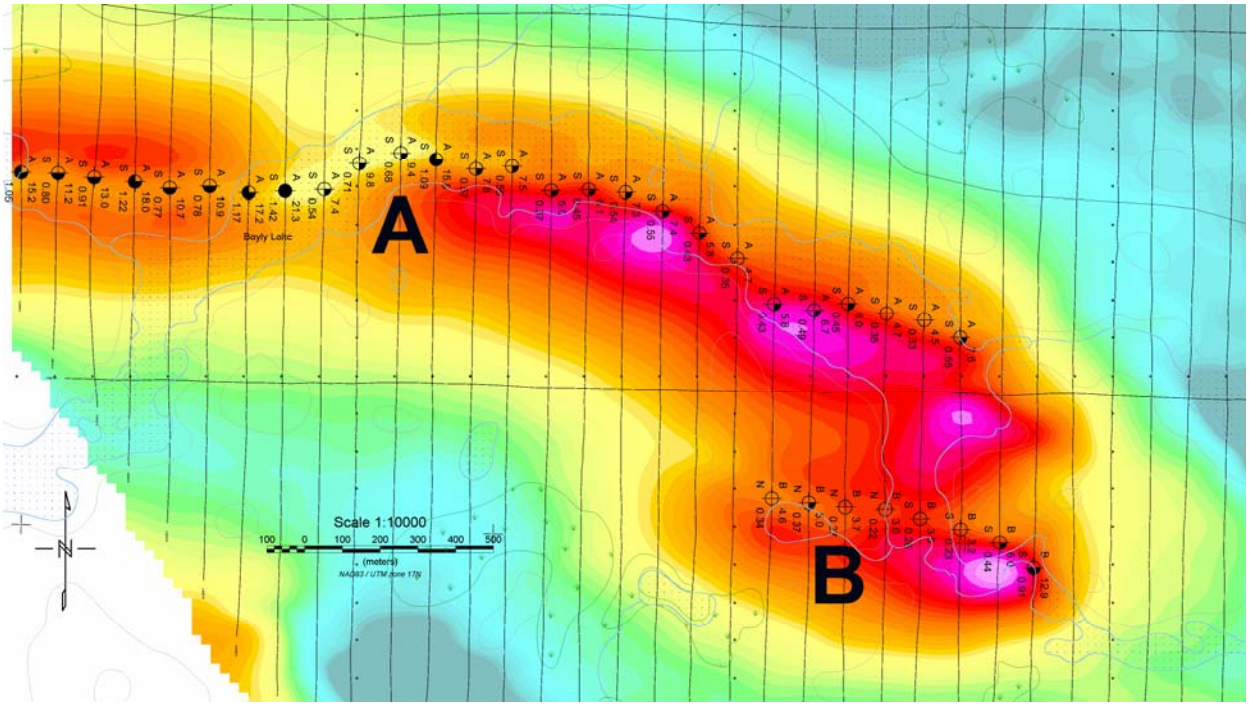

Figure 14 – dB/dt Z-coil 0.339ms image of EM anomalies A & B, Dore block.

Figure 14 shows the EM anomaly symbols of the group of anomalies A and B over the dB/dt Z-coil early time channel 0.339ms image.

Anomaly B, extends for more than 600 meters along strike, is detected from line L3200 to 3270. Its response also corresponds to a thin plate model, changing dip direction from the south (east part) to the north (west part).

With regard to cultural components, care should be taken when interpreting Anomaly D (see Figure 10), since a road is being detected along this group of anomalies.

6.1.3 EM Anomalies of Interest – Heenan Block

Six groups of anomalies from A to F are identified in the Heenan block, as shown previously in Figure 10. Moderate values of conductance (see section 4.3 for conductance calculation) vary from 0.5 to 11 Siemens.

Figure 15 shows the EM time-constant (Tau) image generated from the early timesdB/dt Z-coil response with EM anomaly symbols.

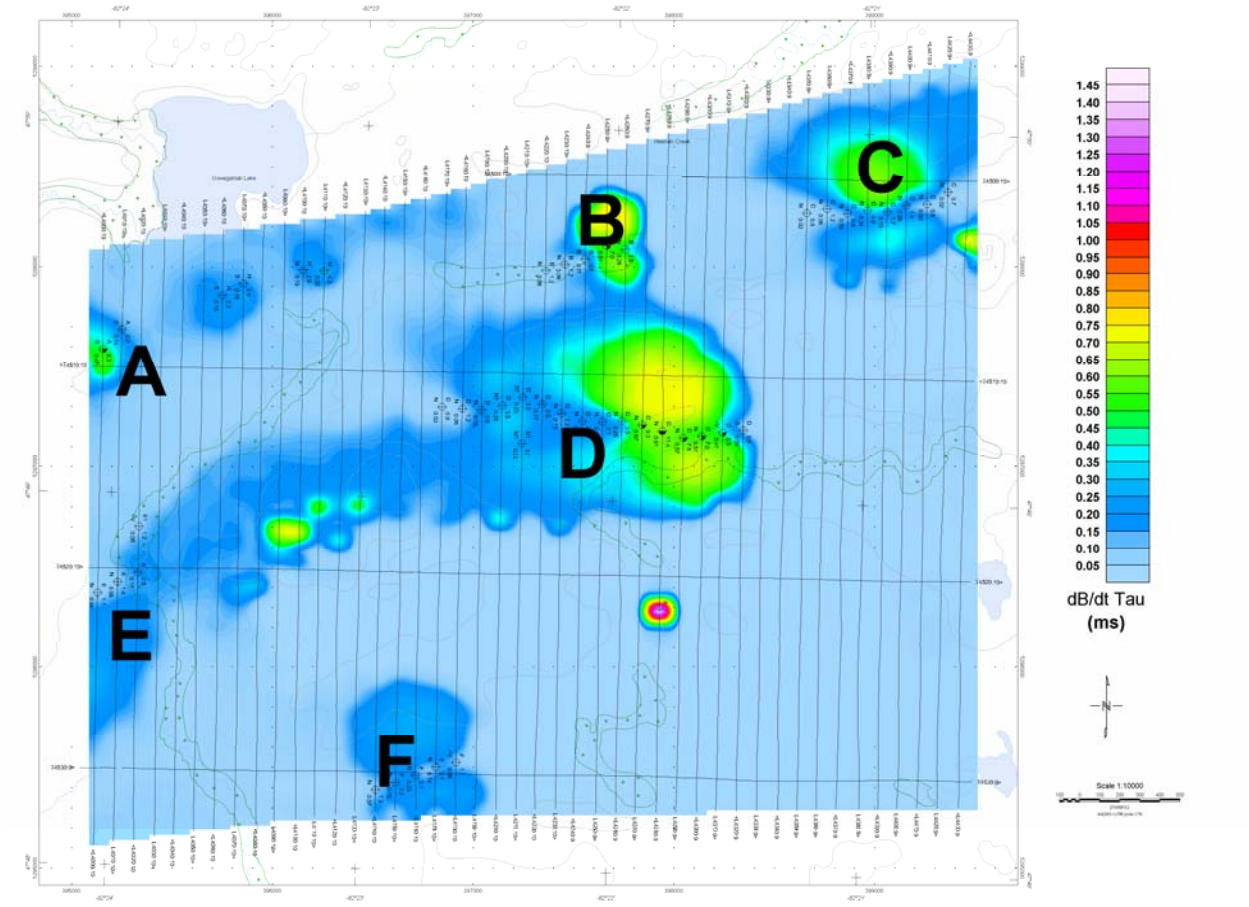

Figure 15 - Tau (dB/dt, Z-coil) and EM anomalies over Heenan block

6.2 Magnetic Data Analysis

The survey area is located in a magnetic region with moderate to strong amplitude variations, of between 56,215 to 58,709 nT.

Variably magnetic trends are observed, as shown in Figure 16 that presents the Total Magnetic Intensity (TMI) image of the three blocks of study. The shading effect in this presentation allows better identification the structures (dikes, faults, contacts) at a large scale. Groups of selected EM anomalies are also presented.

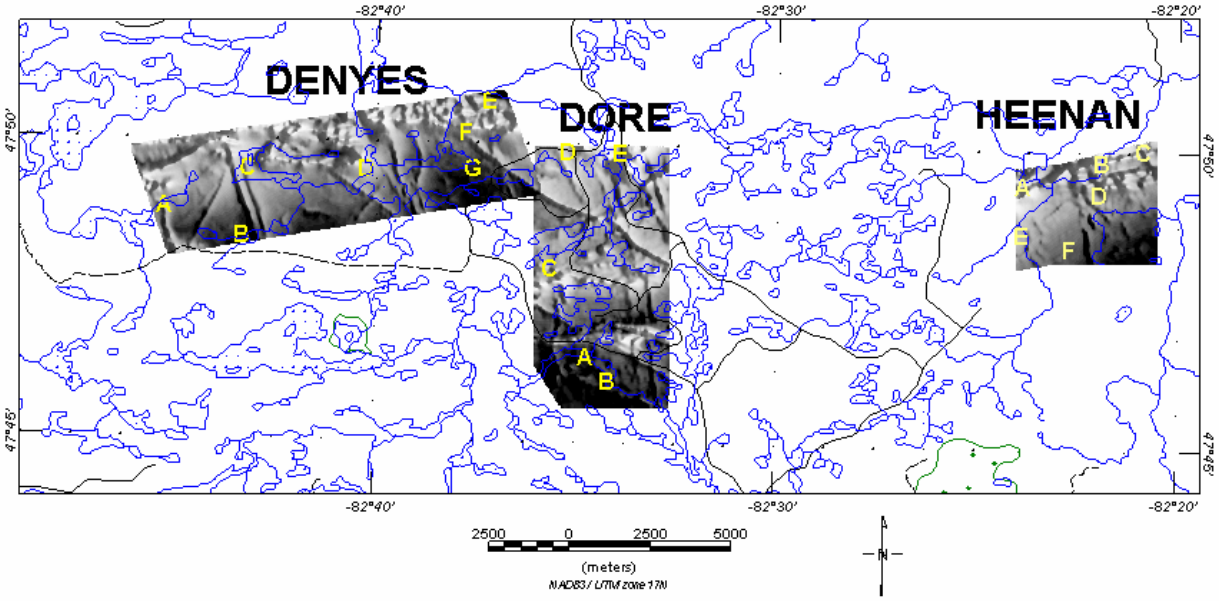

Figure 16 - Grey-shadow image of Total Magnetic Intensity (TMI) of the survey area with EM anomalies.

Detailed comments for each block are found in the following sections.

6.2.1 Magnetic data analysis – Denyes-Swayze Block

Figure 17 shows a Total Magnetic Intensity (TMI) colour-shadow image with EM anomaly symbols of this block. Average value of 56,848 nT with variations of 311 nT are observed in the Denyes-Swayze block.

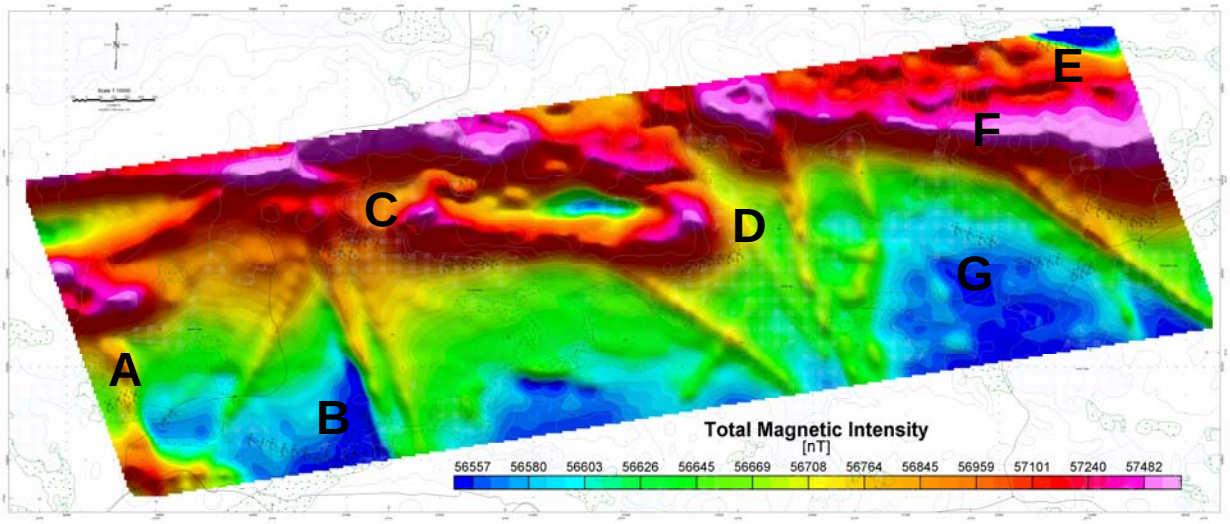

Figure 17 - Total Magnetic Intensity (TMI) for Denyes-Swayze block and EM anomalies

Higher magnetic values are observed in the central to the northern part of the block. Lower amplitude is observed toward the south, south-east and the north-east corner of Denyes-Swayze block.

Several orders of faults at varied direction and depth are detected along the block. More details are observed in the Tilt derivative described in next section.

6.2.1.1 Magnetic Tilt Derivative – Denyes-Swayze block

The Tilt derivative is useful for mapping shallow basement structures and mineral exploration targets (Verduzco et al., 2004)[7].

As shown in Figure 18, the magnetic Tilt derivative image highlights the structural formations of Denyes block. Selected EM anomaly groups are also presented to verify correlation.

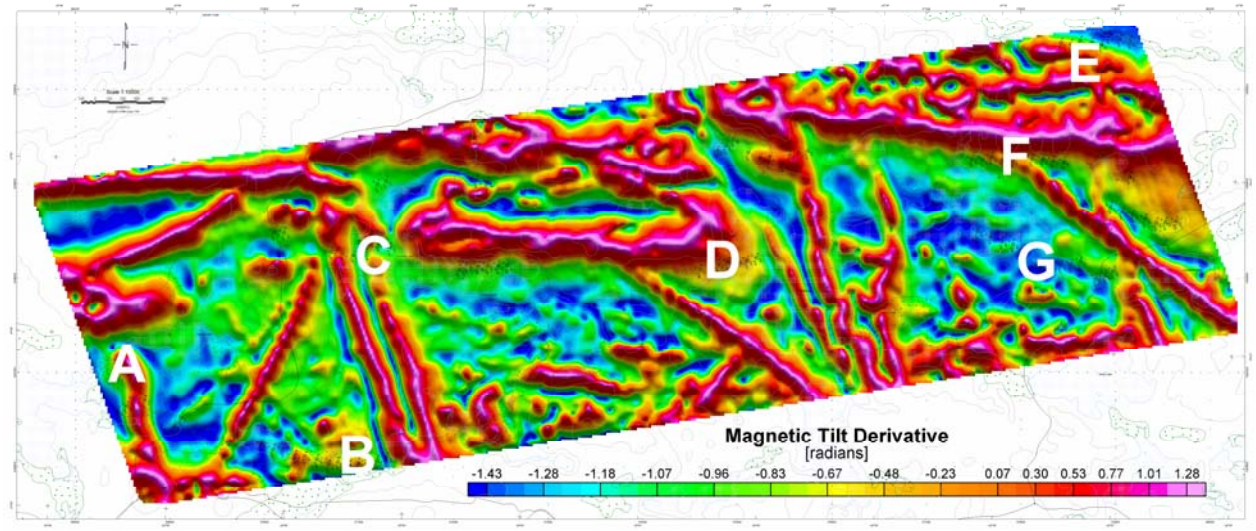

Figure 18 - Magnetic Tilt derivative for Denyes-Swayer block with EM anomalies

As seen in Figure 18, several faults and dikes are observed along the block, favorable to gold-quartz veins that typically occur near major compression faults and are usually localized along associated second-order faults (Dubé and Gosselin, 2007)[6]. It confirms what was discussed for anomaly F (see section 6.1.1), and possibly anomaly C.

Low magnetics detected on Anomaly G, while hosted by metavolcanic rocks, could indicate alteration favorable for gold mineralization.

[7] Verduzco, B. et al., 2004, "New insights into magnetic derivatives for structural mapping", The Leading Edge, v. 23, p. 116-119.

6.2.2 Magnetic data analysis – Dore Block

The Dore block exhibits a magnetic background average of 56,574 nT with weaker variations of 124 nT. Figure 19 shows a Total Magnetic Intensity (TMI) colour-shadow image with EM anomaly symbols of this block.

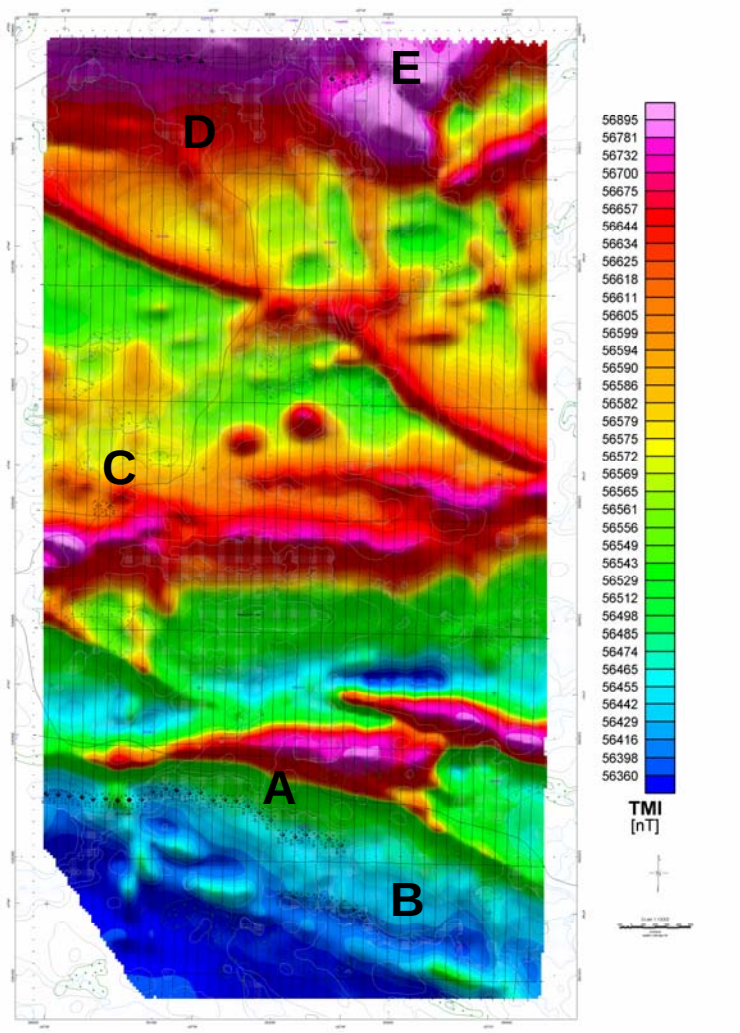

Figure 19 - Total Magnetic Intensity (TMI) over Dore block

Low values of magnetic amplitude are found toward the southern part of the block, favorable for the group of anomalies A and B.

6.2.2.1 Magnetic Tilt Derivative – Dore block

Figure 20 shows the magnetic Tilt derivative image highlighting the structural formations over Dore block. Selected EM anomalies are also presented to verify correlation.

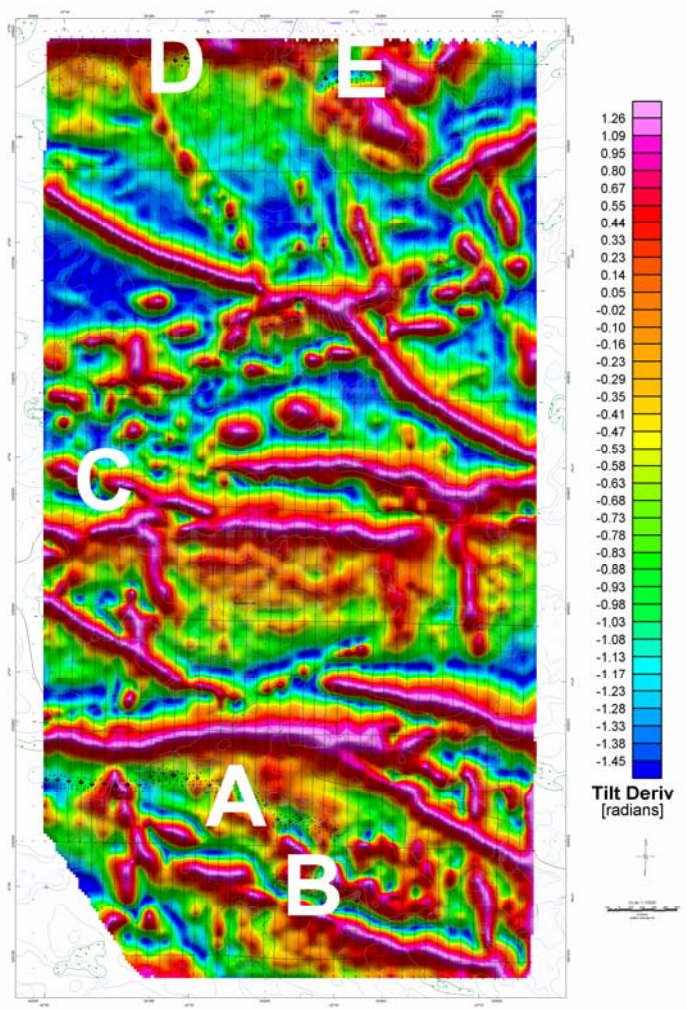

Figure 20 - Magnetic Tilt derivative of Dore block with EM anomalies

6.2.3 Magnetic data analysis – Heenan Block

Figure 21 shows a Total Magnetic Intensity (TMI) colour-shadow image with EM anomaly symbols of the Heenan block. Average value of 56,593 nT with variations of 273 nT are observed in this block.

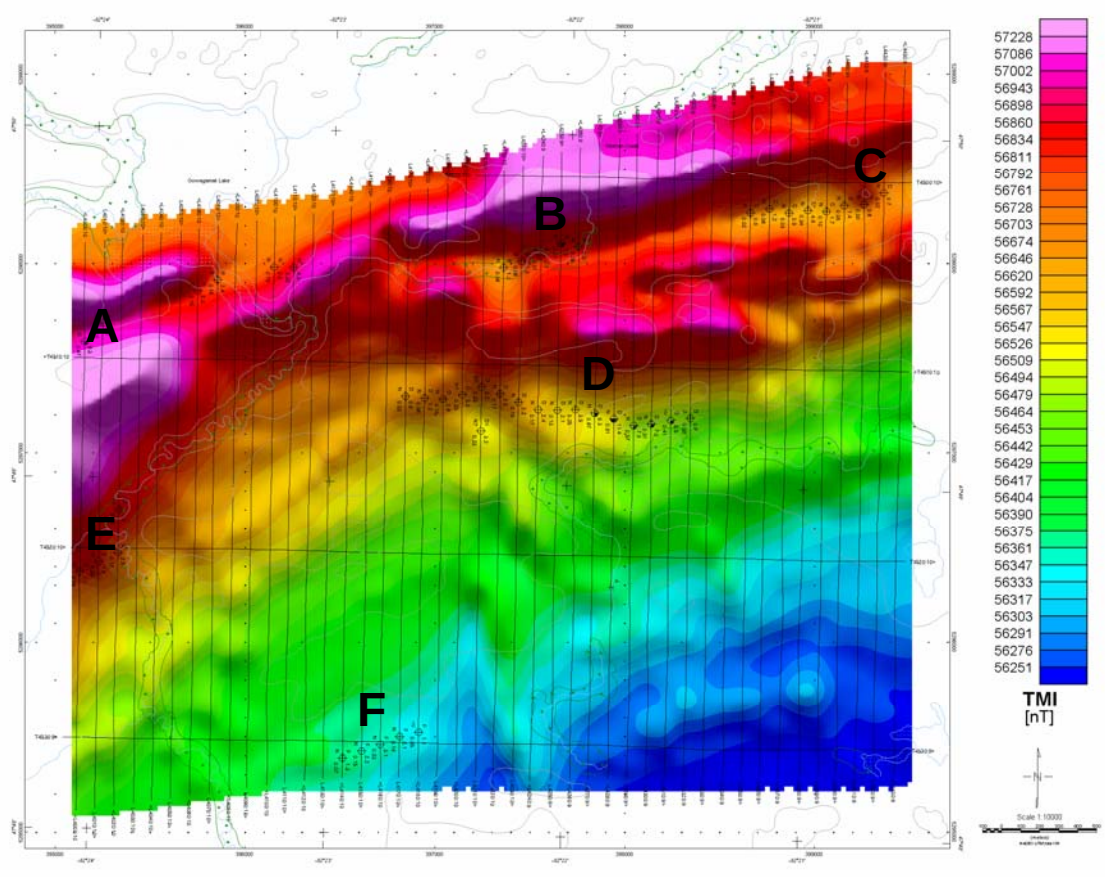

Figure 21 - Total Magnetic Intensity (TMI) for Heenan block

An east–west trend is observed in the total magnetic field, with some visible fault formation in different directions. Highest magnetic values are observed in the northern part of the block, with the lowest in the south-eastern corner of the block.

6.2.3.1 Magnetic Tilt Derivative – Heenan block

As shown in Figure 22, the magnetic Tilt derivative image highlights the structural formations of the Heenan block. Selected EM anomaly groups are also presented to verify correlation.

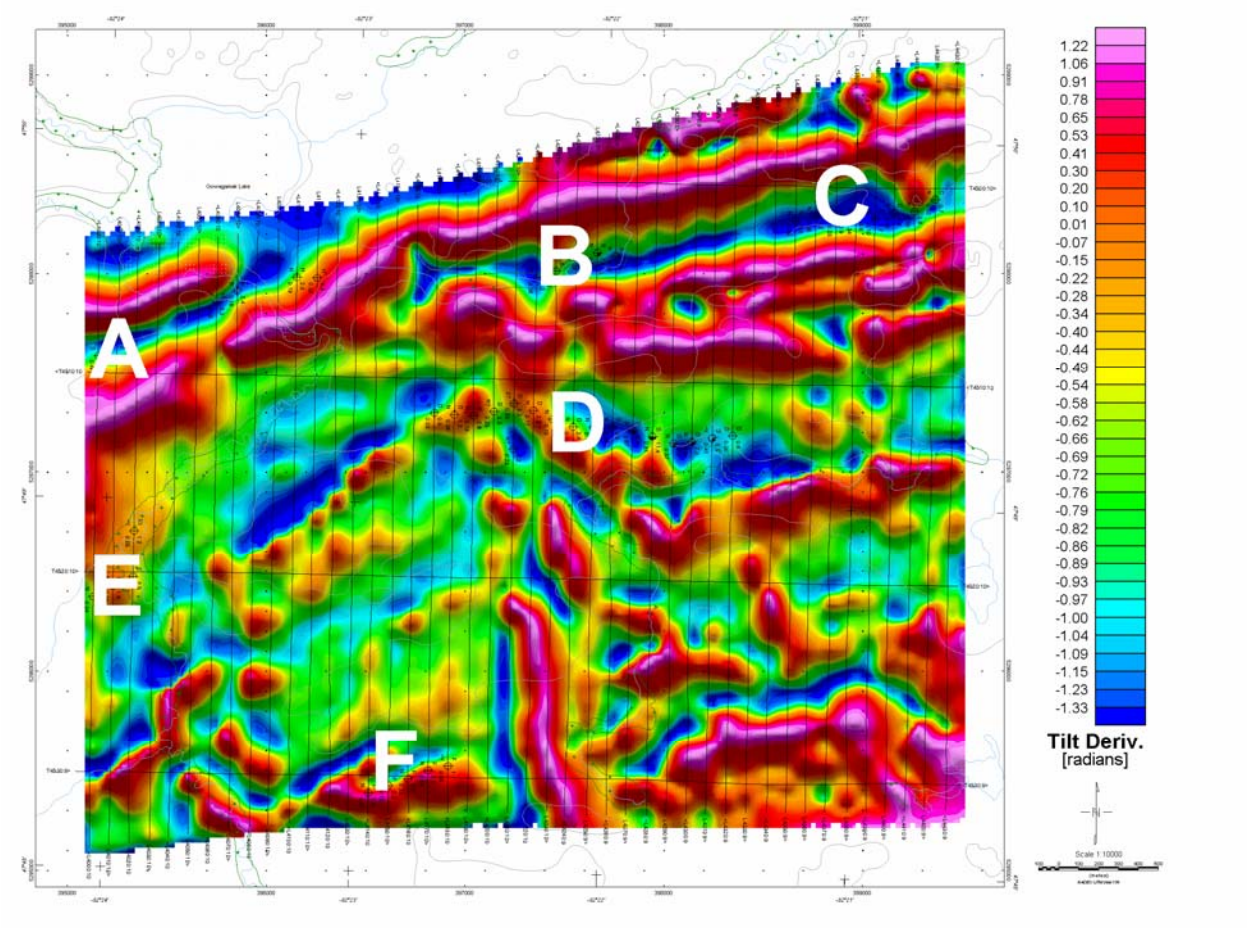

Figure 22 - Magnetic Tilt derivative for Heenan block with EM anomalies

Identified groups of anomalies appear to be located near or intersecting faults of major to medium order, making these targets for gold mineralization, as previously mentioned (Dubé and Gosselin, 2007)[6]

6.3 Gamma-ray Spectrometric Data Analysis

Analysis of gamma-ray spectrometric data focuses on high values of Potassium (K) as an indicator of alteration associated with gold mineralization (Shives et al., 1995)[8].

Care should be taken over water related topographic features such as lakes, rivers, including swamps areas, where gamma-ray spectrometry does not apply.

Figure 23 shows the K image of the survey area with the identified groups of EM anomalies to verify their correlation.

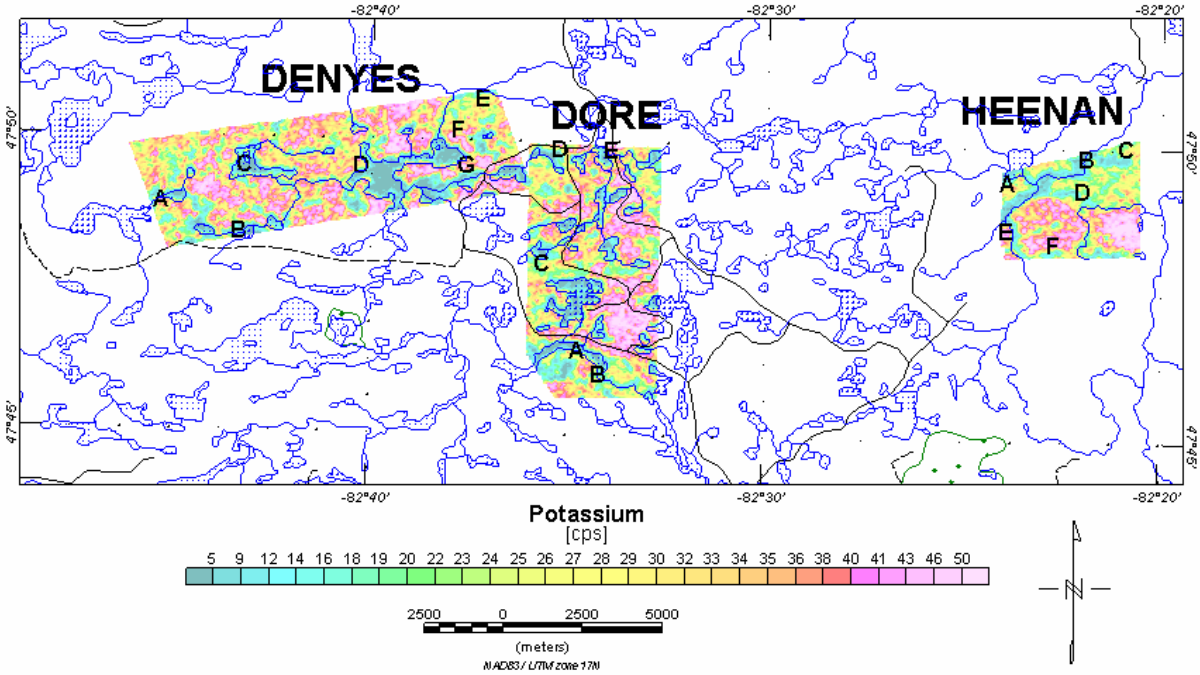

Figure 23 - Potassium image of the survey area with groups of EM anomalies

Where the anomaly is not located over water, high values of K and corresponding low Th/K ratio values are favourable indications of alteration associated with gold mineralization (Shives et al., 1995)[8].

The gamma ray spectrometer analysis for Denyes, Dore and Heenan blocks are further discussed in Appendix H.

[8] Shives, R.B.K., Ford, K.L., and Charbonneau, B.W., 1995, Applications of Gamma-Ray Spectrometric/Magnetic/VLF-EM Surveys – Workshop Manual: Geological Survey of Canada, Open File 3061, 82 p.

7. CONCLUSIONS AND RECOMMENDATIONS

7.1 Conclusions

A helicopter-borne versatile time domain electromagnetic (VTEM) geophysical survey has been completed over the Denyes-Swayze, Dore and Heenan blocks in the province of Ontario, Canada.

The total area coverage is 87.5 km^2. Total survey line coverage is 955 line kilometres. The principal sensors included a Time Domain EM system, a magnetometer and a gamma-ray spectrometer. Results have been presented as stacked profiles and contour colour images at a scale of 1:10,000.

A brief interpretation summary accompanies the report. It supports the EM anomaly picks, EM Time-constant (Tau) analysis as well as magnetic and gamma-ray spectrometric analysis that were performed.

7.2 Recommendations

Based on the geophysical results obtained, a number of EM anomalies of interest were identified across the survey area. The magnetic and gamma-ray spectrometric results also contain worthwhile information in support of exploration targets of interest.

We therefore recommend a detailed interpretation of the available geophysical, in conjunction with the known geology and in close scrutiny for cultural components, prior to ground follow-up and drill testing.

Respectfully submitted[9],

Wendy Acorn
Geotech Ltd.

Jean Legault, P. Geo, P. Eng
Geotech Ltd.

Marta Orta
Geotech Ltd.

Alex Prikhodko, PhD. P.Geo
Geotech Ltd.

July, 2009

APPENDIX A

[9]Note: Final data processing and interpretation of the EM and magnetic data were carried out by Marta Orta; gamma-ray spectrometric data was carried out by Alexander Prikhodko, from the office of Geotech Ltd. in Aurora, Ontario, under the supervision of Jean Legault, P. Geo, Manager of Data Processing and Interpretation.

SURVEY BLOCK LOCATION MAP

Google Earth Location Map of the Blocks

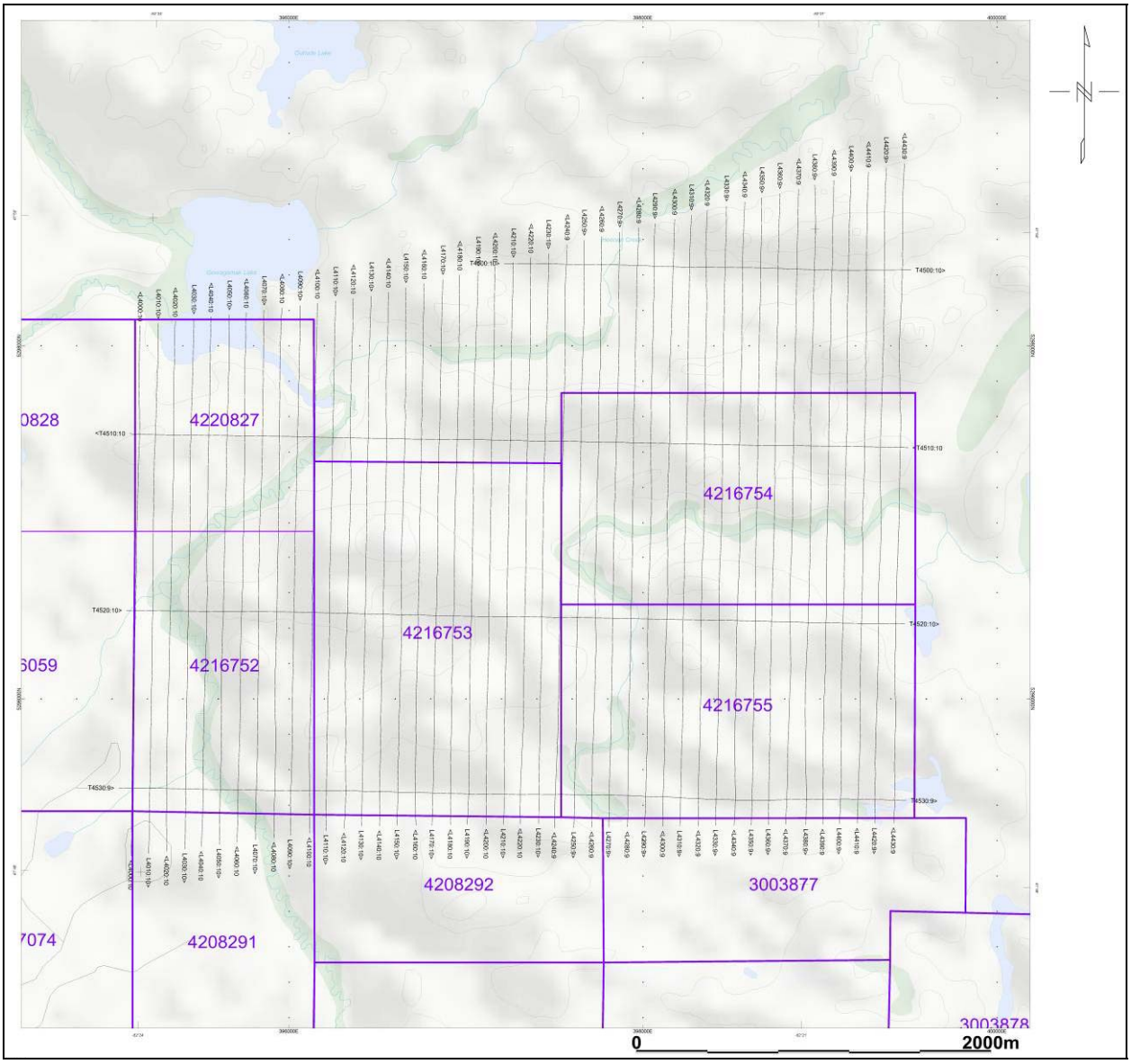

Mining Claims for Heenan Block

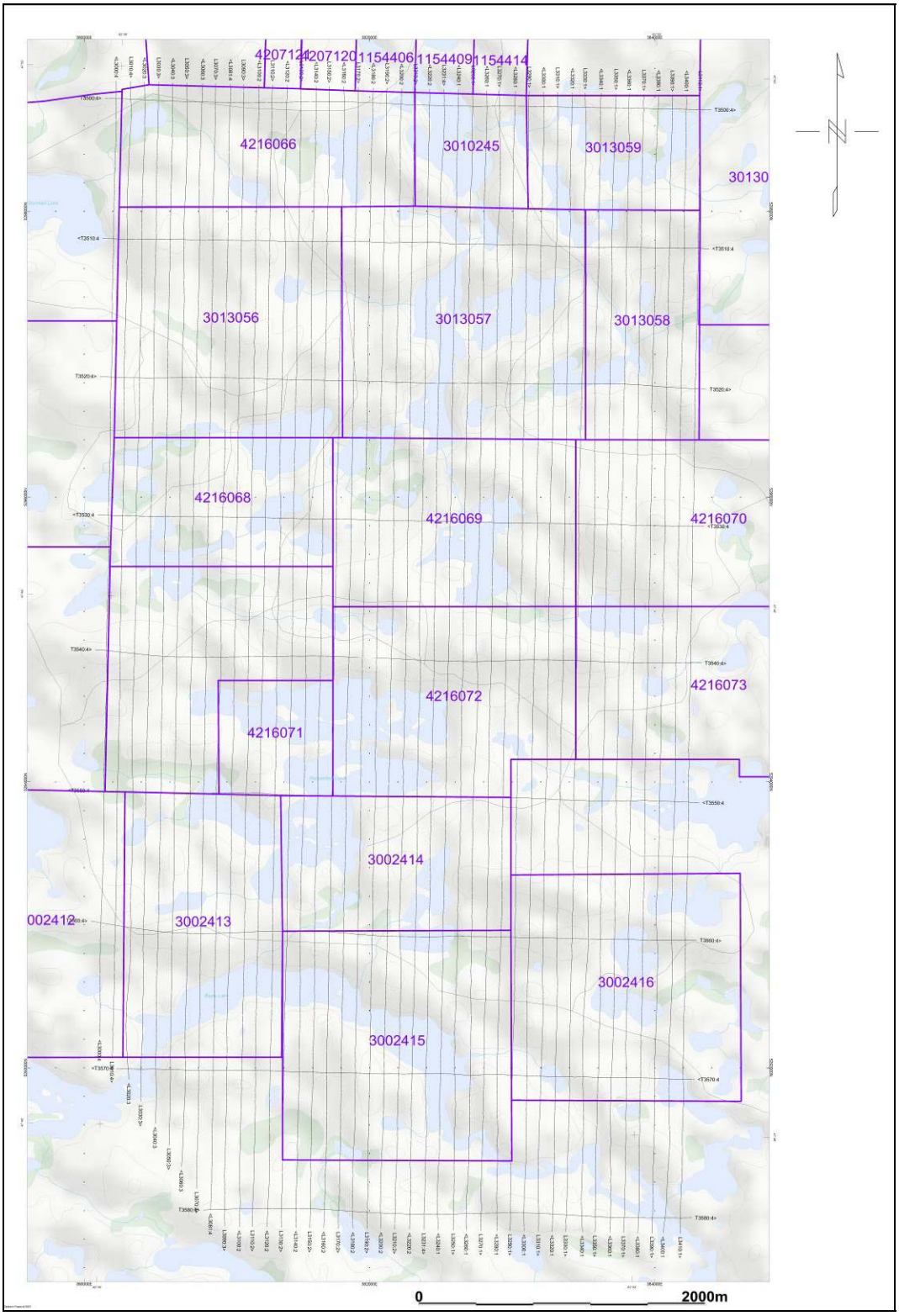

Mining Claims for Dore Block

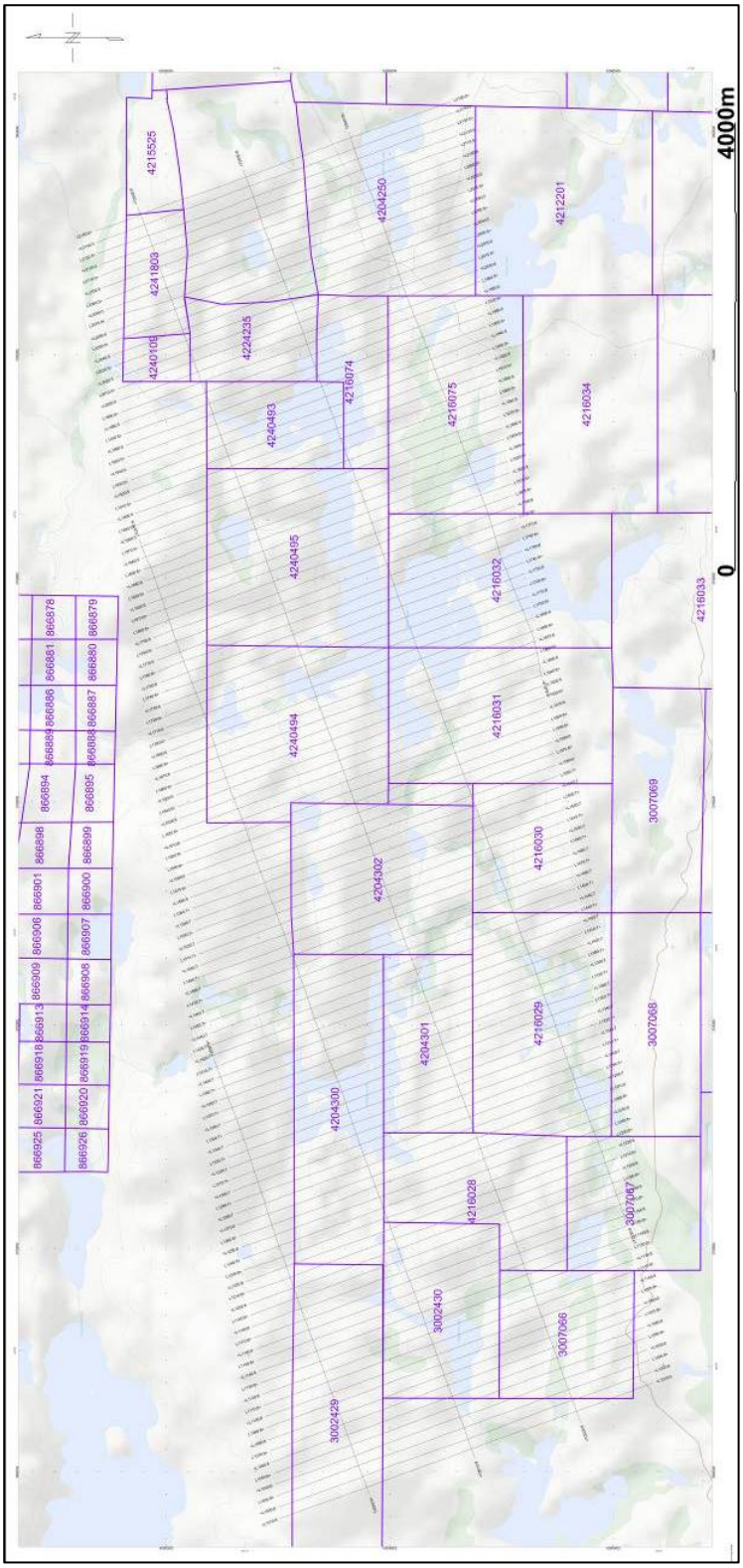

Mining Claims for Denyes-Swayze Block

APPENDIX B

SURVEY BLOCK COORDINATES

(WGS84, UTM Zone 17 North)

Denyes-Swayze Block

X	Y
368457	5299171
373966	5299068
373992	5298010
376997	5298023
377010	5295726
368418	5295662

Dore Block

X	Y
380208	5298887
384332	5298784
384260	5290863
380958	5290914
380106	5292243

Heenan Block

X	Y
395140	5297961
399543	5299022
399422	5295323
395109	5295263

APPENDIX C

VTEM WAVEFORM

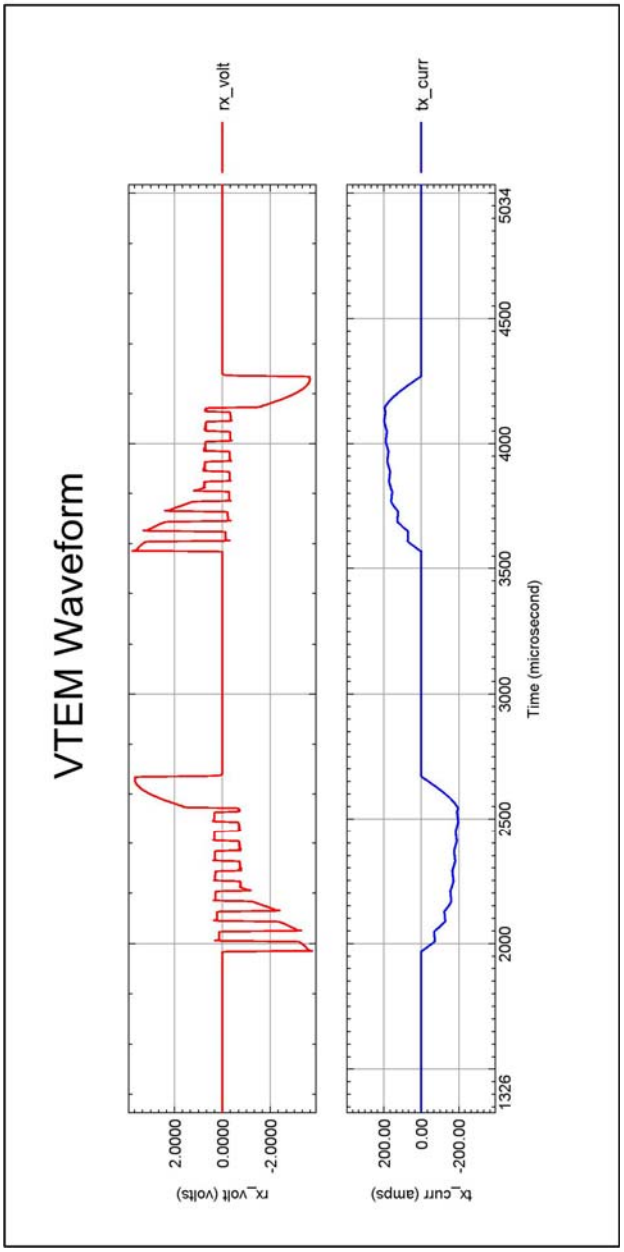

APPENDIX D

GEOPHYSICAL MAPS [1]

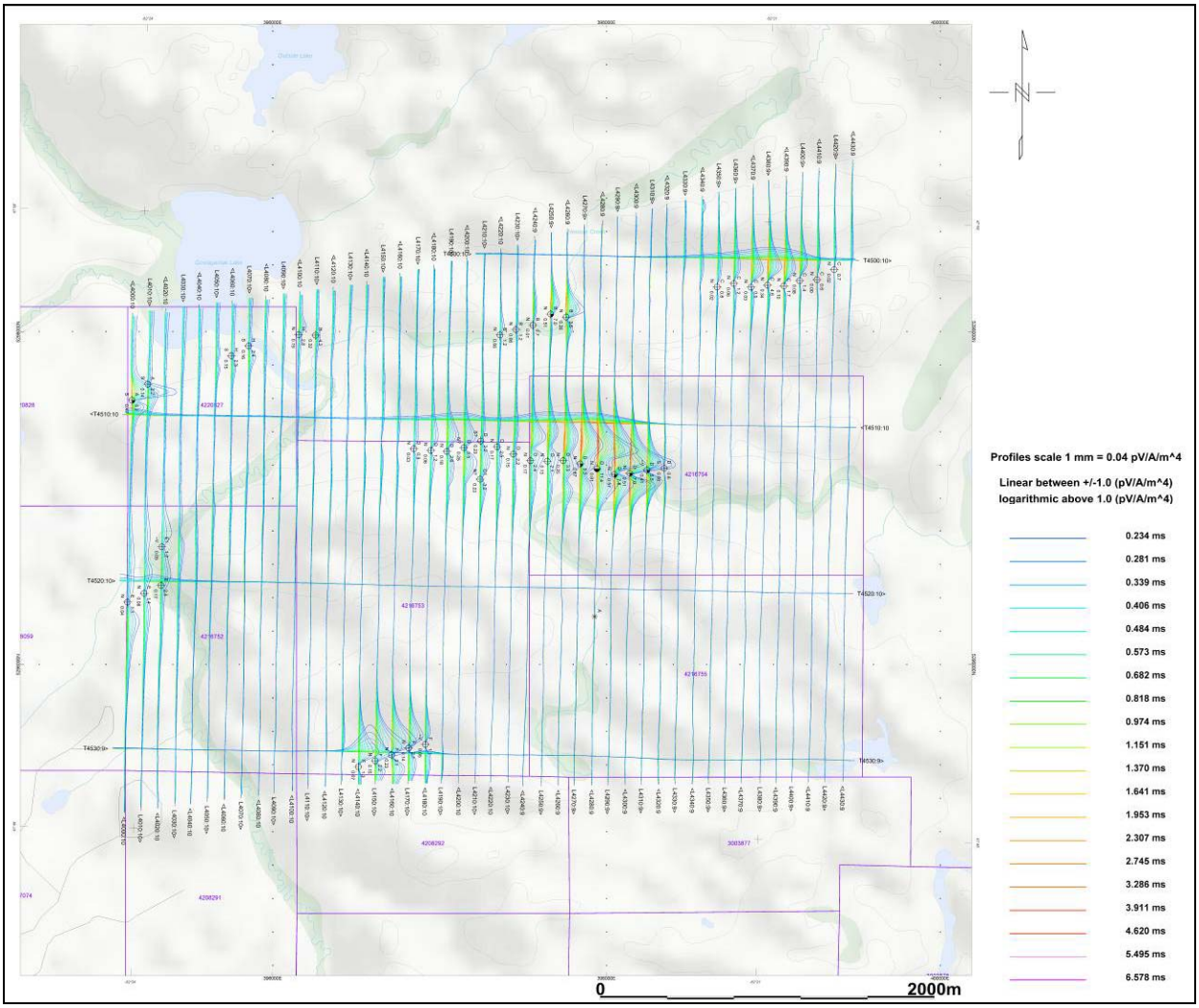

Heenan Block - VTEM dB/dt Profiles with EM anomalies

[1] Full size geophysical maps are also available in PDF format on the final DVD

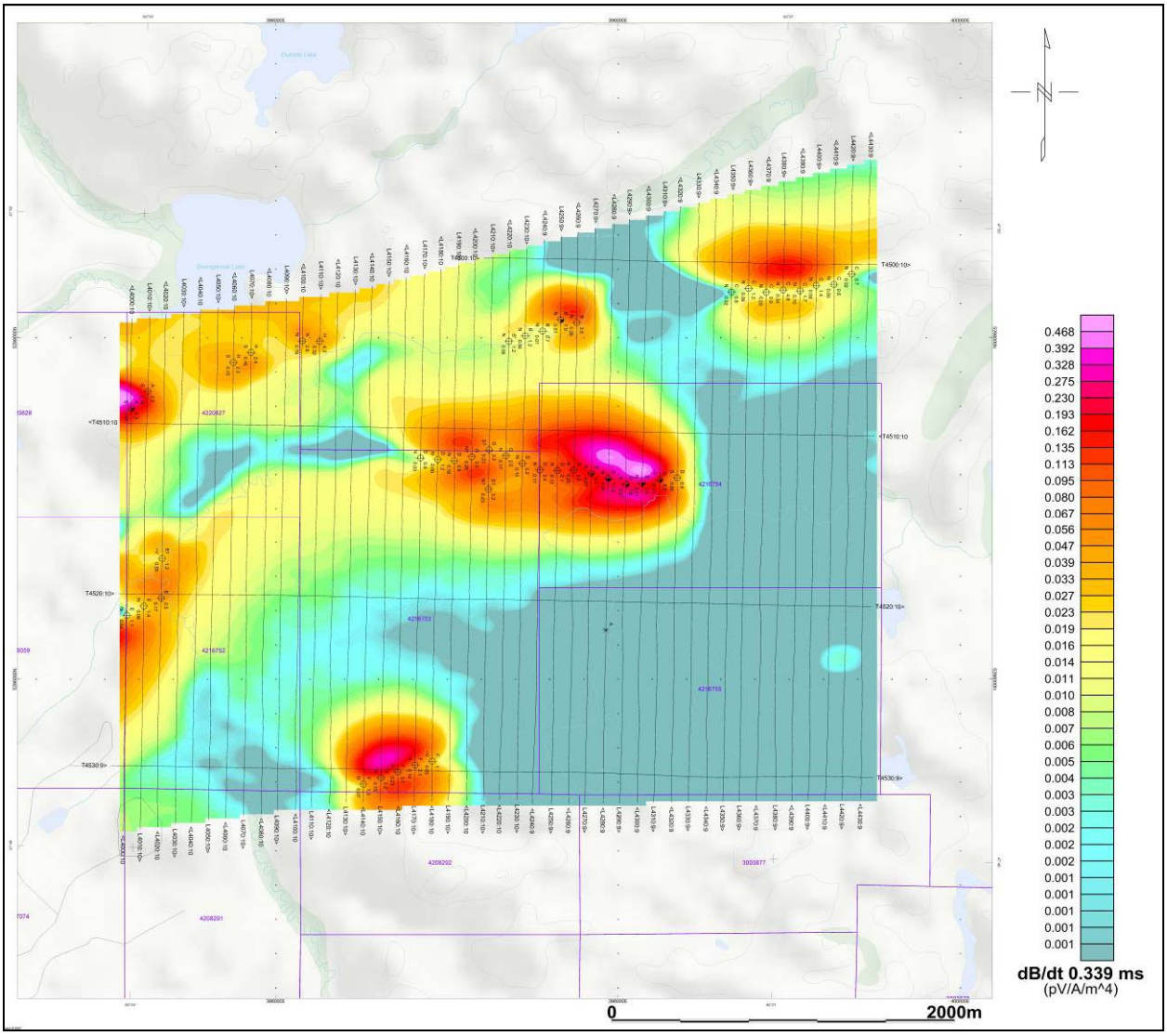

Heenan Block - dB/dt Grid early time channel 0.339 ms with EM anomalies

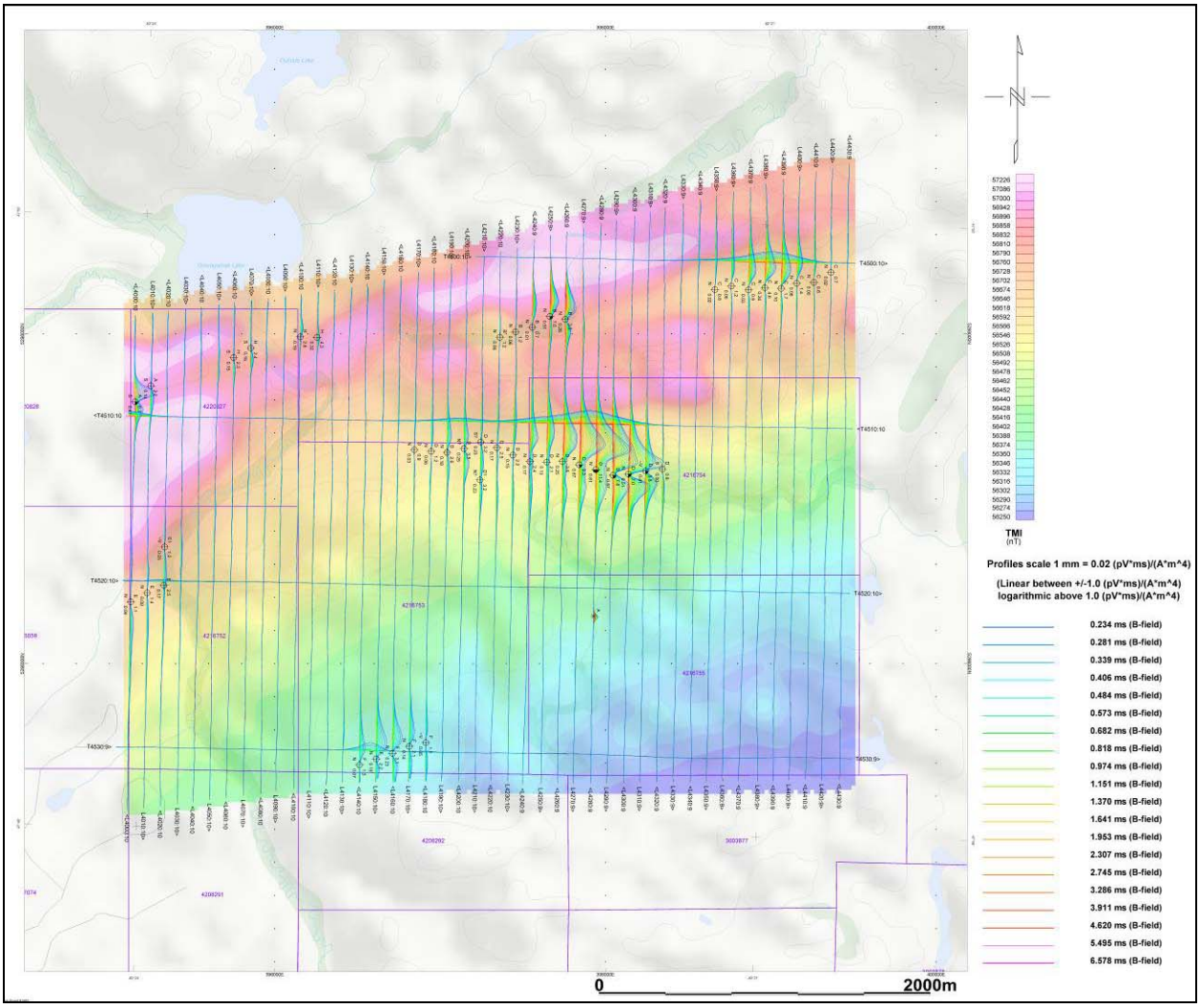

Heenan Block - VTEM B-Field Profiles with EM anomalies

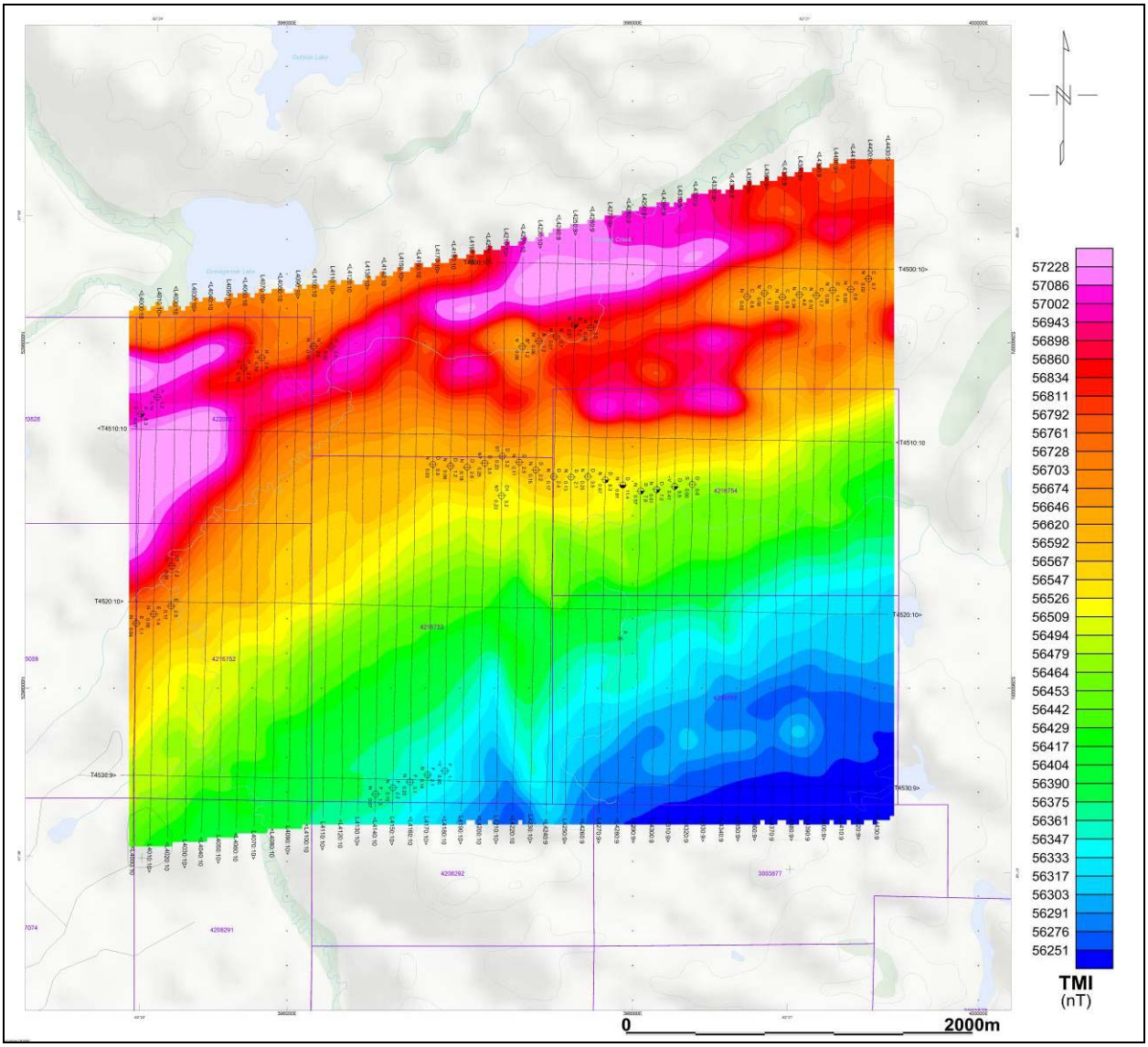

Heenan Block - Total Magnetic Intensity (TMI) Grid with EM anomalies

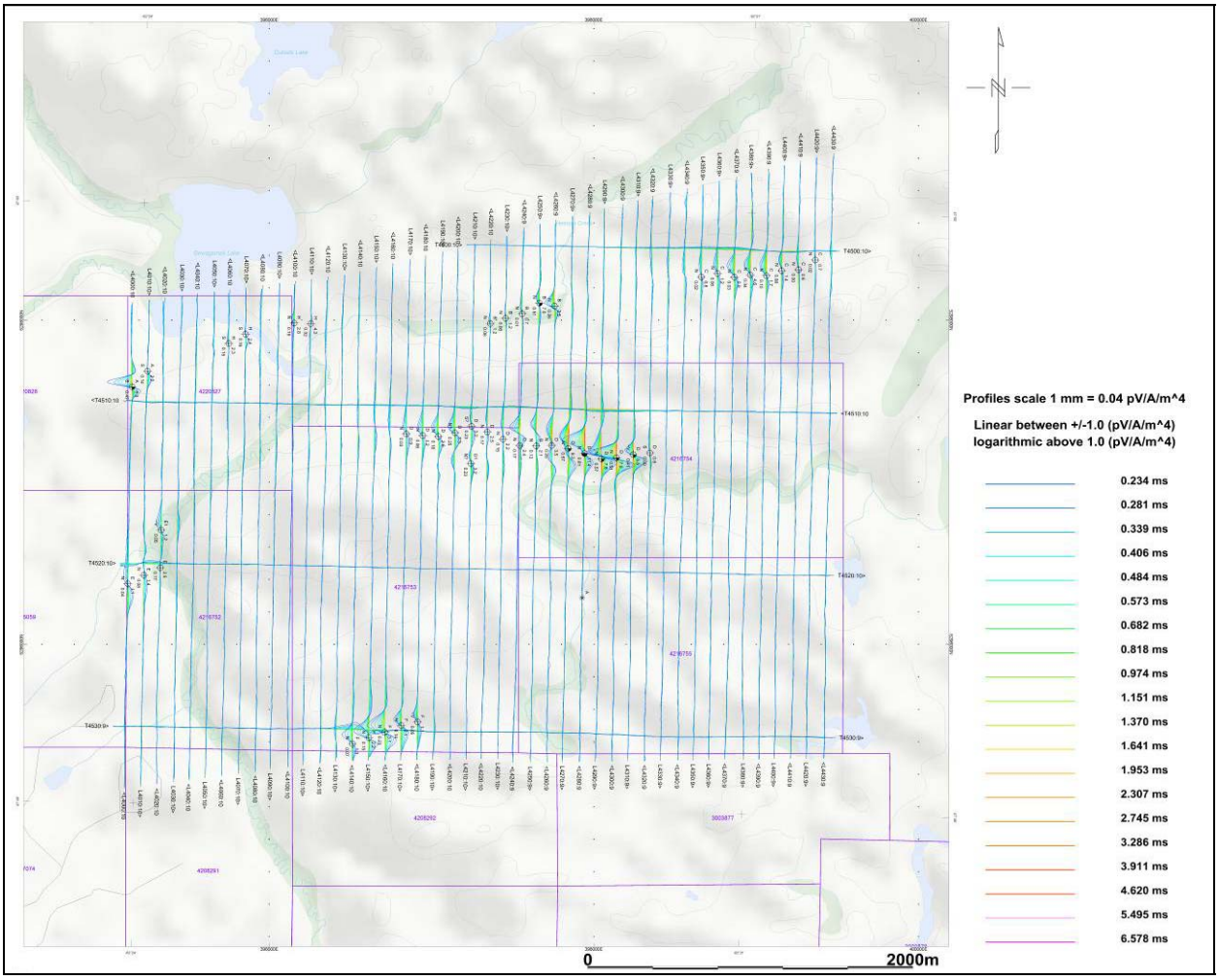

Heenan Block – VTEM X Component Profiles with EM anomalies

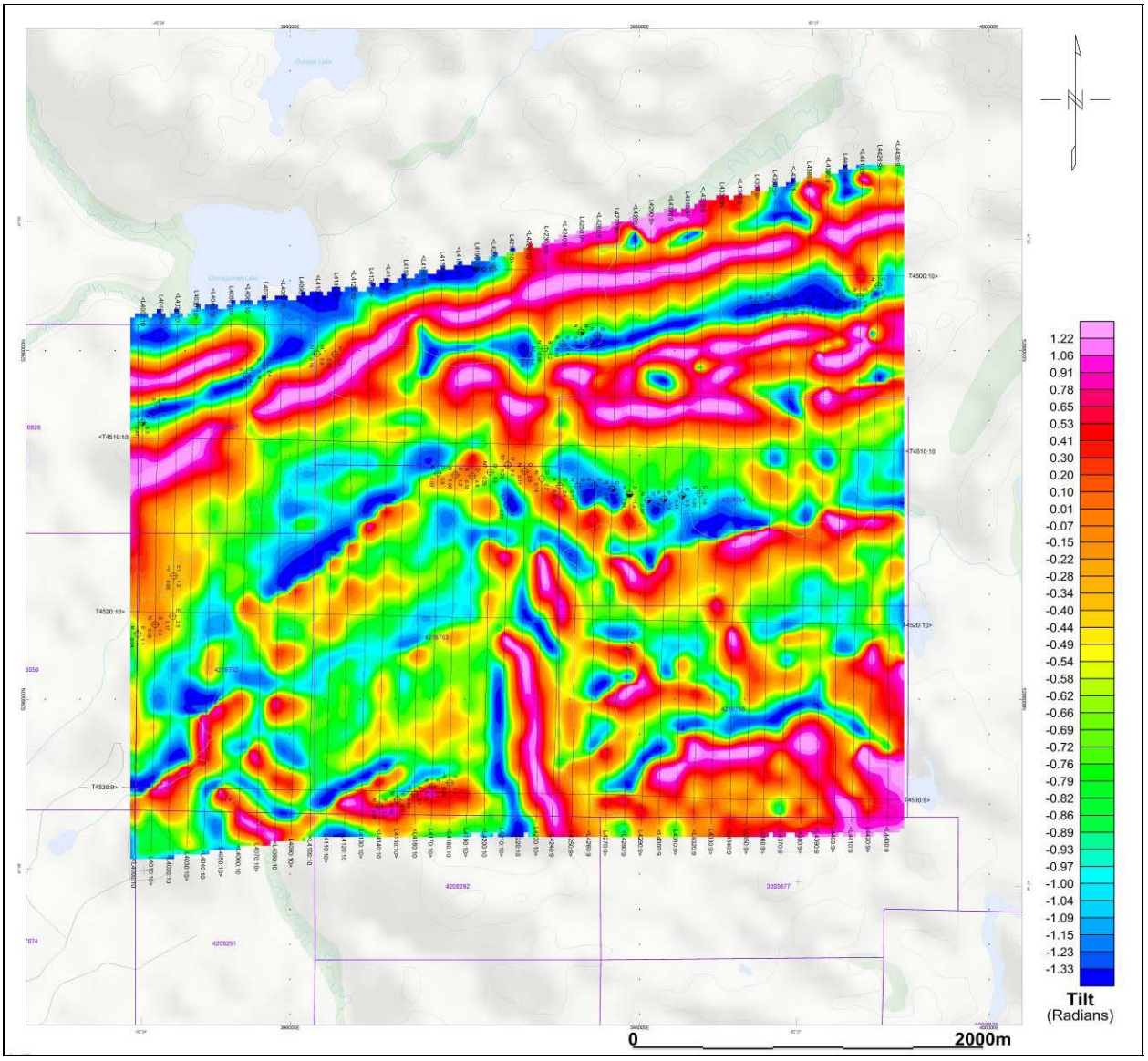

Heenan Block – Tilt Derivative of TMI with EM anomalies

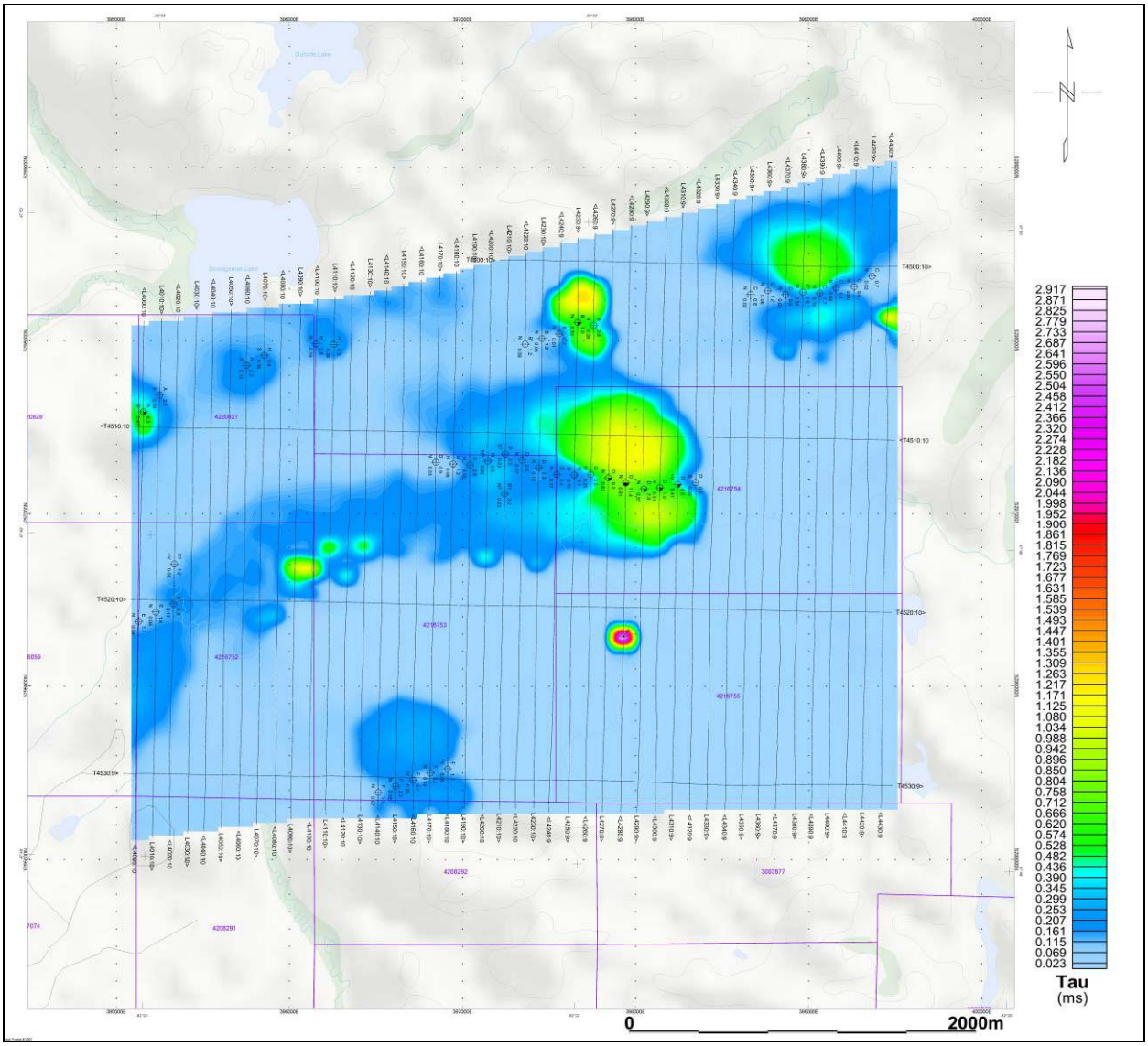

Heenan Block – VTEM dB/dt Z Component Calculated Time Constant with EM anomalies

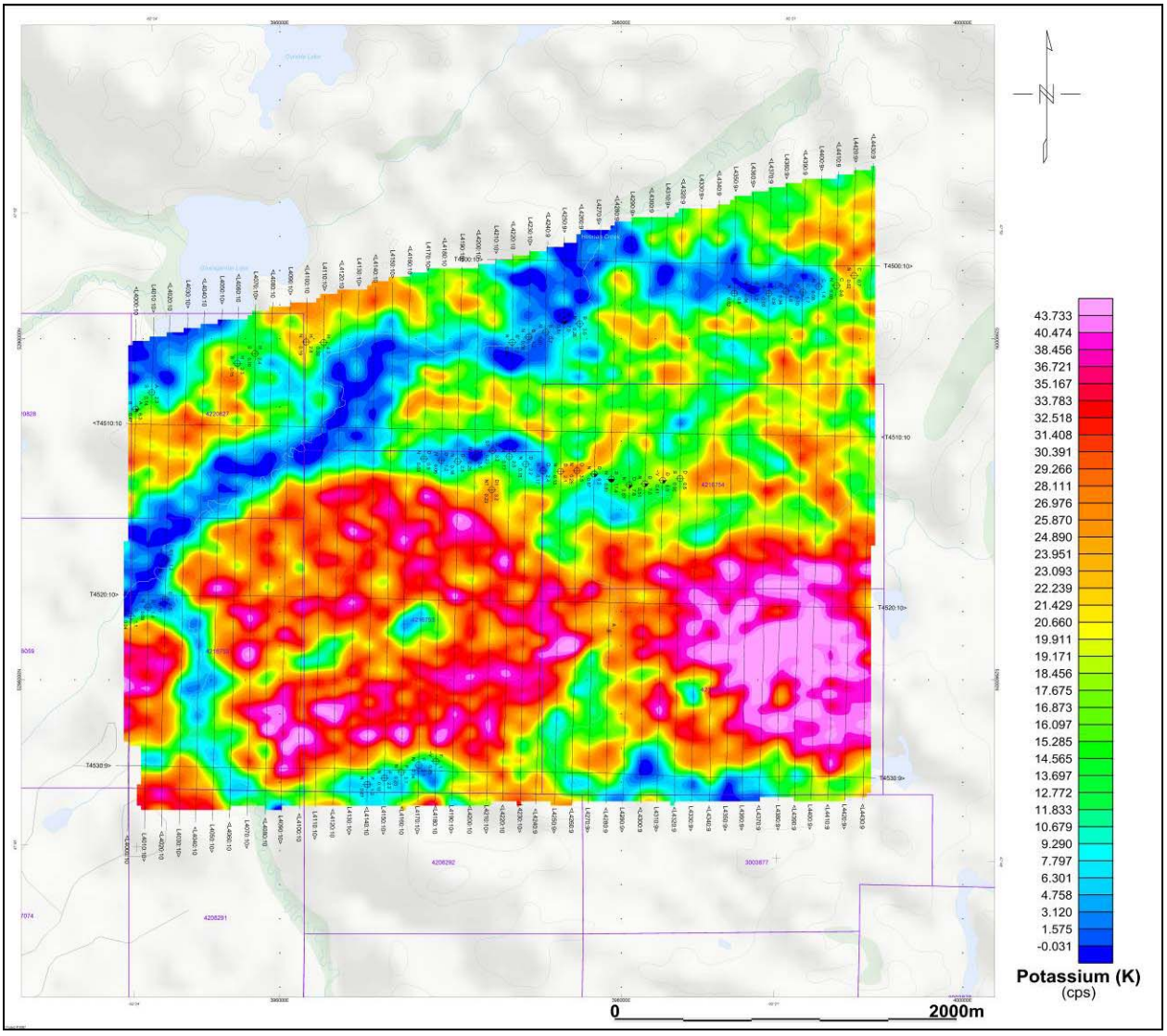

Heenan Block – Gamma Ray Spectrometer Potassium Levels with EM anomalies

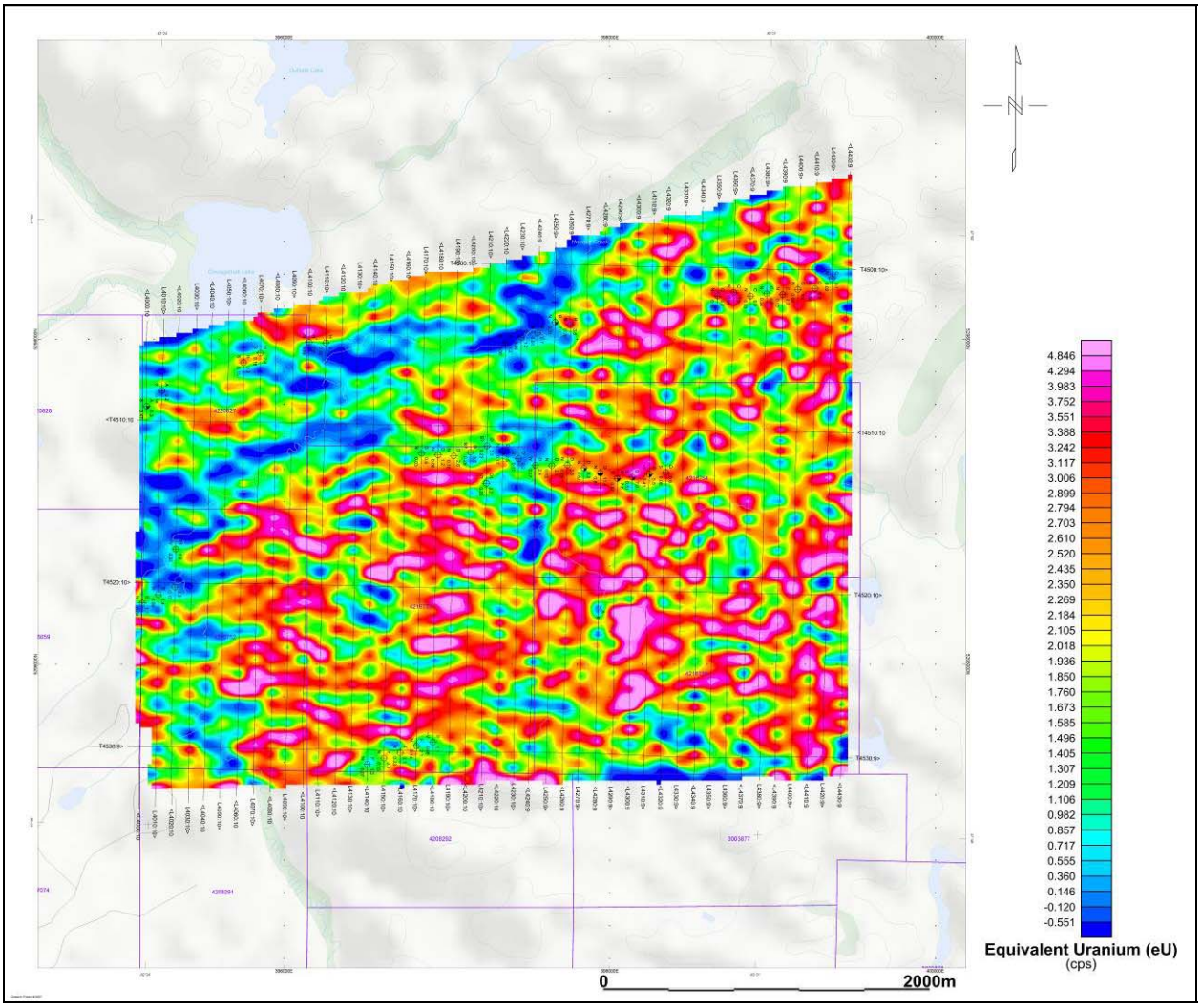

Heenan Block – Gamma Ray Spectrometer Equivalent Uranium Levels with EM anomalies

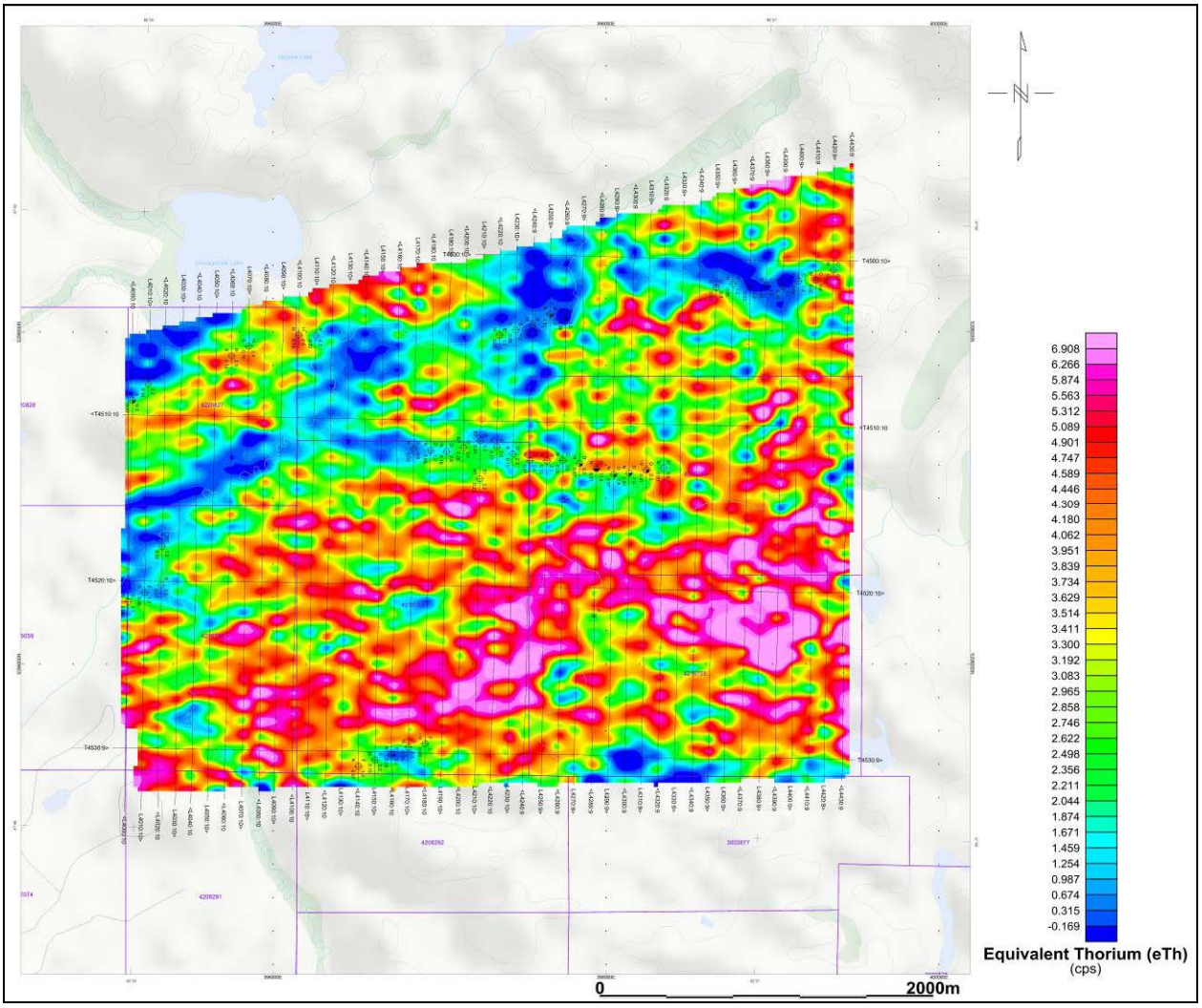

Heenan Block – Gamma Ray Spectrometer Equivalent Thorium Levels with EM anomalies

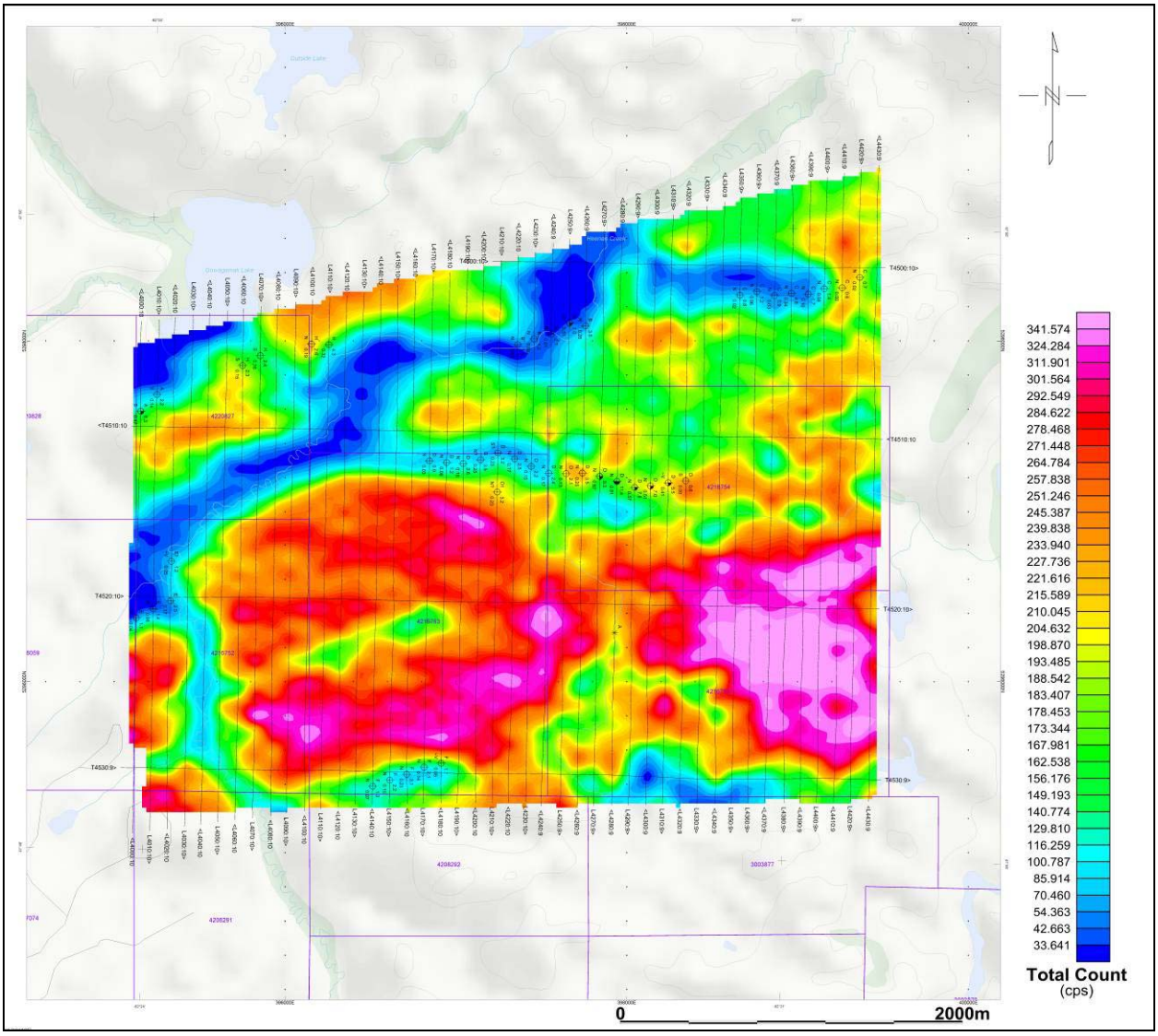

Heenan Block – Gamma Ray Spectrometer K, eU & eTh Total Counts with EM anomalies

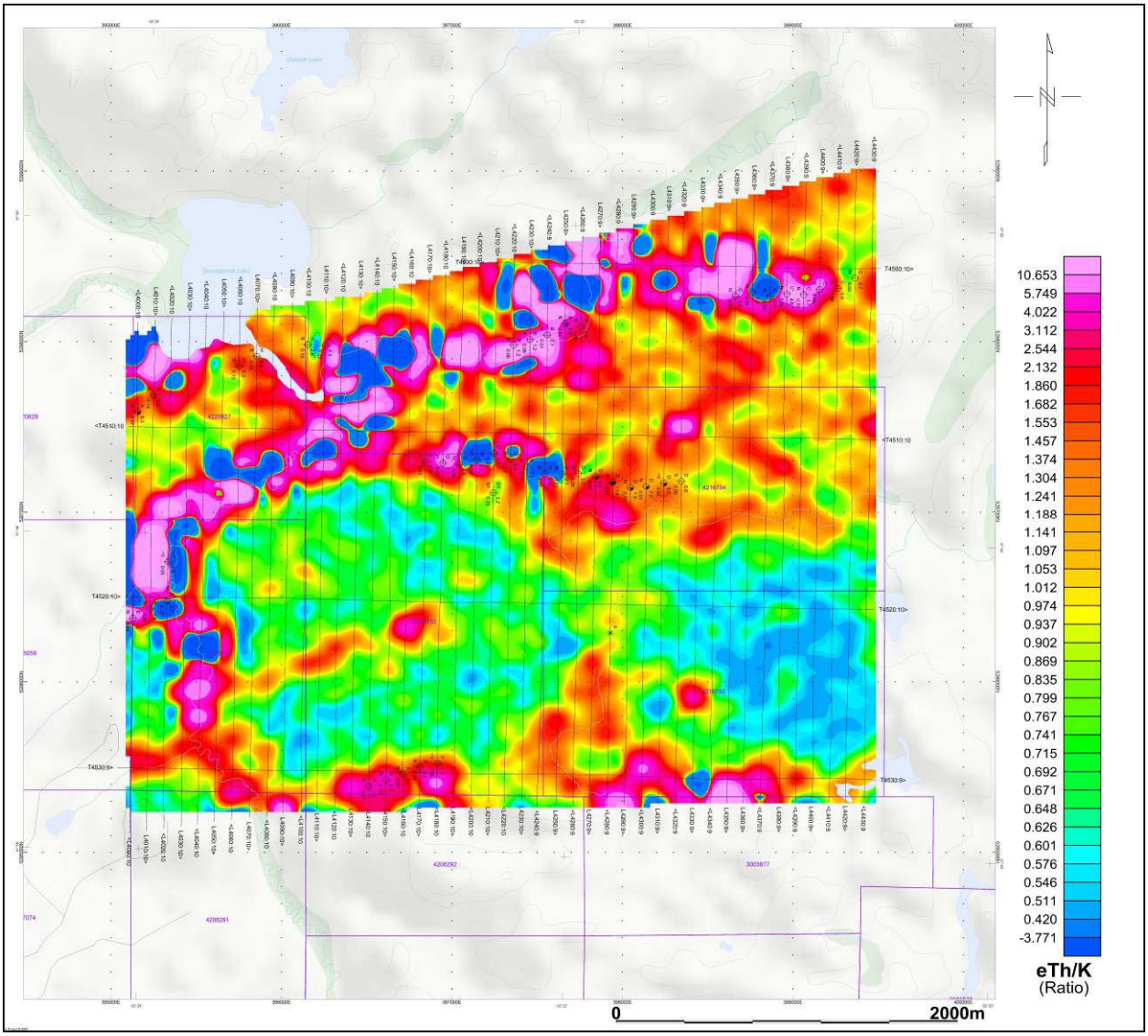

Heenan Block – Gamma Ray Spectrometer equivalent Thorium / Potassium Ratio with EM anomalies

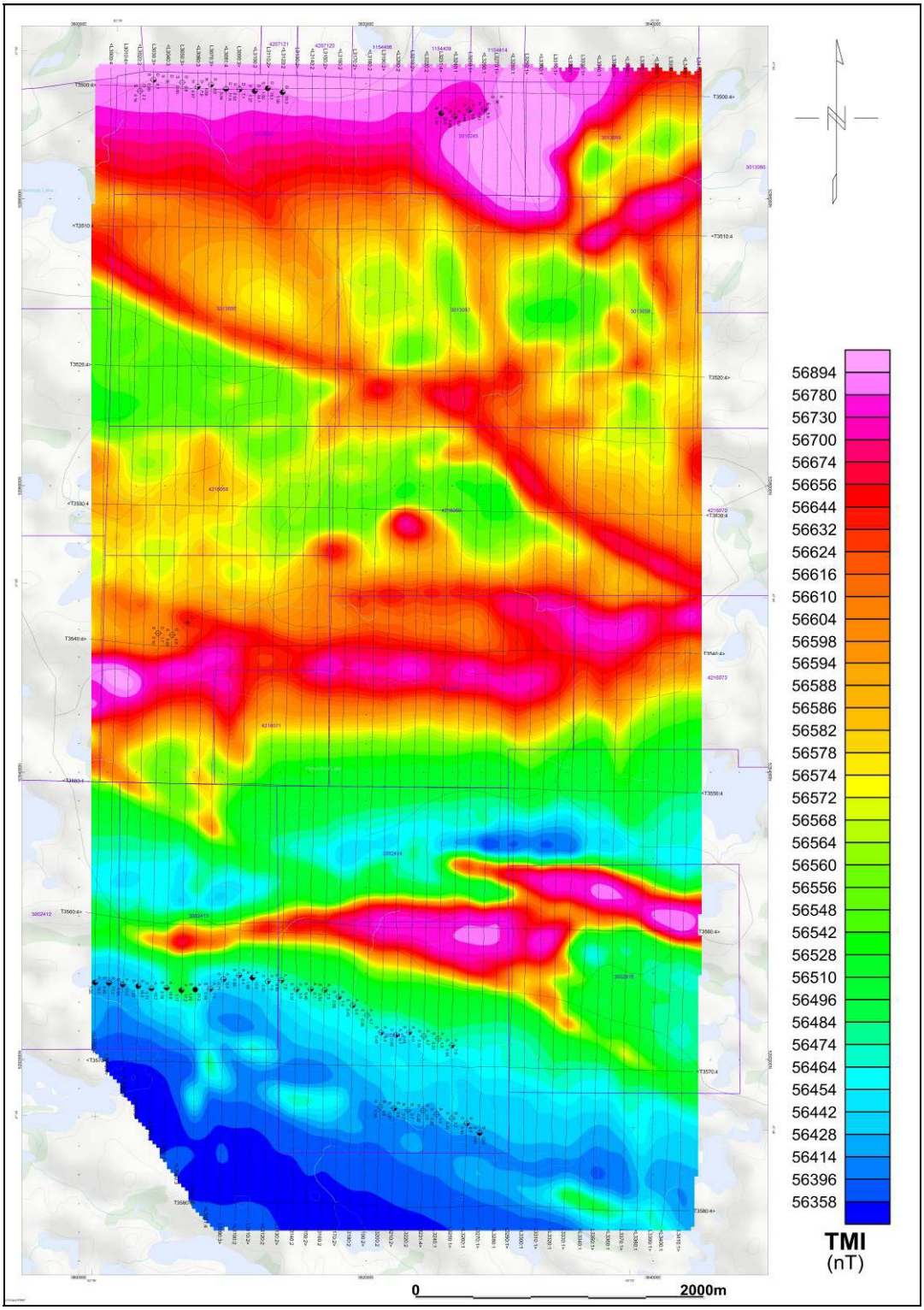

Dore Block - Total Magnetic Intensity (TMI) Grid with EM anomalies

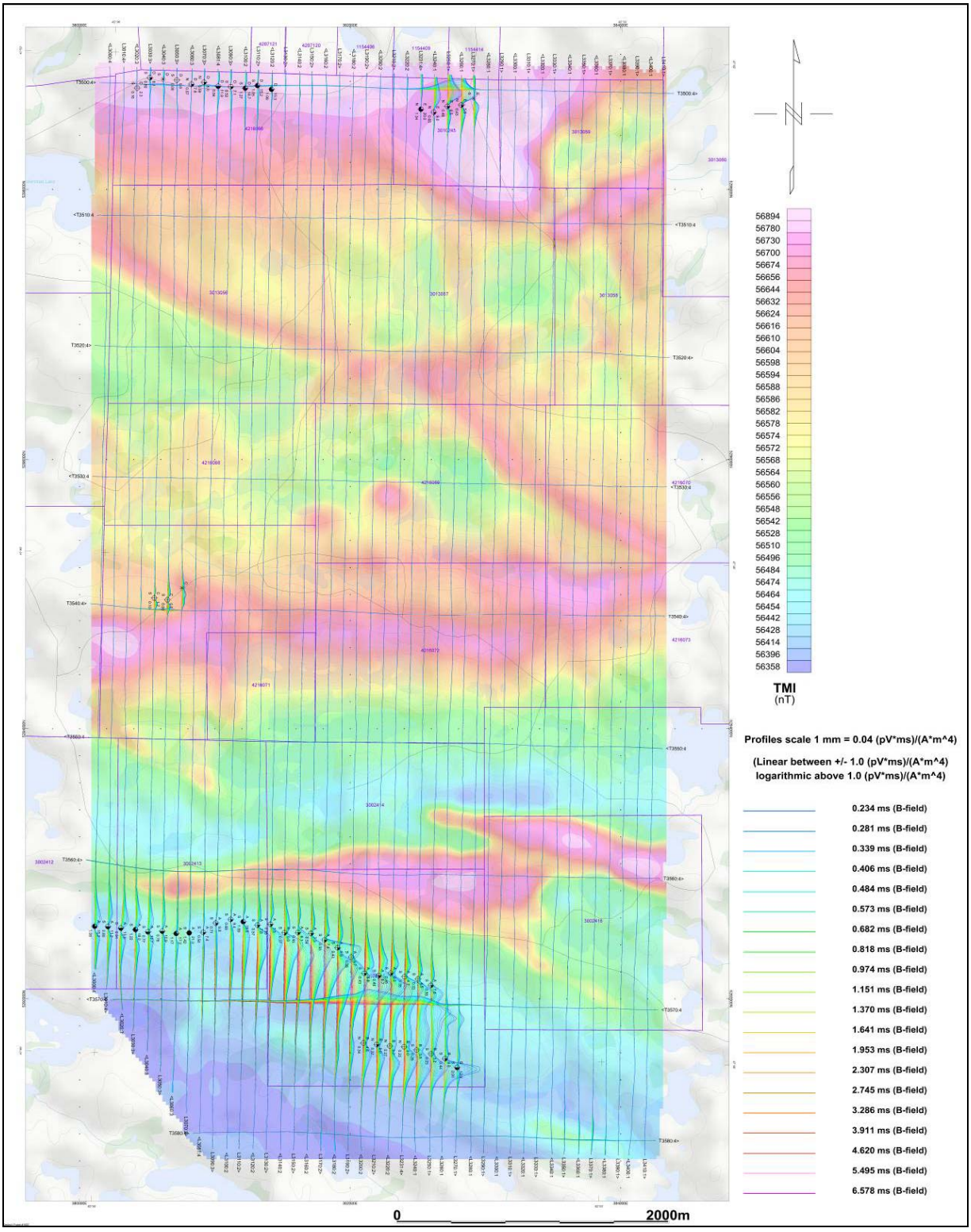

Dore Block - VTEM B-Field Profiles with EM anomalies

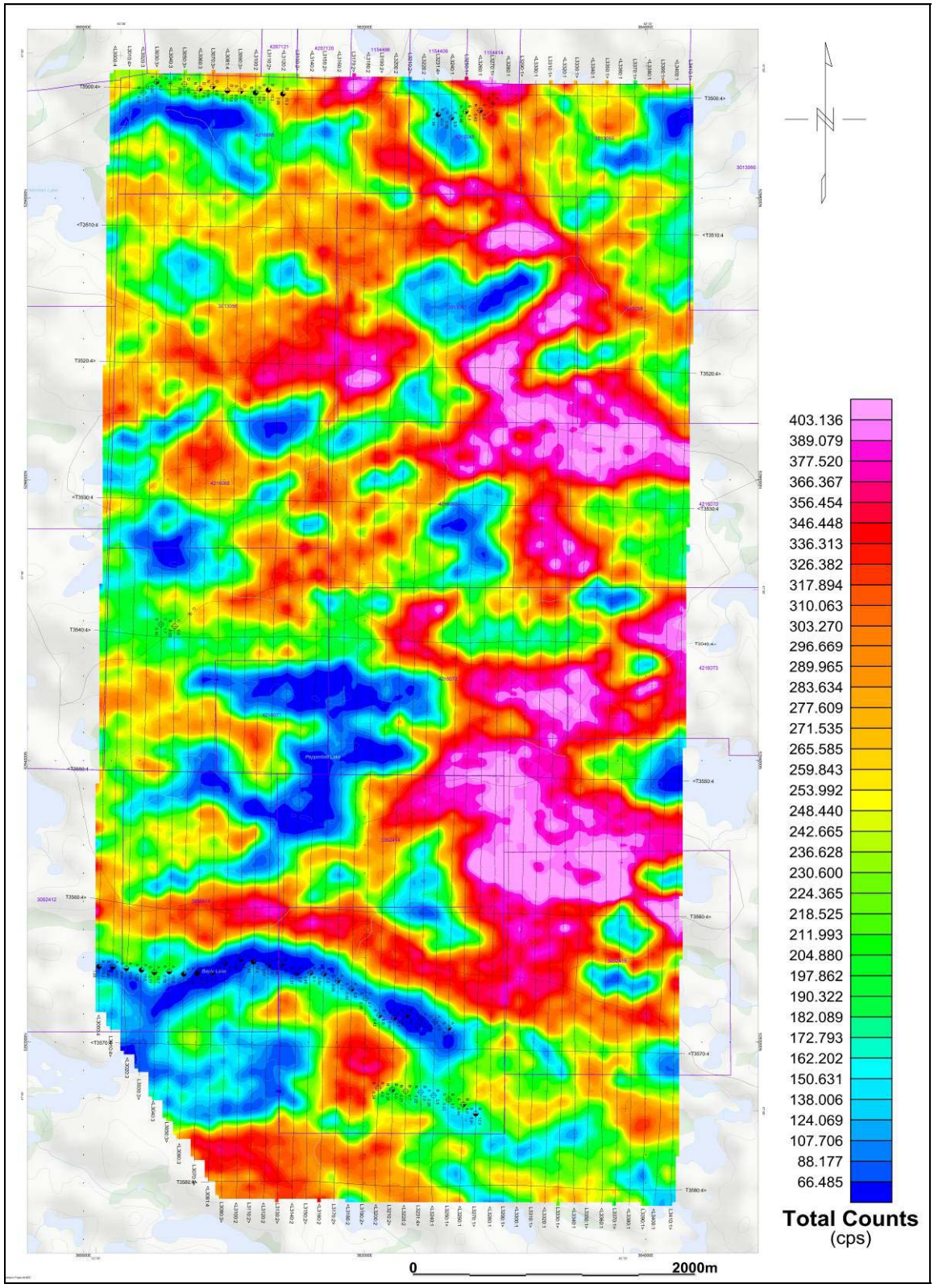

Dore Block – Gamma Ray Spectrometer K, eU & eTh Total Counts with EM anomalies

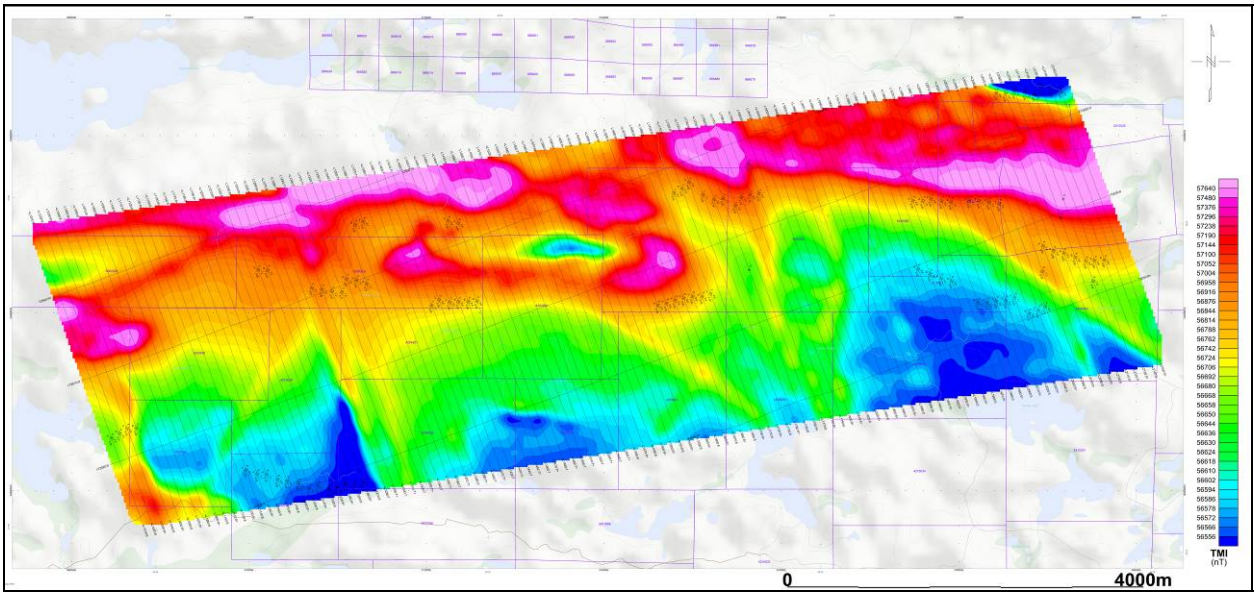

Denyes-Swayze Block - Total Magnetic Intensity (TMI) Grid with EM anomalies

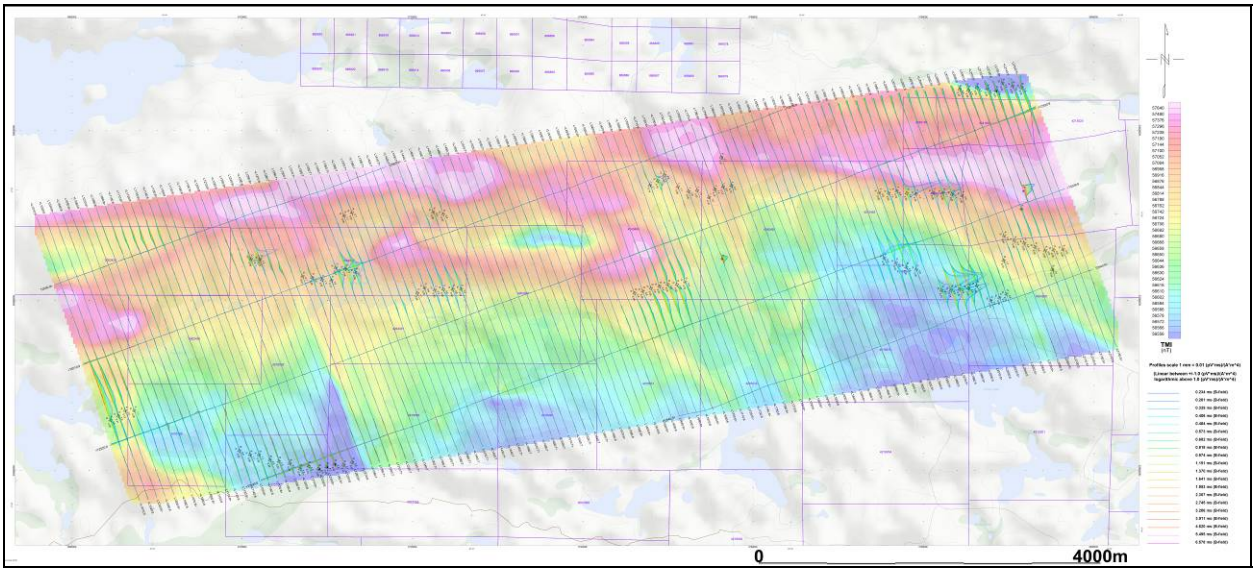

Denyes-Swayze Block - VTEM B-Field Profiles with EM anomalies

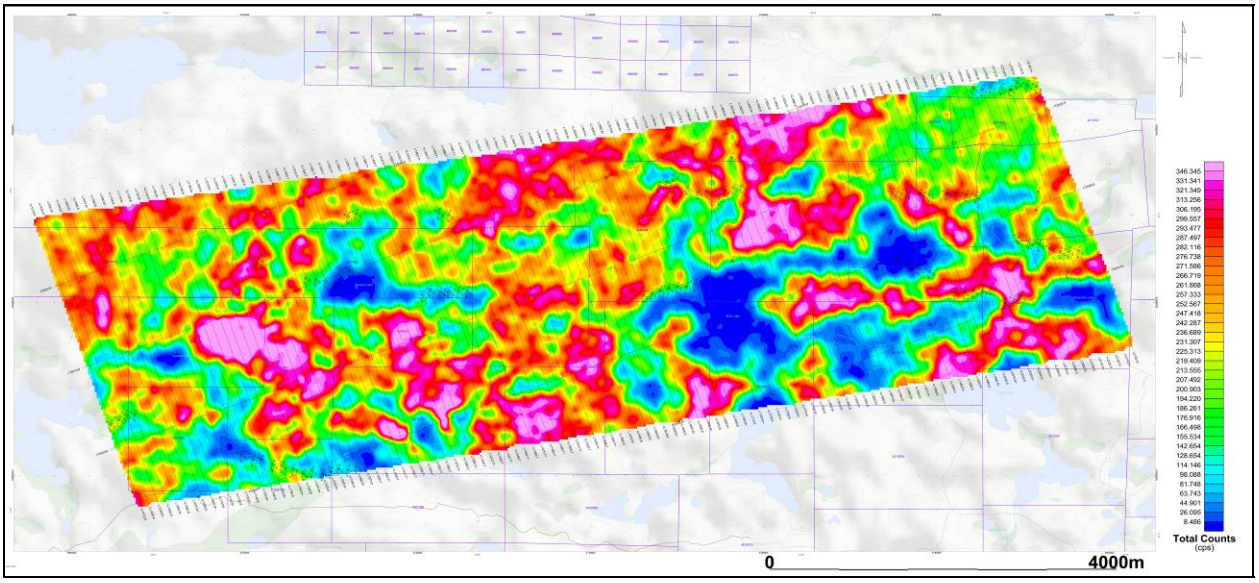

Denyes-Swayze Block – Gamma Ray Spectrometer K, eU & eTh Total Counts with EM anomalies

APPENDIX E

GENERALIZED MODELING RESULTS OF THE VTEM SYSTEM

Introduction

The VTEM system is based on a concentric or central loop design, whereby, the receiver is positioned at the centre of a 26.1 metres diameter transmitter loop that produces a dipole moment up to 404,000 nIA at peak current. The wave form is a bi-polar, modified square wave with a turn-on and turn-off at each end. With a base frequency of 30 Hz, the duration of each pulse is approximately 7.5 milliseconds followed by an off time where no primary field is present.

During turn-on and turn-off, a time varying field is produced (dB/dt) and an electro-motive force (emf) is created as a finite impulse response. A current ring around the transmitter loop moves outward and downward as time progresses. When conductive rocks and mineralization are encountered, a secondary field is created by mutual induction and measured by the receiver at the centre of the transmitter loop.

Measurements are made during the on and off-time, when only the secondary field (representing the conductive targets encountered in the ground) is present.

Efficient modeling of the results can be carried out on regularly shaped geometries, thus yielding close approximations to the parameters of the measured targets. The following is a description of a series of common models made for the purpose of promoting a general understanding of the measured results.

General Modeling Concepts

A set of models has been produced for the Geotech VTEM® system with explanation notes (see models C1 to C18). The Maxwell ^{TM} modeling program (EMIT Technology Pty. Ltd. Midland, WA, AU) used to generate the following responses assumes a resistive half-space.The reader is encouraged to review these models, so as to get a general understanding of the responses as they apply to survey results. While these models do not begin to cover all possibilities, they give a general perspective on the simple and most commonly encountered anomalies.
When producing these models, a few key points were observed and are worth noting as follows:

- For near vertical and vertical plate models, the top of the conductor is always located directly under the centre low point between the two shoulders in the classic **M** shaped response.

- As the plate is positioned at an increasing depth to the top, the shoulders of the **M** shaped response, have a greater separation distance.
- When faced with choosing between a flat lying plate and a prism model to

represent the target (broad response) some ambiguity is present and caution should be exercised.

- With the concentric loop system and Z-component receiver coil, virtually all types of conductors and most geometries are most always well coupled and a response is generated (see Figures C17 & C18). Only concentric loop systems can map such wide varieties of target geometries.

Variation of Plate Depth

Geometries represented by plates of different strike length, depth extent, dip, plunge and depth below surface can be varied with characteristic parameters like conductance of the target, conductance of the host and conductivity/thickness and thickness of the overburden layer.

Diagrammatic models for a vertical plate are shown in Figures C-1 & C-2 and C-5 & C-6 at two different depths, all other parameters remaining constant. With this transmitter-receiver geometry, the classic **M** shaped response is generated. Figures C-1 and C-2 show a plate where the top is near surface. Here, amplitudes of the duel peaks are higher and symmetrical with the zero centre positioned directly above the plate. Most important is the separation distance of the peaks. This distance is small when the plate is near surface and widens with a linear relationship as the plate (depth to top) increases. Figures C-5 and C-6 show a much deeper plate where the separation distance of the peaks is much wider and the amplitudes of the channels have decreased.

Variation of Plate Dip

As the plate dips and departs from the vertical position, the peaks become asymmetrical. Figures C-3 & C-4 and C-7 and C-8 show a near surface plate dipping 80º at two different depths. Note that the direction of dip is toward the high shoulder of the response and the top of the plate remains under the centre minimum.

As the dip increases, the aspect ratio (Min/Max) decreases and this aspect ratio can be used as an empirical guide to dip angles from near 90º to about 30º. The method is not sensitive enough where dips are less than about 30º. For example, for a plate dipping 45º, the minimum shoulder starts to vanish. In Figures C-9 & C-10 and C-11 & C-12, a flat lying plate is shown, relatively near surface. Note that the twin peak anomaly has been replaced by a symmetrical shape with large, bell shaped, channel amplitudes which decay relative to the conductance of the plate.

In the special case where two plates are positioned to represent a synclinal structure. Note that the main characteristic is that the centre amplitudes are higher (approximately double) compared to the high shoulder of a single plate. This model is very representative of tightly folded formations where the conductors where once flat lying.

Variation of Prism Dip

Finally, with thicker, prism models, another algorithm is required to represent current on the plate. A plate model is considered to be infinitely thin with respect to thickness and incapable of representing the current in the thickness dimension. A prism model is constructed to deal with this problem, thereby, representing the thickness of the body more accurately.

Figures C-13 & C-14 and C-15 & C-16 show the same prism at the same depths with variable dips. Aside from the expected differences asymmetry prism anomalies show a characteristic change from a double-peaked anomaly to single peak signatures.

I. THIN PLATE

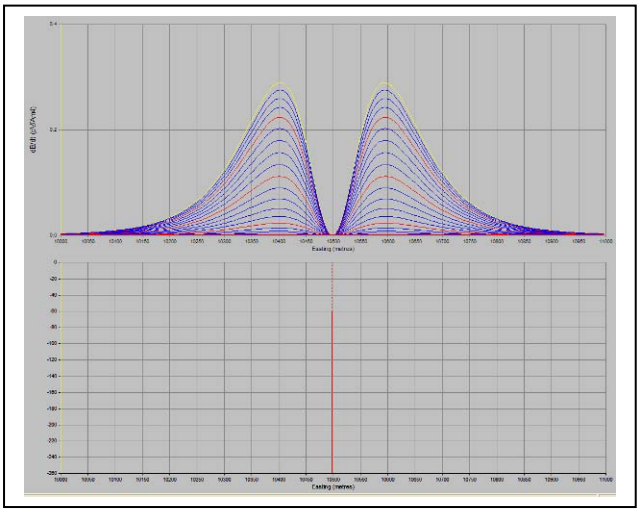

Figure C-1: dB/dt response of a shallow vertical thin plate. Depth=100 m, CT=20 S. The EM response is normalized by the dipole moment and the Rx area.

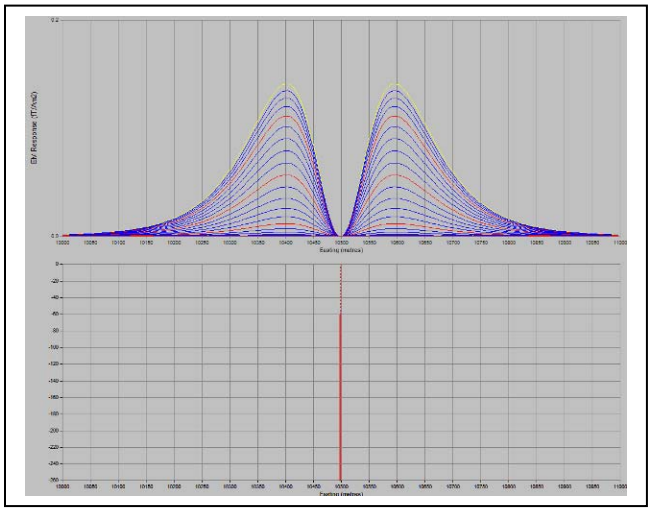

Figure C-2: B-field response of a shallow vertical thin plate. Depth=100 m, CT=20 S. The EM response is normalized by the dipole moment.

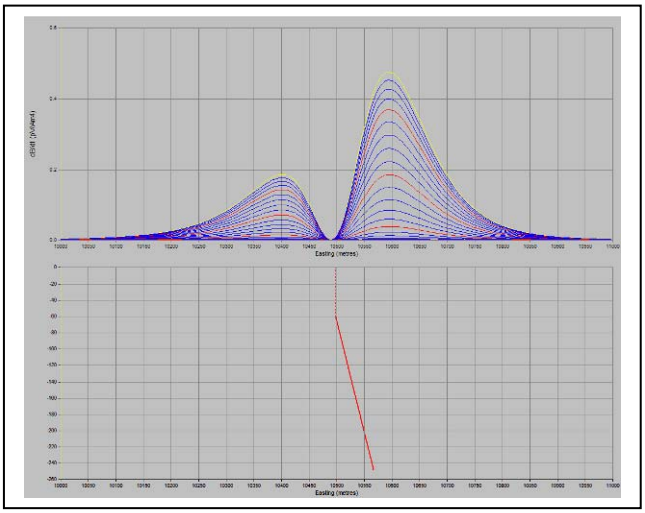

Figure C-3: dB/dt response of a shallow skewed thin plate. Depth=100 m, CT=20 S. The EM response is normalized by the dipole moment and the Rx area.

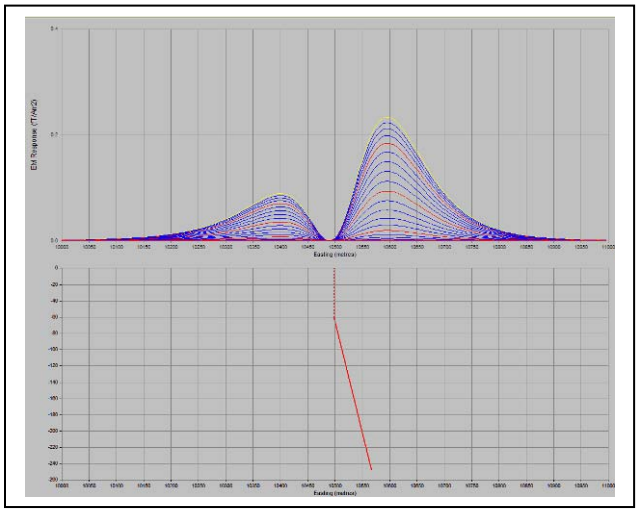

Figure C-4: B-field response of a shallow skewed thin plate. Depth=100 m, CT=20 S. The EM response is normalized by the dipole moment.

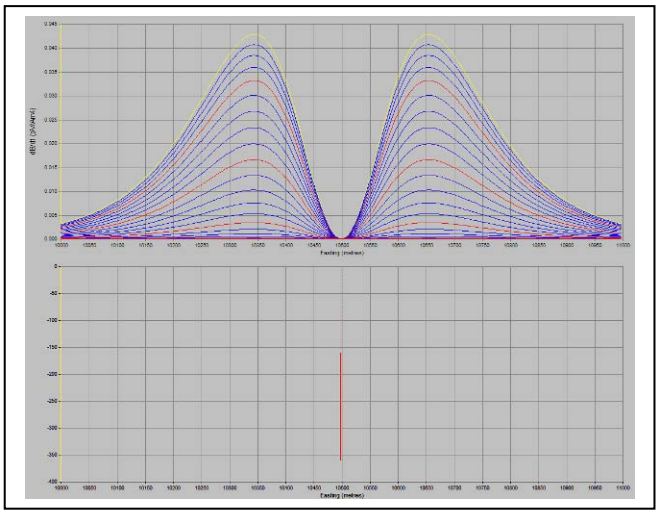

Figure C-5: dB/dt response of a deep vertical thin plate. Depth=200 m, CT=20 S. The EM response is normalized by the dipole moment and the Rx area.

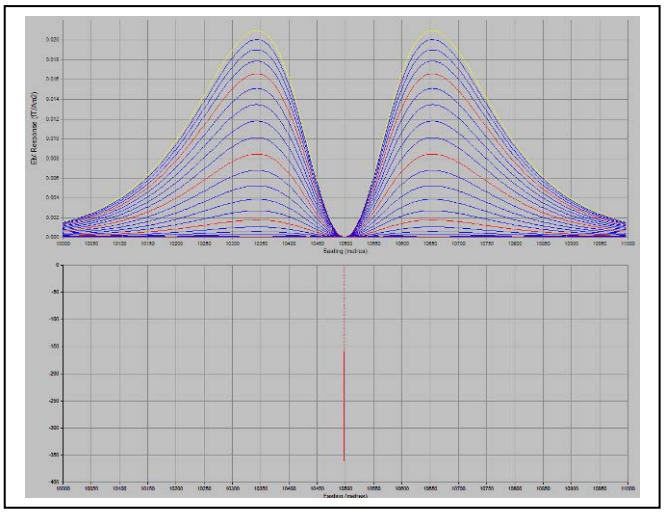

Figure C-6: B-Field response of a deep vertical thin plate. Depth=200 m, CT=20 S. The EM response is normalized by the dipole moment.

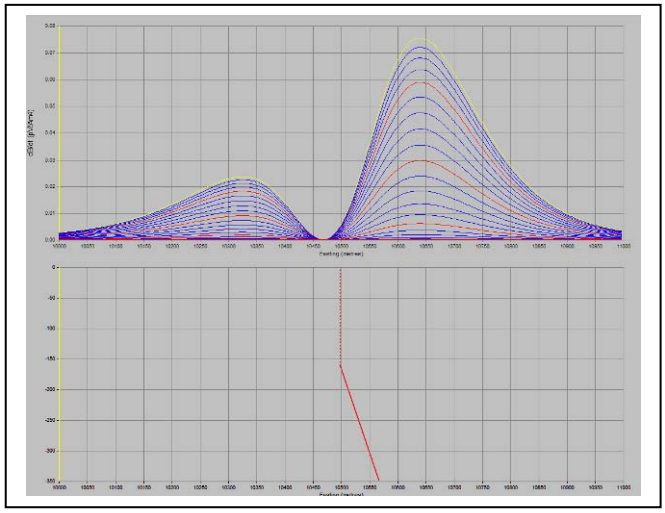

Figure C-7: dB/dt response of a deep skewed thin plate. Depth=200 m, CT=20 S. The EM response is normalized by the dipole moment and the Rx area.

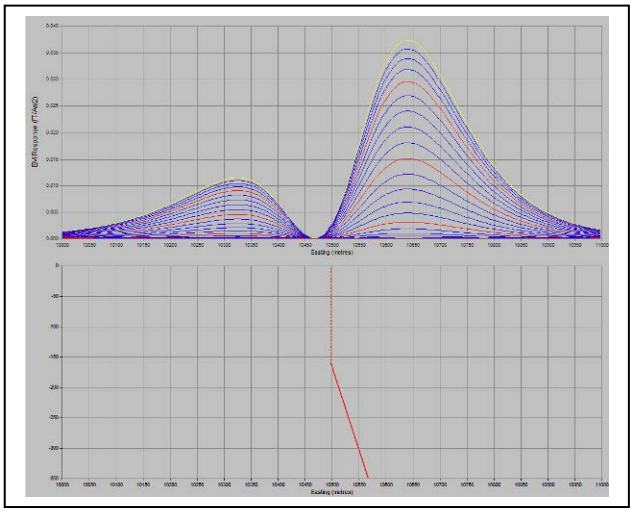

Figure C-8: B-field response of a deep skewed thin plate. Depth=200 m, CT=20 S. The EM response is normalized by the dipole moment.

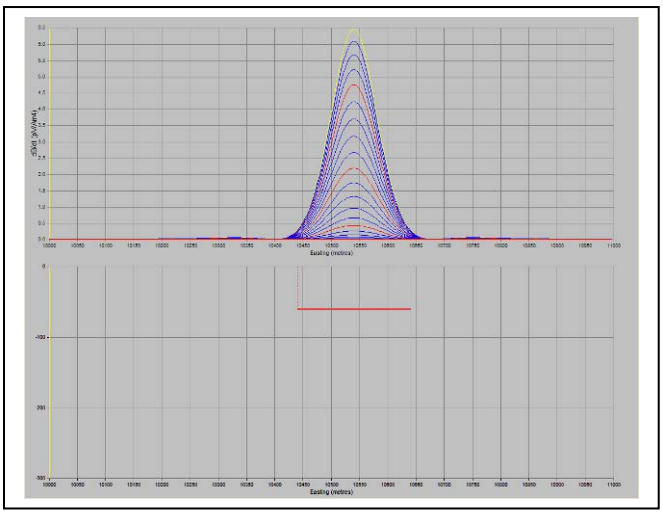

Figure C-9: dB/dt response of a shallow horizontal thin plate. Depth=100 m, CT=20 S. The EM response is normalized by the dipole moment and the Rx area.

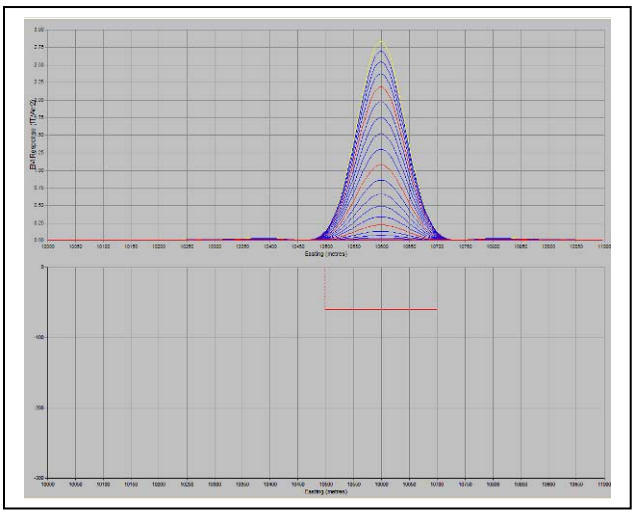

Figure C-10: B-Field response of a shallow horizontal thin plate. Depth=100 m, CT=20 S. The EM response is normalized by the dipole moment.

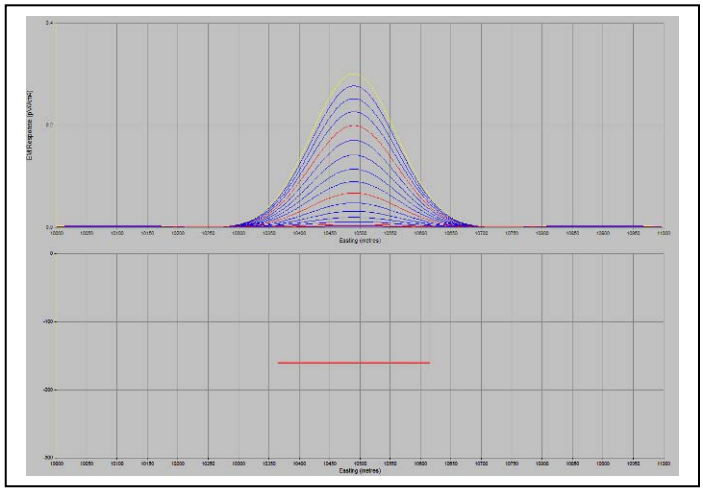

Figure C-11: dB/dt response of a deep horizontal thin plate. Depth=200 m, CT=20 S. The EM response is normalized by the dipole moment and the Rx area.

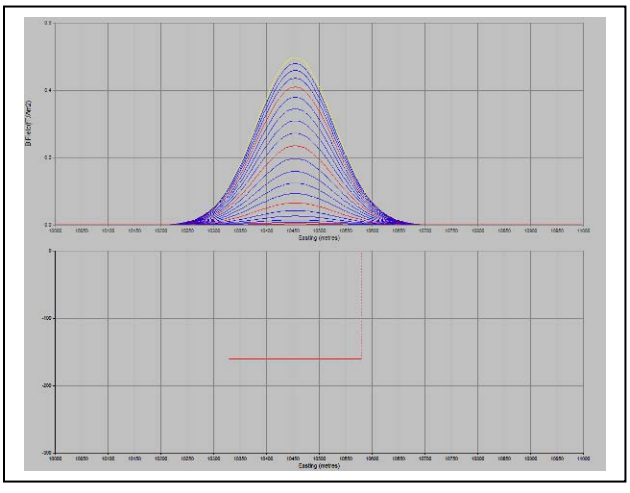

Figure C-12: B-Field response of a deep horizontal thin plate. Depth=200 m, CT=20 S. The EM response is normalized by the dipole moment.

II. THICK PLATE

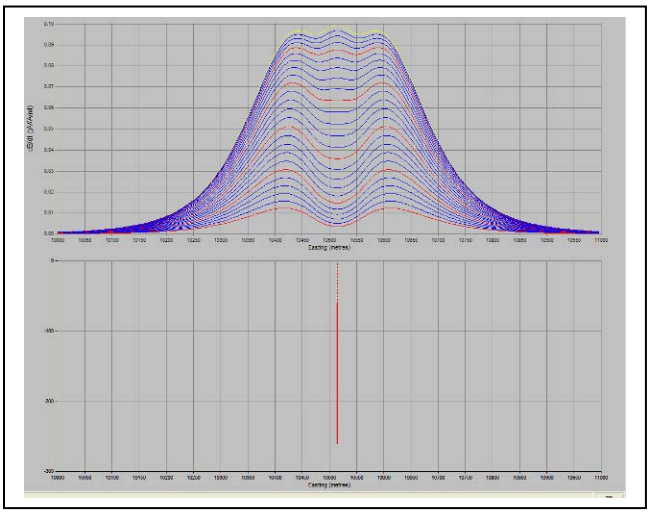

Figure C-13: dB/dt response of a shallow vertical thick plate. Depth=100 m, C=12 S/m, thickness=20 m. The EM response is normalized by the dipole moment and the Rx area.

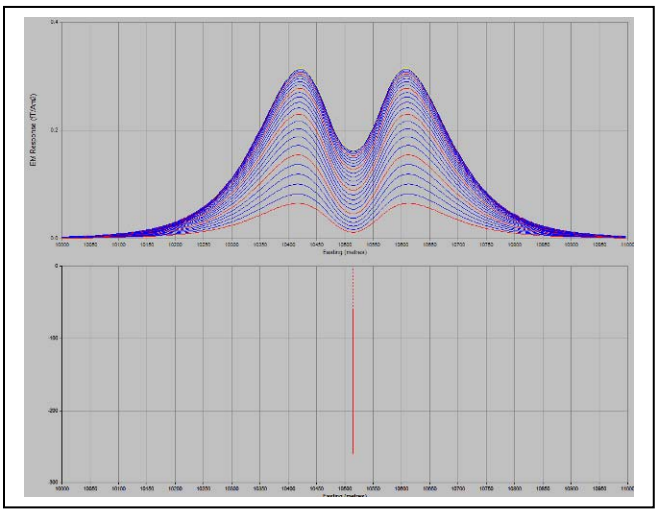

Figure C-14: B-Field response of a shallow vertical thick plate. Depth=100 m, C=12 S/m, thickness= 20 m. The EM response is normalized by the dipole moment.

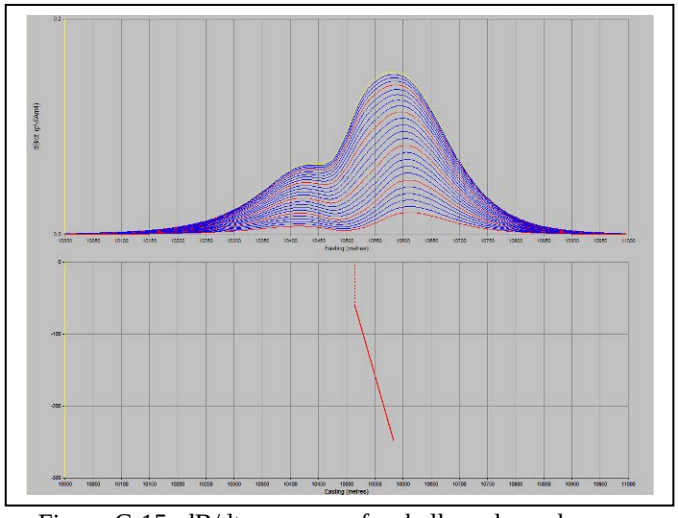

Figure C-15: dB/dt response of a shallow skewed thick plate. Depth=100 m, C=12 S/m, thickness=20 m. The EM response is normalized by the dipole moment and the Rx area.

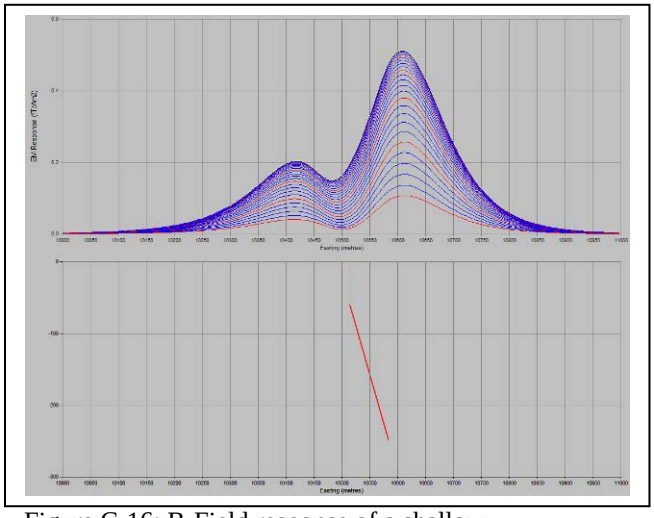

Figure C-16: B-Field response of a shallow skewed thick plate. Depth=100 m, C=12 S/m, thickness=20 m. The EM response is normalized by the dipole moment.

III. MULTIPLE THIN PLATES

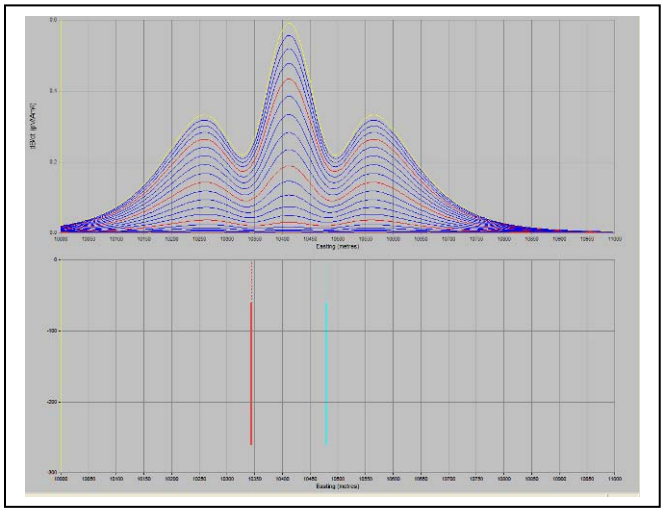

Figure C-17: dB/dt response of two vertical thin plates. Depth=100 m, CT=20 S. The EM response is normalized by the dipole moment and the Rx area.

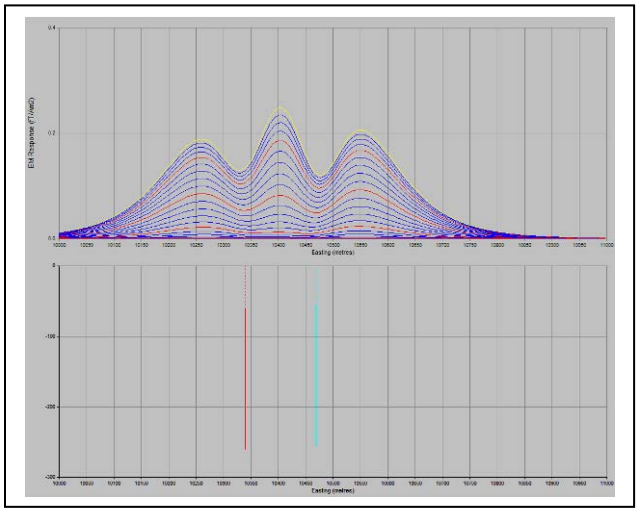

Figure C-18: B-Field response of two vertical thin plates. Depth=100 m, CT=20 S. The EM response is normalized by the dipole moment.

General Interpretation Principals

Magnetics

The total magnetic intensity responses reflect major changes in the magnetite and/or other magnetic minerals content in the underlying rocks and unconsolidated overburden. Precambrian rocks have often been subjected to intense heat and pressure during structural and metamorphic events in their history. Original signatures imprinted on these rocks at the time of formation have, it most cases, been modified, resulting in low magnetic susceptibility values.

The amplitude of magnetic anomalies, relative to the regional background, helps to assist in identifying specific magnetic and non-magnetic rock units (and conductors) related to, for example, mafic flows, mafic to ultramafic intrusives, felsic intrusives, felsic volcanics and/or sediments etc. Obviously, several geological sources can produce the same magnetic response. These ambiguities can be reduced considerably if basic geological information on the area is available to the geophysical interpreter.

In addition to simple amplitude variations, the shape of the response expressed in the wave length and the symmetry or asymmetry, is used to estimate the depth, geometric parameters and magnetization of the anomaly. For example, long narrow magnetic linears usually reflect mafic flows or intrusive dyke features. Large areas with complex magnetic patterns may be produced by intrusive bodies with significant magnetization, flat lying magnetic sills or sedimentary iron formation. Local isolated circular magnetic patterns often represent plug-like igneous intrusives such as kimberlites, pegmatites or volcanic vent areas.

Because the total magnetic intensity (TMI) responses may represent two or more closely spaced bodies within a response, the second derivative of the TMI response may be helpful for distinguishing these complexities. The second derivative is most useful in mapping near surface linears and other subtle magnetic structures that are partially masked by nearby higher amplitude magnetic features. The broad zones of higher magnetic amplitude, however, are severely attenuated in the vertical derivative results. These higher amplitude zones reflect rock units having strong magnetic susceptibility signatures. For this reason, both the TMI and the second derivative maps should be evaluated together.

Theoretically, the second derivative, zero contour or color delineates the contacts or limits of large sources with near vertical dip and shallow depth to the top. The vertical gradient map also aids in determining contact zones between rocks with a susceptibility contrast, however, different, more complicated rules of thumb apply.

Concentric Loop EM Systems

Concentric systems with horizontal transmitter and receiver antennae produce much larger responses for flat lying conductors as contrasted with vertical plate-like conductors. The amount of current developing on the flat upper surface of targets having a substantial area in this dimension, are the direct result of the effective coupling angle, between the primary magnetic field and the flat surface area. One therefore, must not compare the amplitude/conductance of responses generated from flat lying bodies with those derived from near vertical plates; their ratios will be quite different for similar conductances.

Determining dip angle is very accurate for plates with dip angles greater than 30º. For angles less than 30º to 0º, the sensitivity is low and dips can not be distinguished accurately in the presence of normal survey noise levels.

A plate like body that has near vertical position will display a two shoulder, classic **M** shaped response with a distinctive separation distance between peaks for a given depth to top.

It is sometimes difficult to distinguish between responses associated with the edge effects of flat lying conductors and poorly conductive bedrock conductors. Poorly conductive bedrock conductors having low dip angles will also exhibit responses that may be interpreted as surficial overburden conductors. In some situations, the conductive response has line to line continuity and some magnetic correlation providing possible evidence that the response is related to an actual bedrock source.

The EM interpretation process used, places considerable emphasis on determining an understanding of the general conductive patterns in the area of interest. Each area has different characteristics and these can effectively guide the detailed process used.

The first stage is to determine which time gates are most descriptive of the overall conductance patterns. Maps of the time gates that represent the range of responses can be very informative.

Next, stacking the relevant channels as profiles on the flight path together with the second vertical derivative of the TMI is very helpful in revealing correlations between the EM and Magnetics.

Next, key lines can be profiled as single lines to emphasize specific characteristics of a conductor or the relationship of one conductor to another on the same line. Resistivity Depth sections can be constructed to show the relationship of conductive overburden or conductive bedrock with the conductive anomaly.

_____

Roger Barlow
Consultant

_____

Nasreddine Bournas, P. Geo.
Geotech Ltd.

January 2009

APPENDIX F

EM TIME CONSTANT (TAU) ANALYSIS

Theory

As established in electromagnetic theory, the magnitude of the electro-motive force (emf) induced is proportional to the time rate of change of primary magnetic field at the conductor. This emf causes eddy currents to flow in the conductor with a characteristic decay, whose Time Constant (Tau) is a function of the conductivity and geometry of the survey target. The decaying currents generate a proportional secondary magnetic field, the time rate of change of which is measured by the receiver coil as induced voltage during the Off time.

The receiver coil output voltage (**e_0**) is proportional to the time rate of change of the secondary magnetic field and has the form,

$$e_0 \alpha (1 / \tau) e^{-(t / \tau)}$$

Where,

τ = L/R is the characteristic time constant of the target
R = resistance
L = inductance

From the expression, conductive targets that have small value of resistance and hence large value of τ yield signals with small initial amplitude that decays relatively slowly with progress of time. Conversely, signals from poorly conducting targets that have large resistance value and smallτ, have high initial amplitude but decay rapidly with time[2].

EM Time Constant (Tau) Calculation

The EM Time-Constant (TAU) is a general measure of the speed of decay of the electromagnetic response and indicates the presence of eddy currents in conductive sources as well as reflecting the "conductance quality" of a source. Although Tau can be calculated using either the measured dB/dt decay or the calculated B-field decay, dB/dt is commonly preferred due to better stability (S/N) relating to signal noise. Generally, TAU calculated on base of early time response reflects both near surface overburden and poor conductors whereas, in the late ranges of time, deep and more conductive sources, respectively. For example early time TAU distributions in an area that is indicative of conductive overburden are shown in Figure F1.

[2] McNeill, JD, 1980, "Applications of Transient Electromagnetic Techniques", Technical Note TN-7 page 5, Geonics Limited, Mississauga, Ontario.

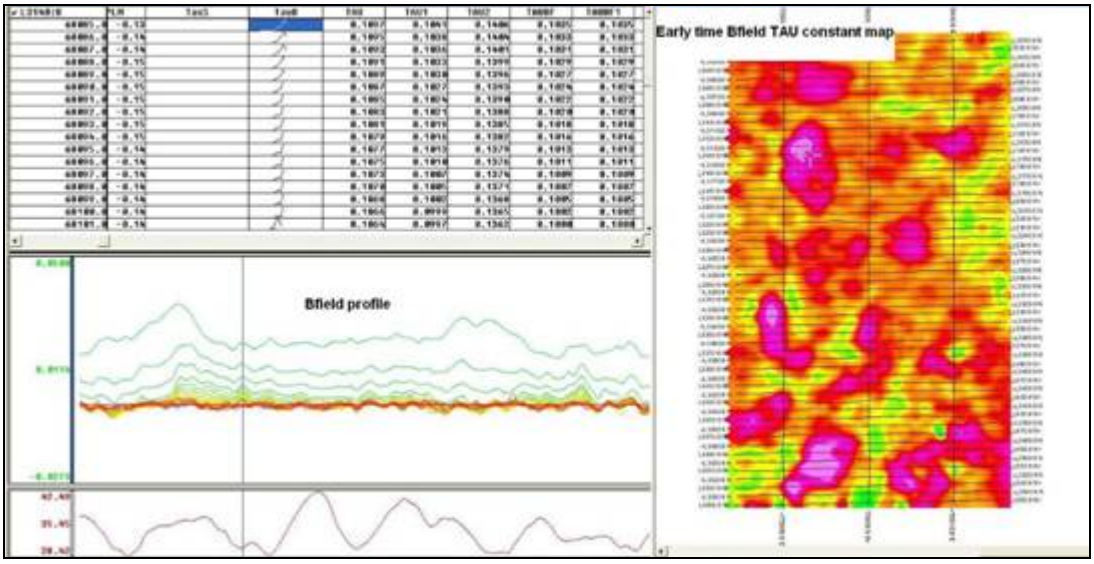

Figure F1 - Area with overburden conductive layer and local sources.

If TAU is calculated across a wide range of time it becomes an integrated parameter and can be used to differentiate conductive sources (Figure F2).

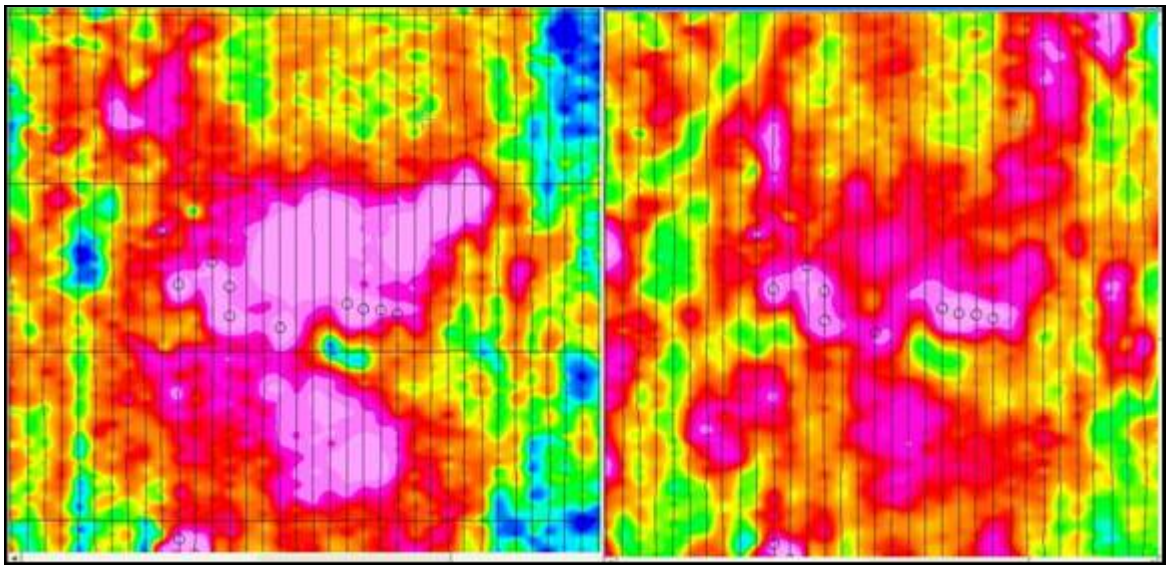

Figure F2 - Map of B-field (left) and TAU (right) with EM anomaly picks due to deep conductive targets.

There are many advantages of TAU maps:

- Because TAU is time integral parameter, all conductive zones and targets are displayed independently of their depth and conductivity on a single map.
- Very good differential resolution in complex conductive places with many sources with different conductivity.

- Signs of the presence of good conductive targets are amplified and emphasized independently of their depth and level of response accordingly.
- Targets which create negative responses in certain known geologic situations, for example due to the relative location of the target, the conductive cover and the coincident geometry of the VTEM system, will usually produce a positive TAU.

In the example shown in Figure F3, three local targets are defined, each of them with a different depth of burial, as indicated on the conductivity depth image (CDI). All are very good conductors but the deeper target (number 3) has a relatively weak dB/dt signal yet also features the strongest total TAU (Figure F4). This example highlights the benefit of Tau analysis in terms of an additional target discrimination tool.

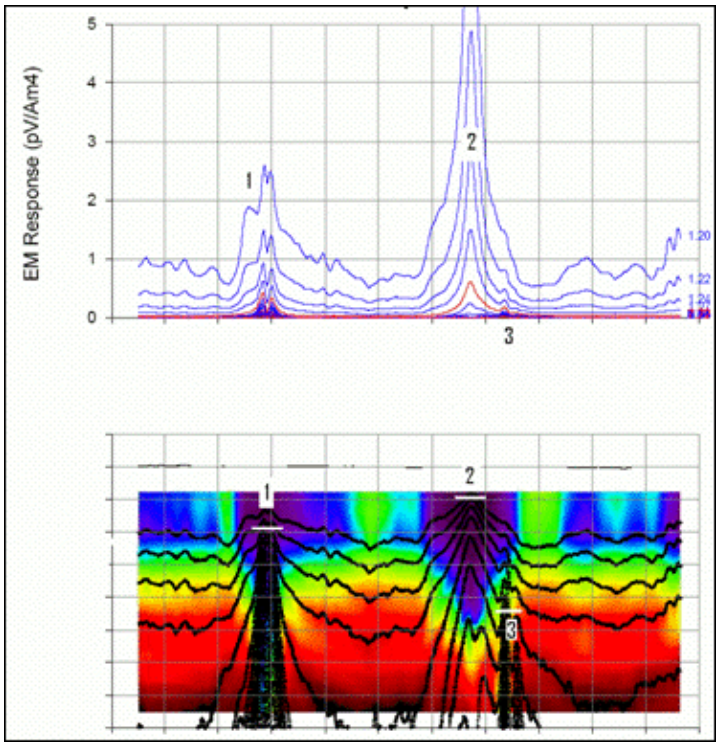

Figure F3 – dB/dt profile and CDI with different depths of sources (white lines).

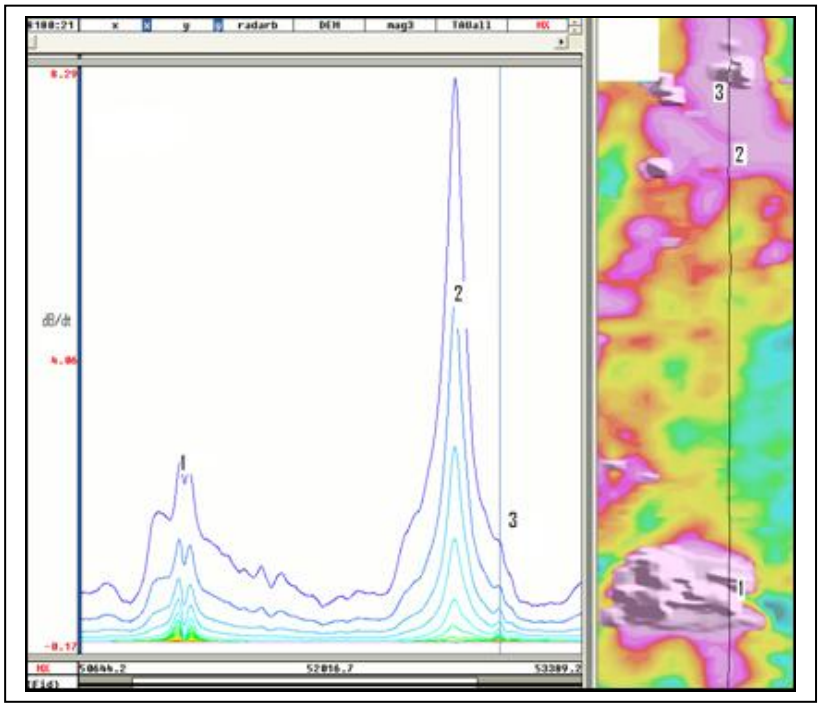

Figure F4 – Map of total TAU and dB/dt profile.

The EM Time Constants for dB/dt and B-field were calculated using the "sliding Tau" in-house program developed at Geotech, using a method similar to the "adTau" of Witherly and Irvine (Condor Consulting Ltd., Lakewood, CO). The EM decays are obtained from all 24 available decay channels, starting at the latest channel (ch33). Time constants are taken from a least square fit of a straight-line (log/linear space) over the last 4 gates above a pre-set signal threshold level (Figure F5).The sliding Tau method determines that, as the amplitudes increase, the time-constant is taken at progressively later times in the EM decay. Conversely, as the amplitudes decrease, Tau is taken at progressively earlier times in the decay. If the maximum signal amplitude falls below the threshold, or becomes negative for any of the 4 time gates, then Tau is not calculated and is assigned a value of 0.0ms by default (M. Orta, Geotech, pers. comm., 07/2009).

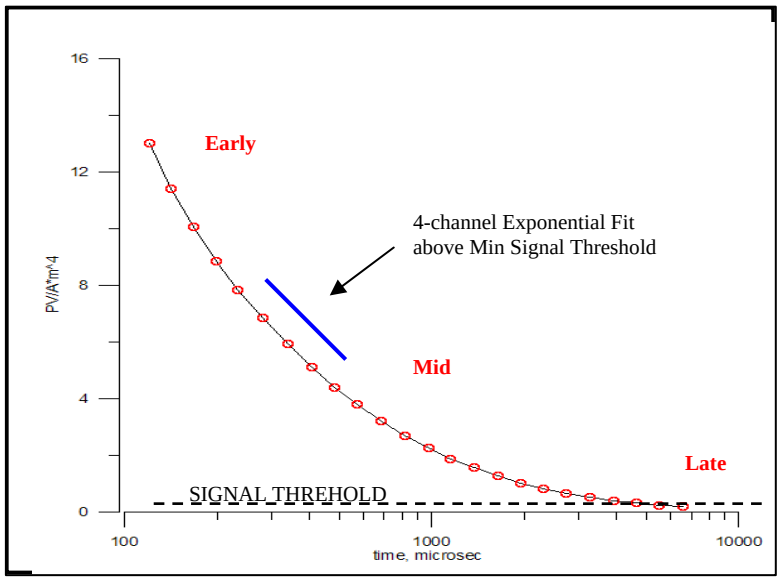

Figure F5 - Typical dB/dt decay and Sliding Tau method for VTEM data

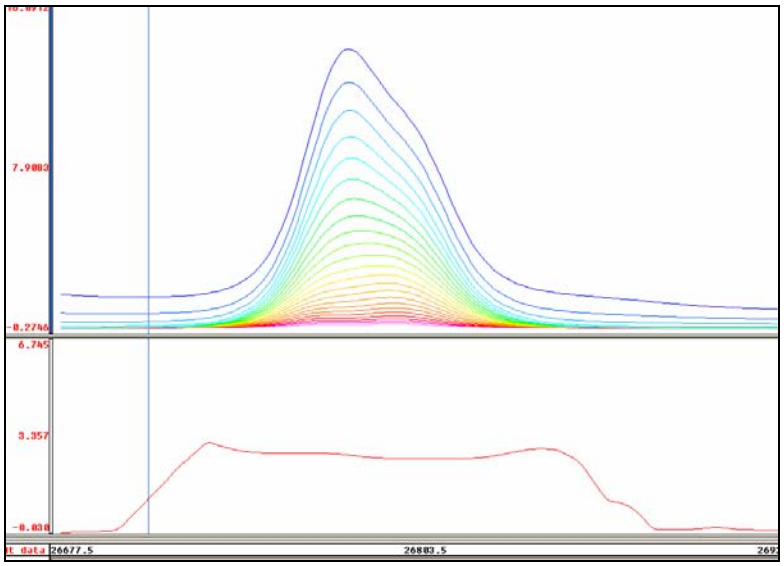

Figure F6 - VTEM anomaly and EM Time constant graph.

Alexander Prikhodko, PhD
Geotech Ltd.

Nasreddine Bournas, PhD, P. Geo.
Geotech Ltd.

July 2009

APPENDIX G

ELETROMAGNETIC ANOMALY LISTING

Denyes-Swayze Block

Line	Anom ID	Anom type	X (m)	Y (m)	Z (m)	EM height (m)	Conductance (Siemens)	Tau dB/dt (ms)	Tau B-Field (ms)	Dipping direction	Cultural effect
L1010	A	Plate	368450	5296591	479	48	3.55	0.26	0.3	N	
L1020	A	Plate	368543	5296642	477	44	3	0.21	0.14	N	
L1030	A	Plate	368625	5296702	487	51	1.97	0.13	0	N	
L1040	A	Plate	368731	5296704	473	42	1.09	0.05	0	N	
L1140	B	Plate	369966	5296233	473	39	0.87	0.03	0	S	
L1150	B	Plate	370092	5296184	477	43	1.09	0.05	0	S	
L1160	B	Plate	370196	5296182	476	41	1.66	0.1	0	S	
L1170	B		370324	5296123	482	47	4.85	0.36	0.37		
L1180	B		370427	5296108	480	43	4.53	0.33	0.65		
L1190	B		370558	5296081	482	48	4.01	0.29	5.81		
L1200	B		370678	5296021	481	45	4.62	0.34	4.13		
L1210	B		370777	5296052	479	45	4.46	0.33	1.32		
L1220	B		370897	5296018	474	41	8	0.59	1.02		
L1230	C	Plate	370103	5298486	477	38	1.19	0.06	0.05	~V	
L1230	B		370990	5296041	475	42	7.19	0.53	1.07		
L1240	C	Plate	370209	5298482	479	43	1.32	0.07	0.04	N	
L1240	B		371083	5296075	473	40	6.99	0.52	1.04		
L1250	B		371191	5296064	479	44	2.05	0.13	1.87		
L1260	B		371293	5296097	476	43	0.83	0.02	0.15		
L1280	C		370708	5298282	477	45	0.69	0.01	0		
L1290	C		370821	5298266	482	47	1.46	0.08	0.07		
L1300	C		370937	5298243	479	46	1.32	0.07	0.06		

Line	Anom ID	Anom type	X (m)	Y (m)	Z (m)	EM height (m)	Conductance (Siemens)	Tau dB/dt (ms)	Tau B-Field (ms)	Dipping direction	Cultural effect
L1310	C		371046	5298236	471	40	1.81	0.11	0		
L1320	C	Plate	371099	5298383	475	44	1.33	0.07	0	S	
L1330	C	Plate	371211	5298371	472	40	0.96	0.04	0	S	
L1340	C	Plate	371327	5298330	477	46	1.65	0.1	0.08	N	
L1350	N	Plate	371196	5298995	491	51	1.06	0.05	0	N	
L1360	N	Plate	371288	5299029	487	48	0.7	0.01	0	N	
L1400	C		372057	5298086	476	44	1.13	0.05	0		
L1410	C	Plate	372142	5298148	477	45	0.58	0	0	~V	
L1420	C	Plate	372262	5298122	483	51	0.61	0	0	~V	
L1430	C	Plate	372361	5298129	489	57	0.58	0	0	N	
L1440	C	Plate	372472	5298128	483	50	0.78	0.02	0	N	
L1450	N	Plate	372242	5299040	495	52	0.58	0	0	N	
L1450	C	Plate	372570	5298134	478	44	0.61	0	0	N	
L1460	N	Plate	372359	5299014	494	51	0.58	0	0	N	
L1640	D	Plate	374608	5298087	488	53	0.58	0	0	S	
L1650	D	Plate	374705	5298108	479	48	0.58	0	0	S	
L1660	D	Plate	374802	5298142	474	46	0.58	0	0	S	
L1670	D	Plate	374900	5298167	472	45	0.58	0	0	S	
L1680	D	Plate	374999	5298186	475	40	0.59	0	0	S	
L1690	D	Plate	375106	5298185	483	53	0.92	0.03	0	S	
L1700	J		374790	5299354	476	45	2.08	0.14	0		
L1700	D	Plate	375202	5298216	465	39	0.94	0.03	0	~V	
L1710	J	Plate	374881	5299404	476	47	2.34	0.16	0.13	S	
L1720	J	Plate	374960	5299476	476	51	0.86	0.03	0	~V	
L1730	J		375117	5299334	478	51	1.07	0.05	0		
L1740	J		375243	5299280	485	54	2.61	0.18	0		
L1750	X	cultural?	375637	5298487	482	53		0.84	1.98		Yes
L1750	J		375344	5299292	483	52	1.35	0.07	0		
L1760	J		375483	5299210	482	49	1.62	0.1	0		
L1770	J		375551	5299306	476	42	1.89	0.12	0		

Line	Anom ID	Anom type	X (m)	Y (m)	Z (m)	EM height (m)	Conductance (Siemens)	Tau dB/dt (ms)	Tau B-Field (ms)	Dipping direction	Cultural effect
L1780	J		375647	5299335	472	42	2.05	0.13	0		
L1790	J		375745	5299349	484	44	1.97	0.13	0.1		
L1790	P		375628	5299680	481	50	0.69	0.01	3.23		
L1930	G	Plate	377541	5298497	469	44	0.82	0.02	0	N	
L1940	G	Plate	377677	5298441	466	42	0.83	0.02	0	N	
L1950	F	Plate	377482	5299266	481	49	0.58	0	0	S	
L1950	G	Plate	377800	5298389	471	46	0.75	0.02	0	N	
L1960	G	Plate	377918	5298362	474	49	0.58	0	0	N	
L1960	F	Plate	377594	5299261	480	42	0.96	0.04	0	S	
L1970	F	Plate	377687	5299286	484	50	0.83	0.02	0	S	
L1980	G	Plate	378216	5298119	470	41	2.05	0.13	0.11	N	
L1980	F		377806	5299260	486	46	3.45	0.25	0.21		
L1990	F	Plate	377913	5299250	484	49	0.99	0.04	0	N	
L1990	G	Plate	378323	5298122	477	48	2.18	0.14	0.12	N	
L2000	G	Plate	378423	5298135	471	44	2.83	0.2	0.24	~V	
L2010	F	Plate	378117	5299268	479	43	1.14	0.05	0	S	
L2010	G	Plate	378530	5298141	480	51	0.91	0.03	0	N	
L2020	G	Plate	378628	5298173	475	45	1.08	0.05	0.01	N	
L2020	F	Plate	378230	5299264	479	44	1.14	0.05	0	S	
L2030	F	Plate	378339	5299248	482	45	1.38	0.07	0.02	N	
L2030	H	Plate	378792	5297998	489	64	2.03	0.13	0	N	
L2040	H	Plate	378895	5298033	489	60	0.58	0	0	N	
L2040	F	Plate	378454	5299233	481	47	0.59	0	0	N	
L2050	H	Plate	378976	5298074	489	51	0.58	0	0	N	
L2060	Q		378942	5298469	482	41	1.67	0.1	0		
L2070	K	Plate	378948	5298757	478	40	0.58	0	0	S	
L2080	K	Plate	379068	5298700	479	45	0.58	0	0	S	
L2080	E		378424	5300482	470	49	3.65	0.27	1.1		
L2090	E		378526	5300469	471	55	3.52	0.26	1		
L2090	K	Plate	379186	5298674	476	47	0.58	0	0	N	

Line	Anom ID	Anom type	X (m)	Y (m)	Z (m)	EM height (m)	Conductance (Siemens)	Tau dB/dt (ms)	Tau B-Field (ms)	Dipping direction	Cultural effect
L2100	K	Plate	379312	5298628	486	52	0.58	0	0	N	
L2100	X	cultural?	379150	5299072	479	42		0.61	1.74		Yes
L2100	E		378626	5300501	473	54	3.07	0.22	0.67		
L2110	E		378748	5300486	476	57	3.95	0.29	0.95		
L2110	X	cultural	379177	5299285	483	46		1.66	4.69		Yes
L2110	K		379431	5298587	490	56	0.58	0	0		
L2110	X	cultural?	379514	5298361	476	51	1.04	0.04	1.64		Yes
L2120	K	Plate	379529	5298592	480	49	0.58	0	0	N	
L2120	E		378852	5300466	469	47	5.49	0.41	1.22		
L2130	E	Plate	378929	5300552	463	48	0.88	0.03	0	N	
L2130	K	Plate	379640	5298599	475	48	0.58	0	0	N	
L2140	E	Plate	379047	5300519	469	55	1.02	0.04	0	N	
L2150	E	Plate	379154	5300503	482	71	1.58	0.09	1.55	N	
T2510	C	Plate	371240	5298373	474	44	1.09	0.05	0	E	
T2510	A?		368328	5297313	483	47	2.58	0.18	0		
T2520	U		379255	5300228	476	47	4.26	0.31	11.18		
T2520	T		379043	5300147	488	36	3.75	0.27	0.47		
T2520	S		377557	5299613	479	38	2.48	0.17	0.72		
T2520	I		369477	5296672	476	42	5.34	0.4	3.71		
T2520	L		369119	5296539	477	43	2.7	0.19	0.33		
T2530	G		370691	5296045	482	49	5	0.37	1.49		

Dore Block

Line	Anom ID	Anom type	X (m)	Y (m)	Z (m)	EM height (m)	Conductance (Siemens)	Tau dB/dt (ms)	Tau B-Field (ms)	Dipping direction	Cultural effect
L3000	A	Plate	380112	5292537	474	44	15.19	1.05	0.63		
L3010	A	Plate	380209	5292535	481	52	11.15	0.80	0.25	S	
L3020	A	Plate	380305	5292524	472	45	13.00	0.91	0.43	S	
L3020	D	Plate	380425	5298750	479	44	2.33	0.16	0.00	S	Yes
L3030	D	Plate	380520	5298827	473	39	8.14	0.60	0.48	S	Yes
L3030	A	Plate	380413	5292512	479	51	18.00	1.22	0.61	S	
L3040	A	Plate	380505	5292496	467	39	10.69	0.77	0.34	S	
L3040	C	Plate	380552	5294974	495	46	1.70	0.10	0.00	S	
L3040	D	Plate	380618	5298816	475	40		1.34	0.58	S	Yes
L3050	D	Plate	380718	5298809	480	41	0.58	0.00	0.00	S	Yes
L3050	C	Plate	380649	5294961	486	43	0.58	0.00	0.00	S	Yes
L3050	A	Plate	380611	5292501	474	43	10.93	0.78	0.33	S	
L3060	A	Plate	380714	5292483	470	46	17.22	1.17	0.52		
L3060	C	Plate	380757	5295049	475	36		0.23	0.04		Yes
L3060	D	Plate	380827	5298779	480	42	7.81	0.57	0.00	N	Yes
L3070	D	Plate	380920	5298793	485	45	8.02	0.59	0.00	N	Yes
L3070	A	Plate	380810	5292488	469	44	21.35	1.42	0.28	S	
L3081	A	Plate	380914	5292493	476	49	7.38	0.54	0.06	S	
L3081	D	Plate	381024	5298764	482	43	11.91	0.84	0.00		Yes
L3090	D	Plate	381118	5298761	483	43	7.08	0.52	0.00	S	Yes
L3090	A	Plate	381006	5292561	469	44	9.85	0.71	0.00	S	
L3100	A	Plate	381116	5292588	476	49	9.38	0.68	0.00	S	
L3100	D	Plate	381224	5298749	484	44	18.73	1.27	0.31	S	Yes
L3110	D	Plate	381315	5298769	483	40	15.22	1.05	0.72	S	
L3110	A	Plate	381210	5292571	468	43	15.80	1.09	0.16	S	
L3120	A	Plate	381315	5292546	471	46	7.79	0.57	0.12	S	
L3120	D		381419	5298741	485	43	15.28	1.06	0.65		
L3130	A	Plate	381411	5292553	473	48	7.47	0.55	0.00	S	

Line	Anom ID	Anom type	X (m)	Y (m)	Z (m)	EM height (m)	Conductance (Siemens)	Tau dB/dt (ms)	Tau B-Field (ms)	Dipping direction	Cultural effect
L3140	A	Plate	381514	5292489	469	46	5.05	0.37	0.08	S	
L3150	A	Plate	381614	5292492	478	52	6.09	0.45	0.31	S	
L3160	A	Plate	381711	5292485	486	56	7.30	0.54	0.04	S	
L3170	A	Plate	381809	5292436	472	47	7.44	0.55	0.15	S	
L3180	A	Plate	381907	5292378	484	57	5.82	0.43	0.00	S	
L3190	A	Plate	382007	5292309	499	73	4.73	0.35	0.01	S	
L3200	B	Plate	382098	5291673	487	55	4.57	0.34	0.00	N	
L3200	A	Plate	382104	5292189	477	52	5.84	0.43	0.15	S	
L3210	A	Plate	382210	5292172	473	49	6.70	0.49	0.20	S	
L3210	B	Plate	382196	5291662	489	58	5.02	0.37	0.00	N	
L3220	B	Plate	382292	5291651	487	53	3.75	0.27	0.02	N	
L3220	A	Plate	382300	5292190	470	45	6.04	0.45	0.01	S	
L3231	E	Plate	382523	5298594	462	42	19.96	1.34	0.11	N	
L3231	A	Plate	382402	5292164	473	47	4.67	0.35	0.00	S	
L3231	B	Plate	382398	5291645	485	56	3.04	0.22	0.00	N	
L3240	B	Plate	382491	5291621	465	42	3.53	0.26	0.02	S	
L3240	A	Plate	382502	5292146	472	47	4.53	0.33	0.00	S	
L3240	E	Plate	382617	5298571	461	43	9.02	0.65	0.35	N	
L3250	E	Plate	382719	5298616	469	51	6.51	0.48	0.12	N	
L3250	A	Plate	382597	5292100	473	46	7.55	0.55	0.12	S	
L3250	B	Plate	382598	5291592	484	54	3.15	0.23	0.05	S	
L3260	B	Plate	382701	5291558	479	50	5.96	0.44	0.25	S	
L3260	E	Plate	382822	5298624	479	55	5.88	0.43	0.04	N	
L3270	E	Plate	382913	5298673	481	49		0.62	0.40	S	Yes
L3270	B	Plate	382791	5291491	470	44	12.91	0.91	0.56	S	
T3500	D		380928	5298764	480	40	20.52	1.37	0.55		Yes
T3540	C	Plate	380553	5294886	495	47	1.99	0.13	0.00	E	
T3570	A		382094	5291957	499	52	0.78	0.02	0.00		

Heenan Block

Line	Anom ID	Anom type	X (m)	Y (m)	Z (m)	EM height (m)	Conductance (Siemens)	Tau dB/dt (ms)	Tau B-Field (ms)	Dipping direction	Cultural effect
L4000	E	Plate	395129	5296373	459	45	1.05	0.00	0.00	N	
L4000	A	Plate	395156	5297589	468	48	6.33	0.10	0.10	S	
L4010	A	Plate	395251	5297686	472	58	2.18	0.42	0.45	S	
L4010	E	Plate	395229	5296427	454	40	1.39	1.84	0.00	N	
L4020	E		395330	5296473	455	42	2.48	0.40	0.89		
L4020	E1	Plate	395335	5296704	454	40	1.16	0.00	0.00	~V	
L4060	H	Plate	395751	5297856	461	45	2.26	0.25	0.62	S	
L4070	H	Plate	395855	5297914	465	49	2.41	0.14	0.30	S	
L4100	H	Plate	396154	5297981	462	45	2.76	0.06	0.19	N	
L4110	H		396257	5297978	465	48	4.28	0.12	0.00		
L4140	F	Plate	396513	5295388	466	47	1.32	0.84	0.09	N	
L4150	F	Plate	396614	5295425	464	45	2.20	0.58	0.81	N	
L4160	F	Plate	396712	5295459	464	45	3.15	0.71	0.32	N	
L4170	D	Plate	396845	5297298	464	50	0.92	0.00	0.00	N	
L4170	F	Plate	396814	5295500	472	54	2.13	0.22	0.45	N	
L4180	F	Plate	396914	5295522	467	47	1.11	0.08	0.00	~V	
L4180	D	Plate	396946	5297288	466	51	1.24	0.76	0.00	N	
L4190	D	Plate	397043	5297282	464	47	2.64	0.00	0.55	N	
L4200	D	Plate	397145	5297304	467	52	3.47	0.11	0.32	N?	
L4210	D	Plate	397246	5297345	473	57	3.24	0.06	0.33	S?	
L4210	D1	Plate	397242	5297115	471	48	3.25	0.08	0.17	N?	
L4220	D	Plate	397344	5297310	468	51	2.47	0.08	0.37	N	
L4220	B	Plate	397362	5297979	457	45	1.22	1.62	0.00	N	
L4230	B	Plate	397457	5298012	467	56	1.20	0.00	0.46	N	
L4230	D	Plate	397441	5297265	475	60	2.20	0.25	0.42	N	
L4240	D	Plate	397544	5297226	463	45	2.42	0.44	0.61	N	
L4240	B	Plate	397558	5298039	455	41	0.68	0.40	0.00	N	
L4250	B	Plate	397665	5298105	468	53	6.97	0.00	0.00	N	

Line	Anom ID	Anom type	X (m)	Y (m)	Z (m)	EM height (m)	Conductance (Siemens)	Tau dB/dt (ms)	Tau B-Field (ms)	Dipping direction	Cultural effect
L4250	D	Plate	397645	5297223	476	57	2.06	0.55	0.59	N	
L4260	D	Plate	397741	5297227	466	45	3.48	0.24	0.29	N	
L4260	B	Plate	397758	5298088	455	42	3.55	0.01	0.08	N	
L4270	D	Plate	397842	5297208	470	53	9.30	0.12	0.12	N	
L4280	X	cultural?	397928	5296286	456	39		0.00	0.00		Yes
L4280	D	Plate	397943	5297178	463	46	11.42	0.00	0.00	N	
L4290	D	Plate	398047	5297144	471	48	7.82	0.00	0.03	N	
L4300	D	Plate	398139	5297151	471	49	6.96	0.00	0.01	N	
L4310	D	Plate	398243	5297170	471	47	5.50	0.00	0.08	~V	
L4320	D	Plate	398345	5297181	474	54	0.58	0.00	0.00	S	
L4350	C	Plate	398662	5298267	473	56	0.82	0.00	0.00	N	
L4360	C	Plate	398763	5298288	471	54	1.20	0.20	0.00	N	
L4370	C	Plate	398866	5298265	460	43	0.85	0.05	0.00	N	
L4380	C	Plate	398964	5298279	469	51	4.62	0.00	0.16	N	
L4390	C	Plate	399063	5298274	467	50	1.70	0.00	0.00	N	
L4400	C	Plate	399157	5298305	469	53	1.40	0.49	0.09	N	
L4410	C	Plate	399261	5298311	475	50	0.58	0.00	0.03	N	
L4420	C	Plate	399365	5298371	477	48	0.75	0.09	0.00	N	
T4500	C		399033	5298428	460	42	11.60	0.00	0.00		
T4510	D3		397904	5297454	468	49	15.61	0.00	0.00		
T4510	D2		397120	5297469	461	41	4.54	0.09	0.20		
T4510	A		395147	5297500	476	48	11.49	0.00	0.00		
T4520	E	Plate	395168	5296498	456	44	1.24	1.17	0.00	W	
T4530	F	Plate	396768	5295470	471	51	0.69	0.00	0.00	W	

APPENDIX H

GAMMA-RAY SPECTROMETRIC DATA ANALYSIS

The analysis of gamma-ray spectyrometric data in support of gold exploration is based on defining regions of low equivalent Thorium correlating versus Potassium ratios, potentially relating to favourable hydrothermal alteration for gold mineralization, as reported by Shieves et al. (1997)[1] and Hetu (1991)[2].

However, care must be taken when considering such spectrometric anomalies in the presence of swamps and other water courses, since these can also cause falsely similar responses.

H1 – Denyes block

Figure H1 shows the ratio image of equivalent Thorium / Potassium with EM anomaly symbols for Denyes block. As shown, most EM anomaly trends either feature high eTh/K or occur along water courses or wetlands and are therefore not considered favourable targets for gold-alteration based on the spectrometric evidence.

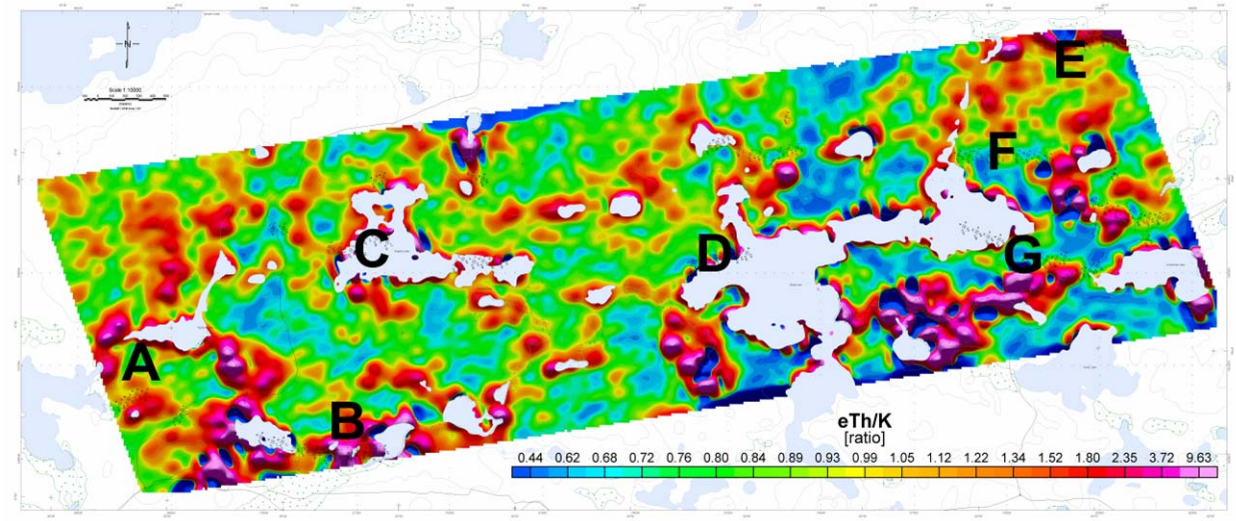

Figure H1 - eTh/K ratio with EM anomalies, Denyes block

However, exceptionally, Anomaly F correlates with favourable high K values (38 counts per second - cps), along L1980. A corresponding low eTh/K ratio of 0.39 correlating with high magnetic values suggests that it represents a potentially favourable indicator for gold mineralization along this EM trend.

---

1 Shives, R.B.K., Charbonneau, B.W., and Ford, K.L., 1997, The detection of potassic alteration by gamma-ray spectrometry - Recognition of alteration related to mineralization, in Gubins, A.G., ed., Proceedings of Exploration 97: Fourth Decennial International Conference on Mineral Exploration: Geophysics and Geochemistry at the Millenium, p. 741-752.

2 Hetu, R.J., 1991, Airborne Geophysical Survey, Red Lake, Ontario: Geological Survey of Canada, Open File 2403, 41 p.

Anomaly G, located in an area of low magnetic amplitudes, also displays low values of eTh/K with moderate K value of 21 cps. This EM anomaly trend, detected from L1980 to L2020 and located west of Ackerman Lake, therefore represents a favourable target for gold mineralization.

H2 – Dore block

The ratio image of equivalent Thorium / Potassium with EM anomaly symbols for Dore block is presented in Figure H2.

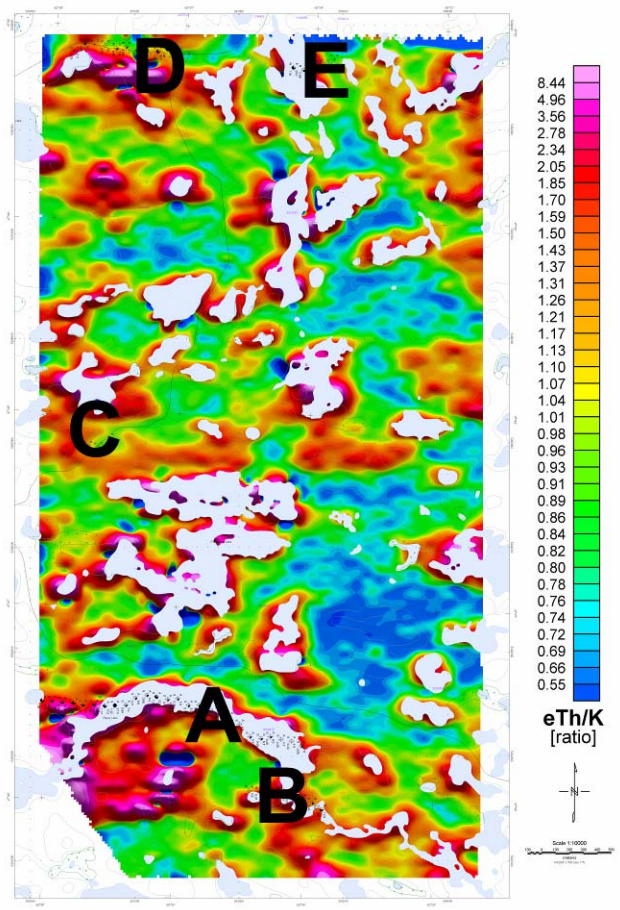

Figure H 2 - eTh/K ratio with EM anomalies, Dore block

Where the EM and spectrometric anomalies are not directly associated detected with wetland or watercourses in Dore block, values of eTh/K are higher than 1 and values of K average 22 cps which is considered moderate. Hence, no low eTh/K anomalies of significance associated with either EM or magnetics appear to be defined on Dore block.

H3 – Heenan block

Figure H3 shows the ratio image of equivalent Thorium / Potassium with EM anomaly symbols for Heenan block.

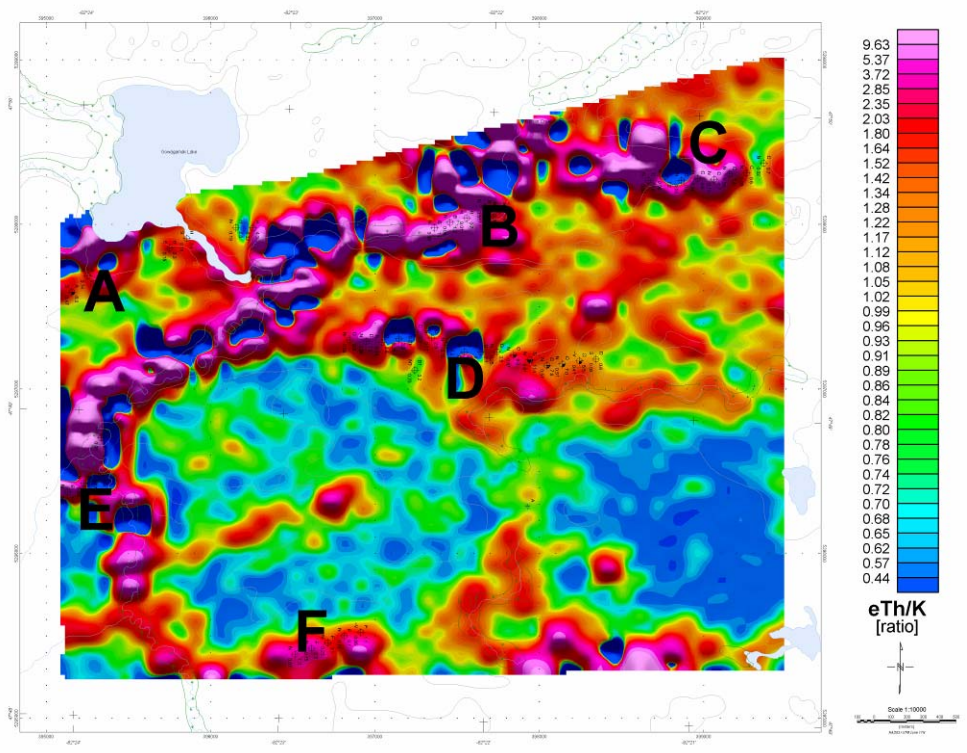

Figure H 3 – eTh/K ratio with EM anomalies, Heenan block

Most of the selected groups of low eTh/K and EM anomalies appear to occur at some point near creeks or swamps, where gamma-ray spectrometry is not applicable. These include EM trends B, C, D and E..

However, no water features are present in the vicinity Anomaly A. Situated between two inferred faults, as shown in magnetics (see Tilt derivative, section 6.2.3.1), this group of anomalies displays low K values of 10 cps with eTh/K value of 0.6, as per line 4000. Anomaly A therefore represents an area favourable for alteration associated with gold, based on the geophysics.